

Fall 2007

# Seafloor characterization of the Historic Area Remediation Site using angular range analysis

Luis A. Soares Rosa

*University of New Hampshire, Durham*

Follow this and additional works at: <https://scholars.unh.edu/thesis>

---

## Recommended Citation

Soares Rosa, Luis A., "Seafloor characterization of the Historic Area Remediation Site using angular range analysis" (2007). *Master's Theses and Capstones*. 313.

<https://scholars.unh.edu/thesis/313>

This Thesis is brought to you for free and open access by the Student Scholarship at University of New Hampshire Scholars' Repository. It has been accepted for inclusion in Master's Theses and Capstones by an authorized administrator of University of New Hampshire Scholars' Repository. For more information, please contact [nicole.hentz@unh.edu](mailto:nicole.hentz@unh.edu).

**SEAFLOOR CHARACTERIZATION  
OF THE HISTORIC AREA REMEDIATION SITE USING  
ANGULAR RANGE ANALYSIS**

BY

**LUIS A. SOARES ROSA**

BSc in Geology, Faculdade de Ciências/Universidade de Lisboa, Portugal, 1993

THESIS

Submitted to the University of New Hampshire  
in Partial Fulfillment of  
the Requirements for the Degree of

Master of Science

in

Ocean Engineering (Ocean Mapping)

September 2007

UMI Number: 1447908

### INFORMATION TO USERS

The quality of this reproduction is dependent upon the quality of the copy submitted. Broken or indistinct print, colored or poor quality illustrations and photographs, print bleed-through, substandard margins, and improper alignment can adversely affect reproduction.

In the unlikely event that the author did not send a complete manuscript and there are missing pages, these will be noted. Also, if unauthorized copyright material had to be removed, a note will indicate the deletion.

**UMI**<sup>®</sup>

---

UMI Microform 1447908

Copyright 2007 by ProQuest Information and Learning Company.

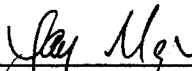
All rights reserved. This microform edition is protected against unauthorized copying under Title 17, United States Code.

ProQuest Information and Learning Company  
300 North Zeeb Road  
P.O. Box 1346  
Ann Arbor, MI 48106-1346

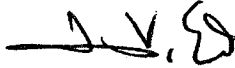
This thesis has been examined and approved.




Thesis Director, ~~Dr.~~ Luciano Fonseca,  
Research Associate Professor of Ocean Engineering, UNH



Dr. Larry A. Mayer,  
Professor of Earth Sciences and Ocean Engineering, UNH



Dr. James V. Gardner,  
Research Professor of Earth Sciences, UNH



Dr. Larry G. Ward,  
Research Associate Professor of Earth Sciences, UNH

08/14/07

Date

## ACKNOWLEDGEMENTS

I would like to thank my wife Ana and little Sofia for making this adventure possible and Dr. Larry Mayer, while CCOM Director, for accommodating all the logistics of a family moving between continents and living in two different states. I also would like to express my thanks to my thesis advisor, Dr. Luciano Fonseca, and to the other members of the committee, Dr. Larry Mayer, Dr. James Gardner and Dr. Larry Ward, whose invaluable guidance and support helped me completing my studies.

Many thanks to SAIC, and especially to Tom Waddington for providing all the multibeam sonar and SPI data used in this study, and also to Natasha Pinckard, Pamela Luey, Michael Cole and the crew of the R/V Beavertail, for all the help during data collection in 2006. Thanks also to Dr. Larry Ward for the use of the Coastal Geology Laboratory – UNH, to the Portuguese Hydrographic Institute, and especially to Dra. Aurora Bizarro and to my colleagues at the Marine Geology Department, for the grain size analysis with laser diffraction.

Many thanks to all my CCOM colleagues and friends, that in one way or the other, made this a fruitful and unforgettable experience.

Finally a word of acknowledgement for my teachers because although I probably learned less than they would expect, I learned much more than I ever imagined.

This work was only possible due to the support of the National Oceanographic and Atmospheric Administration grant NAONOS4001153 and to the leave of absence provided by the Portuguese Hydrographic institute.

## TABLE OF CONTENTS

ACKNOWLEDGEMENTS .....	iii
LIST OF TABLES .....	vii
LIST OF FIGURES .....	viii
ABSTRACT .....	xi

CHAPTER	PAGE
1. INTRODUCTION .....	1
1.1 Remote Seafloor Characterization .....	1
1.2 Interaction of Sound with the Seafloor .....	4
1.3 Geocoder and Angular Range Analysis (ARA) .....	5
1.4 Verification of Model Predictions and the Importance of Mean Grain Size ..	7
1.5 Historic Area Remediation Site (HARS) .....	10
1.6 Objectives .....	15
2. BACKSCATTER MOSAICS AND ANGULAR RANGE ANALYSIS (ARA) .....	16
2.1 Backscatter Mosaics Assembled in Geocoder .....	16
2.2 Angular Range Analysis (ARA) .....	18
2.3 Multibeam Data Collection and Processing .....	22
3. GROUND TRUTH .....	25
3.1 Position Uncertainty .....	26
3.2 Grab Samples .....	27
3.2.1 Surface sediment sampling .....	27

3.2.2	Single sample versus composite sample .....	28
3.2.3	Grab sampler .....	29
3.2.4	Sediment analysis (grain-size and organic content) .....	30
3.2.5	Uncertainties in sediment analysis .....	33
3.3	Sediment Profile Imaging (SPI) and Plan View Image .....	36
4.	GROUND TRUTH AND ACOUSTIC REMOTE SENSING RESULTS, COMPARISON AND DISCUSSION .....	39
4.1	Mean Grain Size .....	39
4.1.1	Calculation of mean grain size .....	39
4.1.2	Error introduced by drying the sample .....	41
4.1.3	Error in the estimation of the mean particle size .....	42
4.1.4	Comparison between the SOP (sieve-laser diffraction) and the sieve- pipette method .....	44
4.1.5	Estimated uncertainties in the determination of mean grain size .....	46
4.1.6	Mean grain size versus penetration of the optical prism .....	47
4.2	Backscatter Strength .....	49
4.2.1	Backscatter strength versus mean grain size .....	49
4.2.2	Comparison of backscatter strength for the same type of sediment .....	53
4.2.3	Differences in backscatter strength between 2005 and 2006 and temporal evolution of the seafloor .....	54
4.2.4	Backscatter strength versus penetration of the optical prism .....	58
4.3	Angular Range Analysis .....	59
4.3.1	ARA in normal mode .....	59
4.3.2	Comparison of ARA results with mean grain size .....	62
4.3.3	ARA in supervised segmentation mode (in areas of horizontal heterogeneity) .....	67

4.3.4	Comparison of ARA results with the estimated mean grain size for the top layer (in areas of vertical heterogeneity) .....	70
4.3.5	Estimation of the consistency of ARA results .....	73
5.	CONCLUSIONS .....	74
	Future Work .....	79
	APPENDICES .....	80
	APPENDIX A - PENETRATION OF THE SOUND INTO THE SEDIMENT .....	81
	APPENDIX B - BACKSCATTER MOSAICS APPLYING DIFFERENT AVGs .....	86
	APPENDIX C - PROCEDURES FOR GRAIN SIZE ANALYSIS .....	93
C.1	Normal procedure for grain size analysis .....	93
C.2	Measurement of the natural occurring particle size .....	95
C.3	Measurement of the effect of drying the sample .....	96
C.4	Pipette analysis .....	96
C.5	Loss On Ignition (LOI) .....	99
	APPENDIX D - EXAMPLES OF ANGULAR RESPONSE .....	100
	REFERENCES .....	104



## LIST OF TABLES

Table 3.1 - Analysis performed on each aliquot of sediment samples. ....	32
Table 4.1 – ARA solutions within the area of the sediment samples.....	73
Table C.1 – Pipettes withdrawal times and depths.....	99

## LIST OF FIGURES

Figure 1.1 – HARS location.....	11
Figure 1.2 - HARS 2006 bathymetry .....	12
Figure 2.1 – Example of backscatter strength and angular response. ....	18
Figure 2.2 – Histogram of backscatter strength.....	20
Figure 2.3 – ARA in theme mode. ....	21
Figure 2.4 – 2005 backscatter mosaic and sampling location. ....	23
Figure 2.5 – 2006 backscatter mosaic and sampling location. ....	24
Figure 3.1 - Example of position uncertainty, station 16. ....	26
Figure 3.2 - Petit Ponar grab sampler. ....	28
Figure 3.3 - Example of the criteria used to decide where to split the sample. ....	32
Figure 3.4 – SPI system.....	37
Figure 4.1 – Histogram of grain size for all samples collected in 2006 .....	40
Figure 4.2 - Mean grain size vs percentage of gravel plus sand for 2006 samples.....	41
Figure 4.3 - Influence of drying the sample on the mean grain size.....	42
Figure 4.4 - Evolution of the grain size distribution with time on laser diffraction. ....	43
Figure 4.5 - Influence of sample preparation on the mean grain size .....	43
Figure 4.6 - Relation between the organic content and particle agglomeration.....	44
Figure 4.7 - Difference in the calculation of Mz by laser diffraction and pipettes. ....	45
Figure 4.8 - Example of grain size distribution using different techniques.....	47
Figure 4.9 - Penetration of the optical prism versus percentage of gravel plus sand. ....	48
Figure 4.10 – SPI penetration vs mean grain size for 2006 data. ....	49
Figure 4.11 - Percentage of gravel plus sand vs BS for 2005 and 2006.....	50
Figure 4.12 - Mz vs BS and mean particle size vs BS (2006).....	50

Figure 4.13 - BS, SPI images and sample photos for stations 26, A4 and P2800.....	52
Figure 4.14 - SPI images from samples 20028, 20064, L1200 and L2400. ....	54
Figure 4.15 - Grain size statistics for samples 20028, 20064, L1200 and L2400.....	54
Figure 4.16 - Difference in the backscatter strength between 2006 and 2005. ....	56
Figure 4.17 - Difference in bathymetry between 2006 and 2005 .....	57
Figure 4.18 – Difference in BS draped over the difference in bathymetry.....	58
Figure 4.19 - Mean BS vs penetration of the optical prism for 2005 and 2006.....	59
Figure 4.20 - ARA solutions for 2006 data .....	61
Figure 4.21 - ARA solutions and backscatter mosaic for station A12 (2006). ....	62
Figure 4.22 - ARA solutions vs Mz from grab samples. ....	63
Figure 4.23 - ARA solutions, SPI images and sample photos for station 17 (2006).....	65
Figure 4.24 - Manual segmentation of the area around station A12 (2006).....	69
Figure 4.25 - SPI images and grab sample photos for station A12 (2006).....	69
Figure 4.26 – Angular response and model fit for station A12 (2006).....	70
Figure 4.27 - Correlation between the mode and sediment layers.....	71
Figure 4.28 - ARA solutions vs Mz from grab samples after corrections.....	72
Figure A.1 - Mean grain size versus k. ....	81
Figure A.2 - Refraction of a ray at 45° grazing angle.....	82
Figure A.3 - Mean grain size vs compressional sound speed.....	82
Figure A.4 - Mean grain size vs attenuation. ....	82
Figure A.5 - $S_B$ versus grazing angle.....	84
Figure A.6 - Estimation of acoustic wave penetration into the sediment. ....	85
Figure B.1 - 2006 backscatter mosaic without any AVG.....	87
Figure B.2 - 2006 backscatter mosaic with AVG Trend. ....	88
Figure B.3 - 2006 backscatter mosaic with AVG Flat. ....	89
Figure B.4 - Difference between AVG Trend and AVG.....	90

Figure B.5 - 2006 backscatter mosaic with a Lambertian correction.....	91
Figure B.6 - Difference between AVG Trend and AVG Lambert.....	92
Figure D.1 - Examples of angular response, stations A2 and N2000 (2006). ....	102
Figure D.2 - Examples of angular response, stations A9 and 97004 (2006).....	103

## **ABSTRACT**

### **SEAFLOOR CHARACTERIZATION OF THE HISTORIC AREA REMEDIATION SITE USING ANGULAR RANGE ANALYSIS**

by

Luis A. Soares Rosa

University of New Hampshire, September, 2007

Angular Range Analysis (ARA) is a physics-based approach to acoustic remote seafloor characterization. In order to better understand the capabilities and limitations of this technique, ARA analyses were performed on multibeam sonar data collected at the Historic Area Remediation Site, an area with high spatial variability. The remotely derived results were compared to grain size information derived from grab samples and Sediment Profile Imaging. Uncertainties in the determination of mean grain size from ground truth were identified and when possible quantified. ARA proved to be an effective remote sensing tool at a regional scale in its main operational mode that has a spatial resolution limited to half-swath width of the sonar and to thirty pings. When the seafloor is heterogeneous within half-swath width of the sonar, textural segmentation of the backscatter mosaic allows the definition of "themes" out which ARA solutions can be calculated, improving the correlation with ground truth.

## CHAPTER 1

### INTRODUCTION

The use and exploration of the seas rely heavily on the propagation of underwater sound. Light and radio waves, commonly used in remote sensing methods, propagate well in air but are scattered and rapidly attenuated when penetrating the water surface. Since direct measurements of seafloor properties are representative of only a single point, are expensive and time consuming, and sometimes even impossible to conduct, we depend on the acoustic remote characterization of the seafloor for a broad range of disciplines including marine geology, offshore engineering and geotechnics, benthic habitat mapping and mine warfare. In this thesis, a novel, physics-based approach to remote seafloor characterization, Angular Range Analysis, is applied to a well-studied area in order to better understand the capabilities and limitations of this technique. Because any acoustically inferred sediment property will need to be validated with direct measurements, an attempt is made to identify sources of uncertainty in common methods of ground truth.

#### **1.1 Remote Seafloor Characterization**

Inferring seafloor properties through the use of acoustic means started with qualitative studies of the echo character by marine geologists and geophysicists, generally using single beam echo-sounder's paper records to make inferences about the nature of the seafloor. For that, the observed echo types were correlated with ground

truth data (usually cores or grab samples) and this information was then extrapolated to the entire survey area (Damuth, 1975; 1980). The same type of approach was extended to analog sidescan sonar paper records, matching the observed acoustic texture with the correspondent seafloor type. This type of approach is strongly dependant on instrumental acquisition settings that often vary in and between surveys as well as on subjective human interpretation.

Since the 1950s attempts have been made to quantify the relationship between geoacoustic and physical properties of sediments (Urick, 1954; Hamilton *et al.*, 1956). By the 1970s, a substantial database of relationships between geoacoustical, physical and geotechnical properties of seafloor sediment was developed (Hamilton, 1970; 1972; 1974; 1976; 1978). Thousands of measurements gave rise to a series of regression equations, relating impedance, reflection coefficient and bottom loss with porosity and density; attenuation with mean grain size and porosity; mean grain size with porosity and density; and sound velocity with porosity, mean grain size and density.

Successful measurement of sediment geoacoustic properties from the acoustic return started with the use of a calibrated chirp sub-bottom profiler. Sediment classification models were developed based on the attenuation, impedance and volume scattering (Mayer and LeBlanc, 1983; Schock *et al.*, 1989; Panda *et al.*, 1994; LeBlanc *et al.*, 1995).

A different type of approach examined the coherency of seafloor echoes as an indicator of seafloor character, and the statistical analysis of echo fluctuations from ping-to-ping was used as a remote sensing tool (Dunsiger *et al.*, 1981; Stanton and Clay, 1986). Coherence in the signal was related with seafloor roughness and bottom type. However, this method only allows a qualitative description in terms of bottom roughness.

By the 1980s, what had been long-used by fishermen in an empirical way was implemented as a seabed classification system: discrimination of seafloor type based on

waveform characterization of the first and second echoes (Orlowsky, 1984). Building on that principle, commercial systems such as RoxAnn (Chivers *et al.*, 1990; Murphy *et al.*, 1995) or QTC View (Collins *et al.*, 1996) use the returned echo of a single beam echosounder to remotely classify the seafloor. RoxAnn uses the final portion of the first return as a measure of roughness and the second multiple of the acoustic signal as measure of hardness. These two parameters are plotted against each other and clusters are defined. QTC View extracts 166 parameters (full feature vectors) from the signal envelope and then combines these into three primary parameters called Q-values. These values, when plotted in a tri-dimensional space tend to group in clusters, each one corresponding to a different type of acoustic response of the seafloor. Both approaches only segment the seafloor into regions of similar response and need ground truth to assign seafloor types to the segmented areas.

With the advent of digital oblique incidence systems (sidescan sonars, multibeam echo-sounders) and the production of digital backscatter mosaics, classification systems based on textural analysis of the image were implemented commercially (QTC Sideview and Multiview, Triton Imaging SeaClass, GeoAcoustics GeoTexture, Arescon, GENIUS). Most of these rely on the use of grey level co-occurrence matrices to segment the image in regions with similar statistical properties (Pace and Dryer, 1979; Reed and Hussong, 1989). More elaborate classification techniques combine multibeam bathymetry with co-registered backscatter data in a hierarchically supervised classification scheme, to segment the seafloor into distinct facies (Dartnell and Gardner, 2004). Other approaches use the signal envelope instead of the image, analyzing the power spectra (Pace and Gao, 1988) or the probability density function of the echo amplitude (Stewart *et al.*, 1994).

All these methods require ground truth to identify the corresponding bottom type. However, since there is no unique relationship between acoustic signature and seafloor



type, an empirical relationship must be established for each survey site. In order to produce a true classification system, the physics of the interaction of sound with the seafloor must be properly understood.

## **1.2 Interaction of Sound with the Seafloor**

Most of the systems used to remotely classify the seafloor fall in the monostatic case, in which the transducer that receives the returned echo is located in the same place where the sound wave was generated. The quantification of the returned echo was first addressed by Urick (1954, p. 233) in terms of target strength, or reverberation strength, per unit area of the bottom:

It remains now to convert these measurements into some sort of scattering coefficient of the bottom. [...] Let a sound wave be incident on a small area  $dA$  of the bottom at a certain grazing angle  $\theta$ . At a distance of 1 yard from  $dA$  back toward the source, let the intensity of backscattering be  $I_s$ . Then we will define a coefficient, which may be called the "scattering strength" of the bottom at angle  $\theta$ , to be the ratio of  $I_s$  to the incident intensity, per unit area of  $dA$ . It is convenient to express scattering strength, referred to one square yard of bottom area, in decibel units. Thus, scattering strength is the ratio of two intensities and is related by the factor  $2\pi$  to the backscattering cross section of a unit area.

In the same experiment, it was observed that backscattering strength is a function of grazing angle and that this relationship changes with bottom type. In another experiment, McKinney and Anderson (1964) recognized the dependence of backscattering strength on the grazing angle, frequency and bottom type, as being of "primary interest". However, only when interferometric sidescan sonars and multibeam echo-sounders became available was it possible to collect acoustic backscatter versus angle of arrival in a systematic manner. At that moment, the potential of this information for remote classification of seafloor types was recognized (de Moustier and Matsumoto, 1993).

One of the components necessary for the use of the backscatter angular dependency as a remote characterization tool, is a high-frequency acoustic backscatter model. Acoustic models predict the acoustic response of the seafloor from its physical and geoacoustic properties. The list of properties can be extensive, due to the fact that sediments are complex assemblages of a variety of particles, pore fluid, organic matter and sometimes free gas. When an acoustic wave reaches the seafloor, part of the energy is scattered back to the transducer due to irregularities at the water/sediment interface and part is transmitted into the sediment and scattered by heterogeneities inside and between the first layers. For a given frequency the amount of scattered energy is mainly dependant on the seafloor roughness, the impedance contrast between the water and the sediment, and the volume heterogeneities that may exist within the sediment. All these processes must be taken into account in a comprehensive acoustic backscatter model. In order to estimate the type of seafloor and remotely characterize its properties from the angular response, an acoustic model has to be inverted. The Angular Range Analysis (ARA) (Fonseca and Mayer, 2007), included in the Geocoder software developed at the University of New Hampshire (Fonseca and Calder, 2005), implements this concept and represents the newest contribution in physics-based approaches for remote seafloor characterization.

### **1.3 Geocoder and Angular Range Analysis (ARA)**

The first step in the remote characterization of the seafloor using ARA is to obtain accurate measurements of backscatter strength. Geocoder radiometrically corrects backscatter intensities registered by the sonar and geometrically corrects and positions each acoustic sample in a projected coordinate system, thus calculating the best estimate of the actual backscatter strength returned from the seafloor.

After the angular response of the seafloor (the variation of backscatter with grazing angle) has been determined, it has to be linked to seafloor properties by an acoustic model. Two modified models are implemented in Geocoder's ARA (Fonseca and Mayer, 2007): 1) a composite roughness model developed by Jackson *et al.* (1986) and 2) an effective density fluid model (Williams, 2001) derived from the Biot theory (Biot, 1956, 1962).

In the Jackson *et al.* (1986) model the sediment is idealized as an acoustically refractive and lossy fluid, and the total backscatter strength is modeled as the sum of two different processes: interface scattering and volume scattering. The acoustic response of the sediment is modeled as function of frequency and grazing angle. This model requires input parameters related to the impedance contrast (sound speed and density in the water and in the sediment), attenuation (loss parameter), roughness (spectral strength and the spectral exponent of bottom relief) and volume scattering (volume parameter).

The Biot theory describes the propagation of acoustic waves in a porous elastic matrix containing a viscous fluid. Models that consider the full Biot theory require parameters related to sediment grains, pore fluid and the sediment frame. Williams' (2001) acoustic propagation model approximates a porous medium as a fluid with a bulk modulus and effective density derived from Biot theory. The implementation of this model in Geocoder's ARA requires, in addition to the parameters used in the implementation of the Jackson's model, the porosity, permeability and tortuosity of the sediment.

The inversion of one of the acoustic models implemented in Geocoder's ARA, which is done by adjustment of the model to the observed variation of backscatter strength with grazing angle, with model parameters constrained by relations between

physical and geoacoustical properties of the sediment, results in a physics-based prediction of seafloor properties.

#### **1.4 Verification of Model Predictions and the Importance of Mean Grain Size**

One possible benefit from the use of a remote sensing technique is to minimize or eliminate the need for ground truth. However, before a remote sensing technique is generally accepted, we have to make sure that the results accurately describe the real world within an uncertainty or resolution that satisfies the objectives of the required application.

The most accurate way of verifying model predictions is the direct measurement of sediment properties, but this poses several problems. The measurement of geoacoustic properties like sound speed and attenuation in the laboratory requires undisturbed samples, but the coring and the sampling process often result in compaction of the sediment and loss of water. Therefore, measured values may not reflect natural conditions. Alternatively, measurements can be made *in situ* using probes pushed into the sediment by divers, from submersibles or by remotely operated vehicles (Mayer *et al.*, 2002), but these properties are frequency dependant and the direct measurement should ideally be done at the same frequency as the one considered in the model. Another problem arises from the temporal variability of seafloor properties and the impossibility of continuous measurements.

Some geoacoustic parameters are either very difficult or nearly impossible to measure (Jackson and Richardson, 2007). For these, the preferred means of obtaining them is through empirical regressions between geoacoustic and physical properties (Hamilton, 1972, 1974; Richardson and Briggs, 2004; Jackson and Richardson, 2007). But the measurement of physical properties is based mostly on core samples and the

determination of properties such as bulk density and porosity, is subject to the same sampling disturbance described above. These errors can be minimized through techniques such as the collection of sediments by divers in slabs or in horizontal corers, or with large box corers (Jackson and Richardson, 2007). Measurement of seafloor roughness can be accomplished using digital stereo photogrammetry and volume heterogeneity can be quantified with X-ray computed tomography (Pouliquen and Lyons, 2004). However, outside designed experiments, measures of seafloor properties seem difficult to obtain.

Because of the difficulties described above, one of the most commonly measured properties is grain size, often expressed by mean grain size or sediment type (e.g. gravelly muddy sand). Jackson and Richardson (2007, p.193 and p.195) comment on the relation between mean grain size and seafloor roughness:

When seafloor roughness, as represented by RMS roughness, is plotted as a function of mean grain size, the result is a scattering of points across the range of sediment types. [...] Sediment mean grain size alone may never yield the types of predictive relationships for roughness required by high frequency acoustic models unless the effects and rates of hydrodynamic and biological process that create, modify and destroy roughness features are incorporated into predictive relationships.

And between mean grain size and geoacoustic and physical properties of the sediment (Jackson and Richardson, 2007, p.150-151):

The coefficient of determination,  $r^2$ , between index of impedance and mean grain size is much lower than the coefficient of determination between index of impedance and sediment bulk density or porosity. This lower coefficient of determination is reflected in the lack of a physical relationship between mean grain size and either sediment bulk density or porosity. [...] Using values of mean grain size as an index, especially in the silt-size range, may be very misleading because of major differences in sorting (standard deviation of the particle size distribution) or due to effects of compaction and packing. [...] Given the aforementioned issues, it is perhaps amazing that empirical regressions between grain size-related parameters and sediment density, porosity, sound speed, or impedance have any predictive value.

Nevertheless, sediment type or mean grain size are typically used indirectly as empirical predictors of acoustic behavior, probably because they are the most common

descriptors found in sediment databases and are often the only sediment physical descriptors available.

An acoustic model may be constrained by relations between physical and geoacoustical properties of the sediment determined in carefully designed experiments, but in a real-world application, when an acoustic measurement is made and the model inverted to remotely characterize the seafloor, there will seldom be any seafloor property data available to verify model results other than the mean grain size.

In this study, mean grain size as predicted by the ARA is compared with mean grain size obtained through common methods of ground truth and sediment analysis. Of particular concern is the use of mean grain size as the object of comparison. Mean grain size as determined by a remote sensing tool such as ARA is always subject to suspicion given the above mentioned apparent lack of physical relationship with other sediment properties used to model the acoustic response of the sediment. However, mean grain size as determined by common methods of ground truth and sediment analysis cannot be considered as an absolute value either. It is affected by uncertainties that are present from sampling to grain size analysis. But most importantly, we have to make sure that we are comparing acoustic and physical samples in the same place, and this is particularly true in areas of high horizontal and vertical heterogeneity.

Horizontal variability can be a limitation for ARA, which in its main operational mode has a spatial resolution limited to half-swath width of the sonar in the across-track direction, and to a certain number of pings (usually between 20 and 30) in the along-track direction. Horizontal variability can also be a limitation for ground truth. The spatial scale of sediment uniformity generally is not known and the size of the sediment sample and the number of samples may not reflect the local variability. Additionally, the sampler may not be precisely positioned.

Vertical variability can lead to errors in the comparison between ARA predictions and mean grain size determined by grab sampling. The penetration of a high-frequency acoustic wave is only in the order of a few centimeters (Appendix A), and if the sediment is layered at a centimeter scale, the grab sampler may transect other types of sediment in the subsurface that are not being sampled acoustically.

This study was carried out on the Historic Area Remediation Site (HARS), off New Jersey, because of the large amount of data available and because of the high spatial variability (the result of anthropogenic actions).

### **1.5 Historic Area Remediation Site (HARS)**

The area of study is located in the New York Bight, northwest of the head of the Hudson Shelf Valley, six nautical miles east of Sandy Hook, New Jersey, with an average depth of 25 m (Fig. 1.1). This area has been a place for disposal of assorted material (garbage, city refuse, cellar dirt and sediments derived from dredging during the maintenance, deepening and construction of new channels in New York Harbor) since the mid-1800s and because of that, very little of the original shelf geology is preserved. The United States Army Corps of Engineers (USACE) web site presents a brief history of the HARS (<http://www.nan.usace.army.mil/business/prjlinks/dmmp/benefic/hars.htm>).

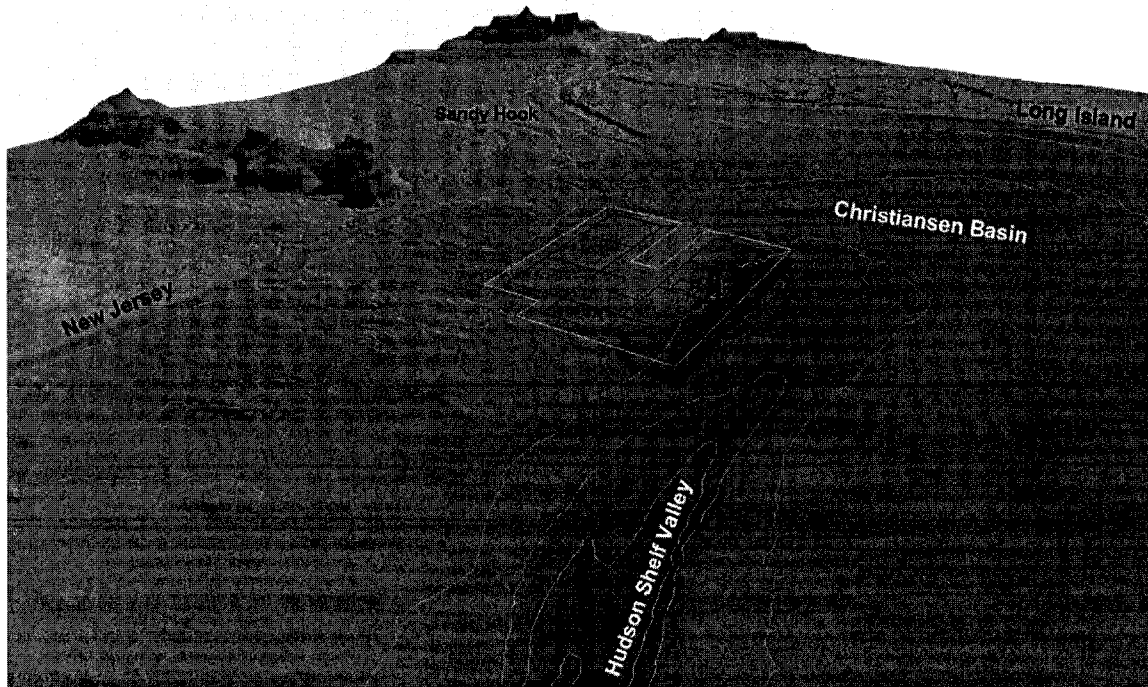


Figure 1.1 – Perspective view from southeast showing the HARS location. With a size of approximately nine by eight km the HARS is located in the Christiansen Basin, northwest of the Hudson Shelf Valley, six nautical miles east of Sandy Hook NJ. Vertical exaggeration: 20 x.

The HARS was established in 1997 through an agreement among the U.S. Environmental Protection Agency (EPA), the U.S. Department of the Army and the U.S. Department of Transportation, in an effort to reduce the elevated contamination and toxicity associated with some of the dredge materials in the area. The HARS comprises the former Mud Dump Site (MDS) and some surrounding dredged material disposal areas. It is divided into nine Priority Remediation Areas (PRAs) where remediation material is to be placed (Fig. 1.2). There is also a Buffer Zone surrounding the PRAs and a No Discharge Zone, which is an area outside the PRAs where no further disposal is permitted.



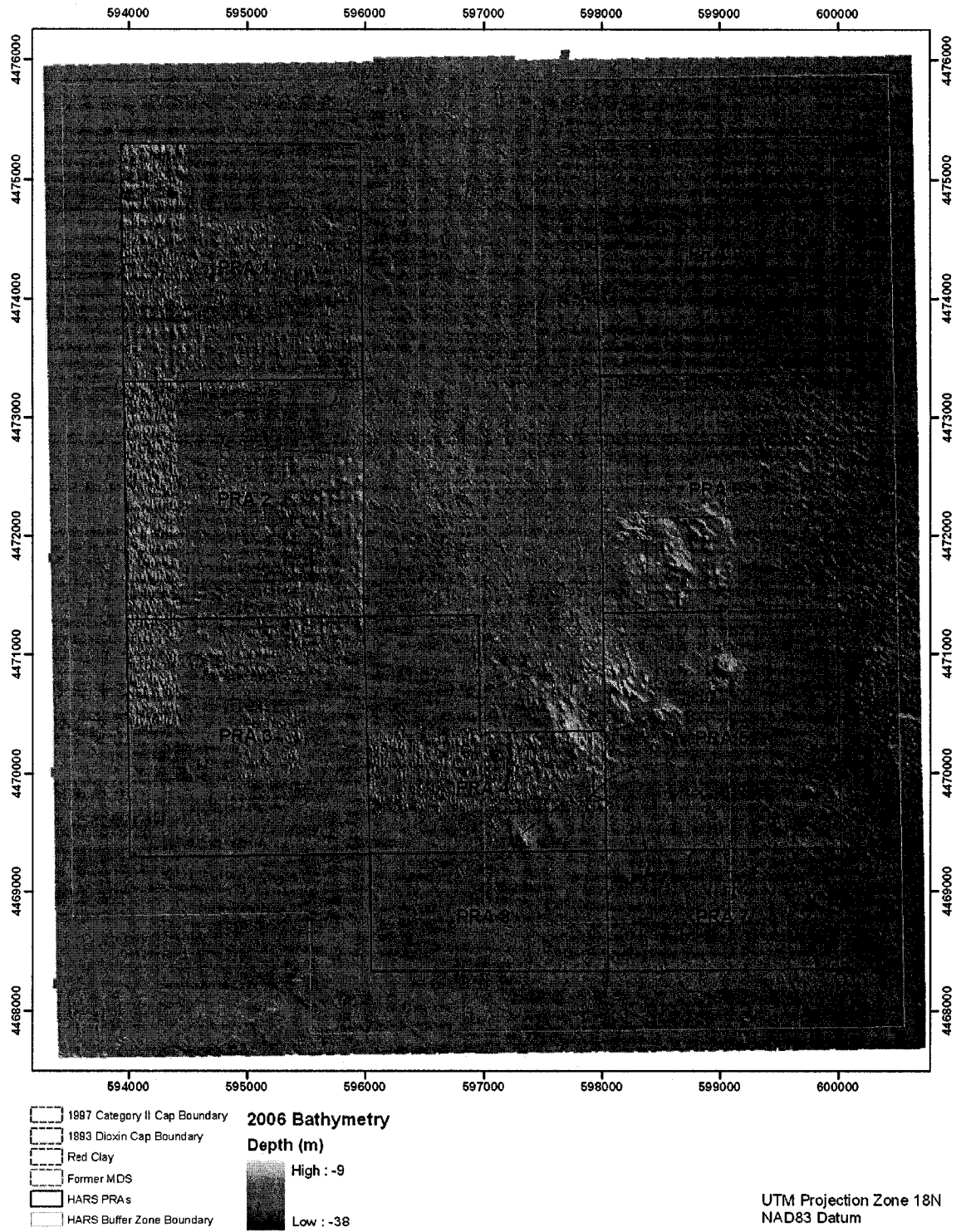


Figure 1.2 - Historic Area Remediation Site 2006 bathymetry. The HARS comprises the former Mud Dump Site (MDS) and some surrounding dredged material disposal areas; it is divided into nine Priority Remediation Areas (PRAs) where remediation material is to be placed.

When surveyed in September 2006, the central region of the HARS was dominated by an elevation produced by dumping, running approximately north-south over depths of 23 to 25 m to the west and 27 to 34 m to the east (Fig. 1.2). The topographic high in the north between PRAs 1 and 9, 15 m below sea level, is designated Castle Hill and corresponds to material dumped prior to the 1930's. In the center of the region, another elevation at a depth of 15 m is the result of material dumped between the 1930's and 1975. To the south, where the shallowest point in the area occurs, at 10 m depth, mounds almost 10 m high were produced by recent disposal of dredged material (Butman *et al.*, 1998, 2002).

North of PRA 4, there are several individual features 50 to 100 m long, about 40 m wide and 1 to 2 m high, aligned northwest-southeast. Butman *et al.* (1998) hypothesize that these features are individual dumps from barges. To the northeast, there is a clay deposition area. Throughout the region to the northwestern corner of the HARS, there are several features with the same alignment. These may correspond to historic dumps because the orientation is the same as that taken by vessels when entering the New York Harbor (Butman *et al.*, 1998; Schwab *et al.*, 2000).

Two, approximately circular, smooth regions, lie in the south of the site. They correspond to the capping of dioxin mounds with more than 1 m of clean sand (SAIC, 2005b), the 1993 Dioxin Project (to the west) and the 1997 Category II Project (to the east). Between 1997 and 1998  $1.83 \times 10^6$  m<sup>3</sup> of sand were used to cap  $0.5 \times 10^6$  m<sup>3</sup> of Category II sediments previously deposited (Butman *et al.*, 2002). Sediments classified as Category II meet ocean dumping criteria but present a potential for bioaccumulation (EPA, 1996).

PRAs 1, 2, 3 and 4 present well-preserved individual mounds that formed from the placement of remediation material that has been ongoing since 1997. From 1997 to 2000  $4.3 \times 10^6$  m<sup>3</sup> of remediation material were placed in this area. The general

morphology reflects the placement procedure, which follows sequentially the cells of a grid in order to obtain a uniform coverage of 15 to 75 cm across the area of the grid.

The deepest area, in the southeastern part of the HARS, is aligned with the head of the Hudson Shelf Valley and corresponds to a channel 300 to 400 m wide and 2 to 4 m deep. The channel is limited on the northeast by outcrops of southeastward-dipping coastal plain strata, probably of Cretaceous age (Butman *et al.*, 1998) and on the southwest, by a smooth slope. The characteristic morphology of the channel gradually disappears to northwest. All this area is relatively smooth and probably corresponds to fine sediments winnowed from the northwest and transported eastward and downslope toward the head of the Hudson Shelf Valley.

The rock outcrops (Fig. 1.2) probably extend in the subsurface to PRA 6. This is an area with several topographic highs aligned northwest-southeast, which are approximately 1 m high. To the north of this region, throughout PRA 9, there are several circular depressions 30 to 50 m in diameter, up to 0.5 m deep, with a small high in the center, with the same alignment. These may correspond to dumps of rocky material (Butman *et al.*, 1998) and/or to the disruption of the subsurface geology. The southwest corner of the HARS is characterized by long-wavelength bedforms.

The HARS contains a wide variety of sediment types, ranging from clay to gravel, in a relatively small area. This small-scale variability is particularly suited for a test of the spatial resolution of the ARA approach. Datasets acquired by Science Applications International Corporation (SAIC) in 2005 and 2006 were used for this study. Each dataset consists of a multibeam sonar survey conducted with a Reason 8101 MBES, Sediment Profiling Imaging (SPI), plan view images, and grab samples. All these data were acquired over a relatively short period of time, which minimizes the effect of temporal variability of the seafloor and, consequently, yields a better correlation between remote sensing and ground truth data.

## **1.6 Objectives**

The primary objective of this study is to determine the applicability of ARA to an area with high spatial variability such as the HARS in order to understand the capabilities and limitations of ARA. Since any acoustically inferred sediment property will need to be compared to direct measurements, an attempt was made to identify sources of uncertainty in common methods of ground truth.

Chapter 2 outlines the acoustic methods used to predict seafloor properties in terms of mean grain size. The ground truth methods used to verify ARA predictions are detailed in Chapter 3. In Chapter 4, results from grain size analysis and from acoustic remote sensing are presented, and a comparison is made between the two. A discussion of the degree of confidence in these results is also included in Chapter 4. Chapter 5 summarizes the conclusions and suggests new experiments and paths for improvement.

## CHAPTER 2

### BACKSCATTER MOSAICS AND ANGULAR RANGE ANALYSIS (ARA)

#### 2.1 Backscatter Mosaics Assembled in Geocoder

As discussed in Chapter 1, backscatter mosaics have been used to remotely classify the seafloor, usually through textural segmentation into several classes followed by ground truth to define attributes for each class. Until the mid 1990s only backscatter mosaics constructed from sidescan sonar data were available. However, the position and attitude of the sidescan sonar towfish usually is not known with precision. Also, backscatter intensities are recorded as a long time series for each side of the sidescan sonar and there is no information about the angle from where the sound is being received. This results in an ambiguity when two arrivals from different places reach the sonar at the same time. Multibeam sonars provide a time series of backscatter values for each beam in each ping, from which water depth measurements can be extracted. The knowledge of the precise position and attitude of the multibeam sonar allows the accurate determination of the position and the geometry of each beam over the seafloor. However, what is usually recorded by the sonar is not the true backscatter strength but the backscatter intensity as affected by system settings at the time of acquisition (Beaudoin *et al.*, 2002).

Geocoder (Fonseca and Calder, 2005) assembles a time series for port and starboard sides from the backscatter intensity time series of each beam, accounts for transmitting power, receiver gains and time varying gains applied by the system,

corrects for transmitting and receiving beam patterns, as well as attenuation and spherical spreading in the water column. It also accounts for the range to the transducer, seafloor slope, transmit and receive beamwidths and pulse length in order to calculate the area of ensonification. After these radiometric corrections are made, the backscatter strength is calculated per unit solid angle per unit area. A filter is also applied to remove speckle noise. Additionally, the geometric corrections account for refraction in the water column and movement and attitude of the transducer, after which each backscatter sample is mapped to a mosaic cell in a projection coordinate system. A mosaic obtained with this process shows the spatial distribution of the best estimates of backscatter strength, preserving its angular dependence, but as can be observed in Figure B.1 (Appendix B) the mosaic is difficult to interpret.

The final step in the assemblage of a backscatter mosaic is the removal of the angular dependence of the backscatter. In order to apply the proper correction and normalize backscatter intensities across the swath, detailed information about geoacoustical and physical properties of the sediment is needed because the angular dependency is a property of the seafloor type. If this information could be obtained for each ping, along the entire swath and vertically into the sediment up to the depth of acoustic penetration, it would then be possible to build a precise Angular Varying Gain (AVG) table, different for each ping, and then obtain a truly normalized backscatter mosaic. Inasmuch as it is virtually impossible to obtain detailed information about the geophysical properties of the sediment concomitantly with the acoustic survey (and if that type of information was available, the acoustic survey would not be necessary), it is common to apply a generalized AVG filter to remove the effect of the backscatter angular dependence and normalize the acoustic response across the swath. Examples of the effect of using different AVG filters in the assemblage of backscatter mosaics are

shown in Appendix B. For different AVG filters, the difference in backscatter values for the same portion of the seafloor can be greater than 10 dB in certain areas.

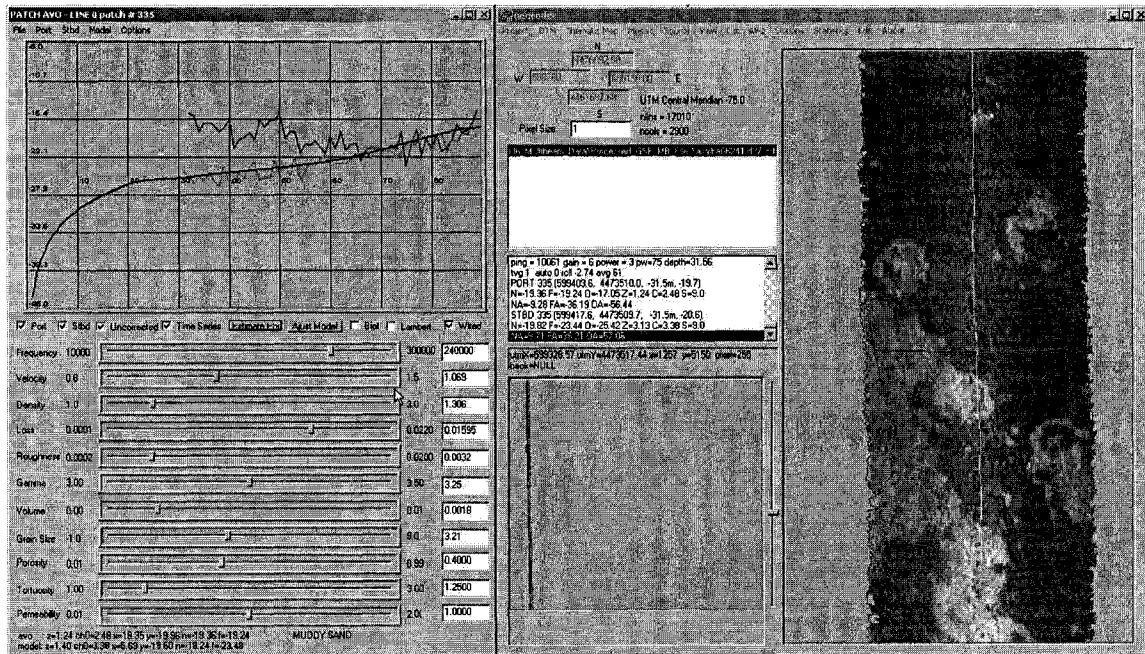


Figure 2.1 – Right: backscatter strength for a portion of the line 06241d27 with all corrections applied and without AVG to normalize the acoustic response across the swath, the red and green rectangles overlaying the backscatter mosaic correspond to the patch of the seafloor where ARA is performed. Left: average angular response for each of the rectangles depicted on the right panel, the green curve corresponds to the seafloor acoustic response on starboard, the red line to port side. The blue curve is the modeled acoustic response fitted to the observations on the starboard side, predicting a muddy sand seafloor. The angular resolution of the method does not allow correct predictions when the seafloor varies significantly within half-swath as on the port side, the angular response is a mixing between the characteristic curve of a fine sand/coarse silt in the near range and coarse sand/gravel for the outer beams.

## 2.2 Angular Range Analysis (ARA)

The backscatter angular response is an intrinsic characteristic of the seafloor and is used by the Angular Range Analysis implemented in Geocoder (Fonseca and Mayer, 2007) for its characterization. The analysis is performed for each patch of the seafloor defined by the half-swath width in the across-track direction and by a stack of consecutive pings in the along-track direction, normally between 20 and 30 (stacking

several pings is important to reduce speckle noise), and this determines the spatial resolution of the method (Fig. 2.1).

From the observed backscatter angular response, a set of ARA-parameters is extracted, containing the slope and intercept for different parts of the angular response curve, and the orthogonal distance (the distance of a point to the general trend in an intercept-slope plane). The variation of these parameters is strongly influenced by seafloor roughness, impedance and volume heterogeneities, respectively.

As described in section 1.3, two high-frequency acoustic propagation models are embedded in the software, modeling the angular response for a given frequency as a function of seafloor properties. Several combinations of seafloor properties may lead to the same angular response so the acoustic models implemented in the software are constrained by relations between seafloor properties determined by Hamilton (1972; 1974; 1976; 1978).

The prediction of seafloor properties from the observed angular response is accomplished by model inversion, iteratively adjusting the model ARA-parameters to the ARA-parameters calculated from the observations, but not in a free way. The model ARA-parameters are constrained by the parameters of the forward model that are tied by Hamilton's empirical relations.

Given accurate measurements of backscatter strength, the main obstacle for ARA is the nature of seafloor across the swath, which is assumed to be uniform. One possibility to overcome this limitation would be to segment areas in the backscatter mosaic with similar tones and textural patterns (Haralick, 1979) and then calculate average angular responses for the segmented areas. Fonseca and Calder (2007) point out that this sort of reasoning is difficult to justify since an assumption about the angular response of the sediment was already made when building the first mosaic and applying an AVG filter. In order to combine the spatial resolution of the backscatter mosaic with



the angular resolution of the ARA, Fonseca and Calder (2007) clustered ARA parameters as a feature vector in a multidimensional space using an unsupervised clustering algorithm. Each cluster is expected to represent areas on the seafloor with similar properties and similar angular responses. This technique implies an *a priori* definition of the number of sediment types present in the area.

For highly complex areas like the HARS, it is difficult to define *a priori* how many sediment types are present. One possibility would be to take sediment samples on a dense and evenly spaced grid but that would destroy the purpose of a remote sensing approach. Another option, although subjected to *a priori* assumptions about the angular response, would be to use a backscatter mosaic to define the number of classes, but in the case of the HARS, the size of the surveyed area compared with the degree of spatial heterogeneity presents a scaling problem. The area is too big to differentiate classes and all transitional classes seem to exist. So, the best that can be done is to classify areas of high and low backscatter. Figure 2.2 depicts the backscatter histogram for the entire 2006 backscatter mosaic presented in Figure 2.4.

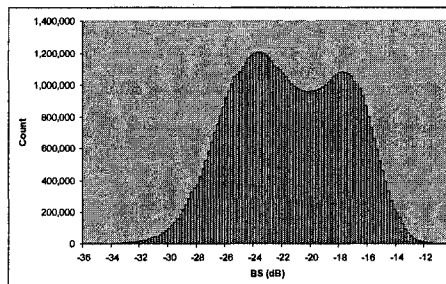


Figure 2.2 – Histogram of backscatter strength across the HARS using the average between the two more reliable values that fall within each 1 m cell, as calculated by Geocoder.

If, in a limited area, a marked contrast between different seafloor types can be observed, it may be assumed that the applied AVG did not mask that limit, but only harmonized the textural appearance of the deposits. Within each deposit, sediment heterogeneity may exist but that will not be resolved even with ground truth

measurements. Therefore, average properties for the deposit must be assumed as much on the ground truth as on the remote sensing side. For those areas where different sediment types can be clearly identified, segmenting areas on the backscatter mosaic with similar tones and textural patterns may be a valid method to determine the average angular response for each deposit.

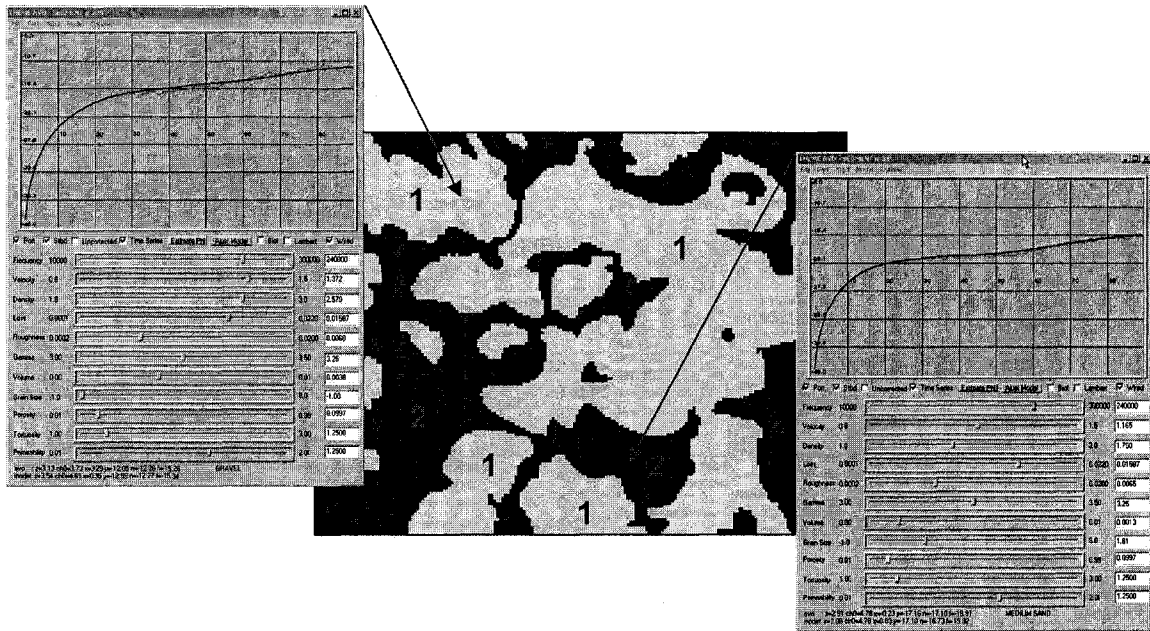


Figure 2.3 – ARA in theme mode. In this example two themes were defined based on the observation of the backscatter mosaic, each one is expected to correspond to areas of the seafloor with similar geophysical properties. For each theme the average angular response is calculated (green lines). The ARA-model is then fitted to the angular response of each theme (blue lines) and seafloor properties are predicted. In this example theme 1 corresponds to gravel and theme 2 to medium sand.

The Angular Range Analysis for a specific area of the seafloor defined by the user is implemented in Geocoder's ARA with the designation "theme mode" (Fig. 2.3). The first step in the ARA is the manual segmentation of the backscatter mosaic in areas with similar tonal and textural patterns, called "themes". Each theme is expected to correspond to portions of the seafloor with similar geoacoustic and physical properties. The second step is the calculation of the average angular response for each theme. This calculation considers all the snippets that fall within each theme, independently of the

line they belong to, and is not restricted to the half-swath width of the sonar and to a stack of pings as in the normal mode (Fig. 2.1). The final step, extraction of ARA-parameters, model inversion and prediction of seafloor properties, follows the same process as for the “normal mode”.

### **2.3 Multibeam Data Collection and Processing**

Multibeam sonar data was acquired by SAIC onboard *M/V Atlantic Surveyor* with a Reson 8101 multibeam system (240 kHz, 101 beams  $1.5^\circ \times 1.5^\circ$ ) on August 26<sup>th</sup> to 31<sup>st</sup> 2005 (SAIC, 2005b) and on August 29<sup>th</sup> to September 14<sup>th</sup> 2006. Data was processed by SAIC and archived in .gsf file format. Bathymetry post processing was done following a CARIS HIPS processing pipeline.

The backscatter time series for each beam in each ping (snippet) was imported into Geocoder directly from the processed .gsf files. Since digital numbers on the 8101 Reson system do not represent the true backscatter strength, Geocoder software corrected for radiometric and geometric distortions and positioned each acoustic sample in a projection coordinate system (Fonseca and Calder, 2005). The result is the correct angular response of the seafloor. An AVG filter (option “Trend” in Geocoder) was applied to normalize the backscattering strength across the swath and the final backscatter mosaic was produced with 1 m cell resolution (Fig. 2.4 and Fig. 2.5). Backscatter strength, as normalized by Geocoder when assembling mosaics, is the average between  $35^\circ$  and  $55^\circ$  grazing angles (Fonseca, L. personal communication, 2007). ARA was applied in its normal mode, averaging a stack of 30 pings along-track to calculate the angular response for an across-track range of half the swath width of the sonar. In this study the effective density fluid model (Williams, 2001) implemented in

Geocoder's ARA was used; model results in terms of mean grain size are presented in Chapter 4.

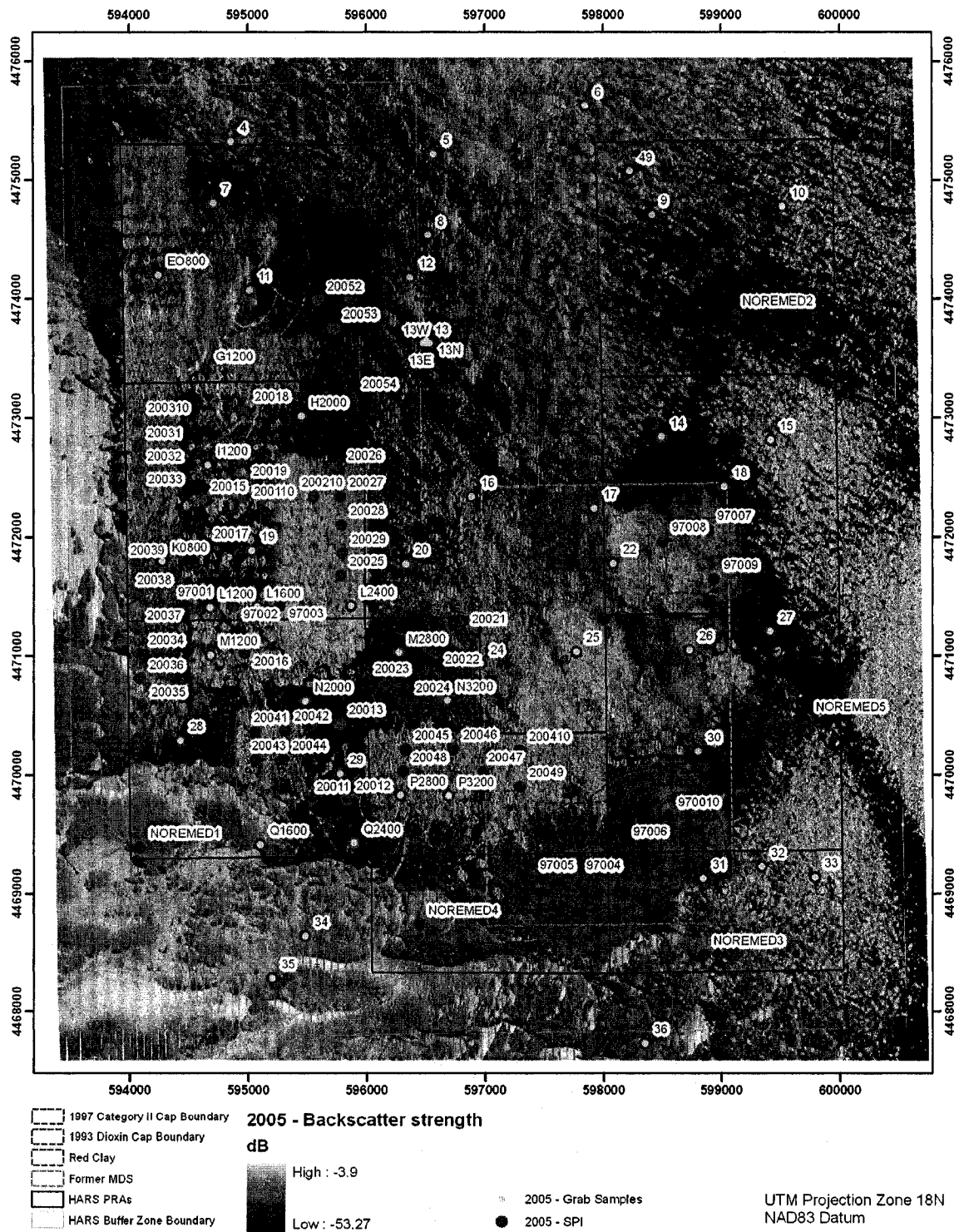


Figure 2.4 – Position of the grab samples and profile images acquired in 2005 over the backscatter mosaic assembled with Geocoder.

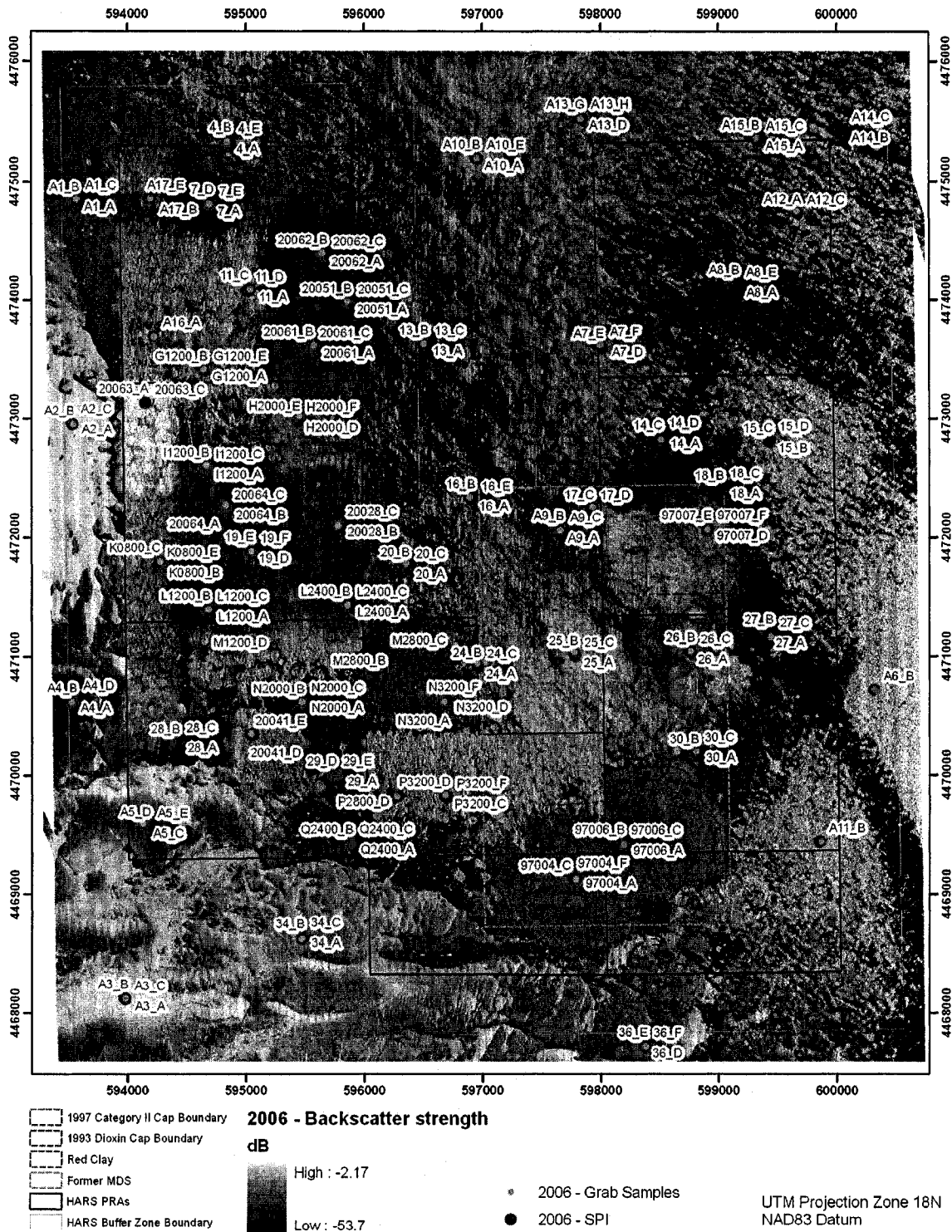


Figure 2.5 – Position of the grab samples and profile images acquired in 2006 over the backscatter mosaic assembled with Geocoder.

## CHAPTER 3

### GROUND TRUTH

To evaluate the effectiveness of ARA, model results must be compared to ground truth data. Although the empirical relations among mean grain size and sediment physical and geoaoustic properties (Hamilton, 1972; 1974; Richardson and Briggs, 2004; Jackson and Richardson, 2007), and backscattering strength, are subject to large errors (Jackson and Richardson, 2007), mean grain size and sediment type are the most common descriptors of seafloor properties.

Mean grain size is widely used as an environmental and geotechnical proxy, but values are often reported without reference to the method used for sample collection or analysis, as well as the associated uncertainty. This study tried to identify, and estimate when possible, the limitations of the methods most commonly used for sediment collection and analysis.

In addition to sediment sample data, Sediment Profile Imaging (SPI) and plan view images were collected in the HARS by SAIC to evaluate benthic recolonization status and the degree of benthic habitat disturbance at each station (SAIC, 2005a). Profile images of the undisturbed water/sediment interface and top centimeters of sediment allow comparison of the observed sediment type with grab sample results and an estimation of seafloor roughness and volume heterogeneity. The penetration of the SPI optical prism, which acts like a static load penetrometer, also provides a

geotechnical parameter that can be used for comparison with mean grain size and acoustic measurements.

### 3.1 Position Uncertainty

SPI and grab sampling positions are affected by an uncertainty. In the 2006 survey the position of each individual sample was referenced to the position of the GPS antenna. Considering the uncertainty of the differential GPS ( $\pm 3$  m), the distance from the antenna to the place where the SPI system was deployed (6.7 m) and to where the grab was deployed (3.6 m) and the maximum cable angle ( $10^\circ$  for the SPI system and  $30^\circ$  for the Petit Ponar grab sampler), total position uncertainty varies between  $\pm 15$  m to  $\pm 25$  m for the grab and from  $\pm 12$  m to  $\pm 15$  m for the SPI system, depending on the depth. Figure 3.1 shows the position uncertainty for station 16.

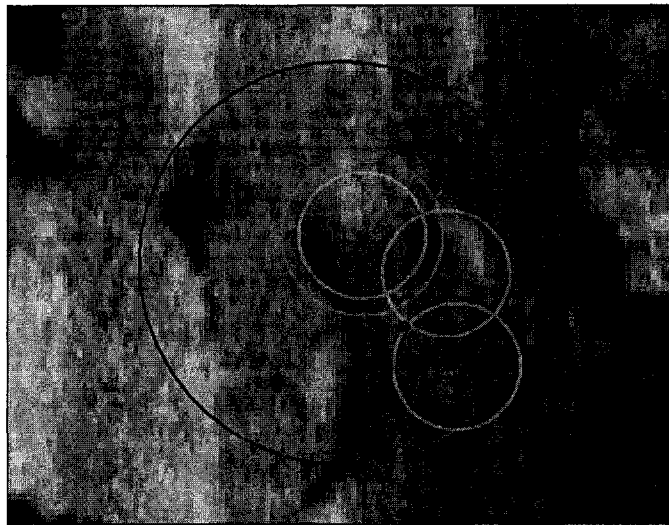


Figure 3.1 - Station 16. In 2005, data is referenced to the nominal position of the station, depicted as a blue dot. The blue circle represents the estimated uncertainty and has a radius of 40 m. In 2006 all the replicas for the nominal station are depicted as red dots, the yellow circle (12 m radius) corresponds to the estimated uncertainty for successful SPI samples and the green circle (15 m radius) corresponds to the estimated uncertainty for successful grab samples. The 2006 backscatter mosaic with 1 m cell size is used as background to show the small scale variability of the area and why there is an uncertainty about the sedimentary deposit that is being sampled.

Positions for the 2005 data followed a different approach, as all the replicas within each station were referenced to the position of the planned station (SAIC, 2005a). Therefore, the grain size and the penetration of the optical prism (SPI) can be considered as average properties within the radius of uncertainty for each station. Considering that the survey vessel was the same, maneuvered by the same people, and in similar weather conditions, one can assume the observed dispersion of replicas around each planned station in 2006 to be on the same order of magnitude of what occurred in 2005. The uncertainty associated with this practice of referring measurements to the planned station was estimated to be approximately 40 m (Fig. 3.1).

### **3.2 Grab Samples**

#### **3.2.1 Surface sediment sampling**

Surface sediments were collected on September 1<sup>st</sup> and 2<sup>nd</sup>, 2005, with a 0.1 m<sup>2</sup> Van Veen grab sampler, onboard the *R/V Beavertail*, to determine the toxicity of surface sediments. The grab was deployed one or more times (usually no more than two) around the nominal position of the stations shown in Figure 2.3. If the sediment was acceptable (bucket more than half full and without evidence of washout or disturbance), the entire content was placed in a large mixing bowl and the sampling continued until enough sediment was collected (SAIC, 2005a).

The sampling strategy for 2006 was a compromise between revisiting primary stations from 2005, in order to observe the temporal evolution of benthic recolonization at a given station, and the need to obtain data in areas that were not previously sampled (Fig. 2.4). On August 21<sup>st</sup> and 22<sup>nd</sup>, 2006, onboard *R/V Beavertail*, sediment samples were collected with a Petit Ponar grab sampler (Fig. 3.2) at the same time as SPI



images were obtained. This grab sampler allowed for the collection of surface sediments to a depth that varied between the thickness of the first layer of grains in gravelly bottoms up to approximately 10 cm in muddy sediment. The grab did not trip in some stations, even after three attempts (stations 15, 18, 27, 28, 29, 20063, A1, K0800, M2800, N2000 and Q2400). When available, sediment that was stuck to the frame was collected and labeled with the station name (samples 27\_C, A1\_C, K0800\_C and N2000\_C). At other stations, the sampler closed without any sediment (stations A8 and A14) or collected only a single pebble or cobble (samples A6\_B, A10\_B and P3200\_B).

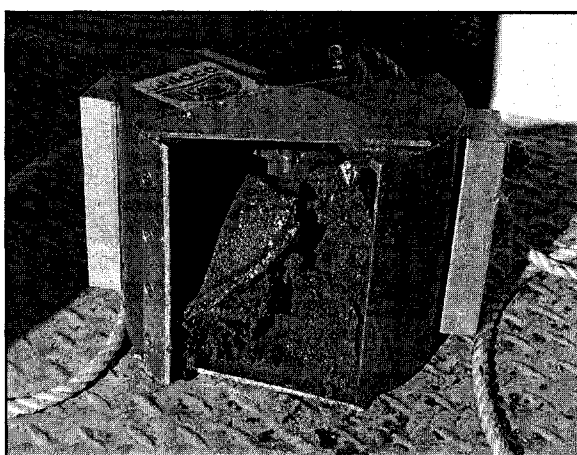


Figure 3.2 - Petit Ponar grab sampler used to collect sediment samples in 2006.

### **3.2.2 Single sample versus composite sample**

The two different approaches followed in 2005 and 2006 bring up the issue of the number of replicas needed to characterize the deposit at the sample locality. One approach considers that a given deposit has an internal spatial heterogeneity that cannot be resolved. In this case, the best sampling is a composite sample that reflects average characteristics. Krumbein and Pettijohn (1938) suggest that at least four discrete samples (replicas) should be combined into a single composite in order to reduce the ratio, of the error of the mean of a set of observations  $n$  ( $E_m$ ), over the error of a single

observation ( $E$ ) to 0.5, the point when the error starts to decrease more slowly as more samples are taken. The error of the mean of a set of observations  $n$  varies inversely with the number of observations,  $E_m = E/\sqrt{n}$ .

In the other approach, position uncertainty is considered to be good enough to attribute the sample to a homogenous patch of the seafloor. Since the position of a sample is hardly repeatable, a second replica would sample a different patch of the seafloor and describe sediment characteristics in a different place.

Collier and Brown (2005) report a minimum error in the calculation of the mean grain size from four repeated grabs at the same station with position uncertainty  $\pm 15$  m to vary from  $\pm 1.2 \Phi$  to  $\pm 0.3 \Phi$  in gravelly silt sediments of the Loch Linnhe on the west coast of Scotland. Although this example is valid only for a specific sediment type and spatial variability of the seafloor, this adds to the concern about sampling representativeness.

### **3.2.3 Grab sampler**

The type and size of the grab sampler is another contributor to the uncertainty in a grain-size measurement. For instance, the size of the grab may not be large enough to collect a representative sample of the sediment population. Larger grains may not be sampled at all, and if that is the case, frequency distributions of grain size will be open on the coarser size, or coarser grains may be sampled in a way that does not reflect the true distribution of the population. As an example, a 20 mm single pebble represents 9% in weight of a 1 kg sample and sampling one more or one less pebble may shift significantly the mean grain size.

Krumbein and Pettijohn (1938) present a table of practical sample weights, based on Wentworth's (1926) work and suggest that 125 to 500 g should be collected in order to obtain a representative sample for mechanical analysis if the coarsest size is within the sand size (0.06 to 2 mm), 1 kg for granule size (2 to 4 mm) and from 2 to 16 kg for pebble size (4 to 64 mm). Unfortunately, the efficiency of a grab is in the opposite direction, as the volume of sampled sediment decreases with larger grain sizes.

The type of grab used may allow washout of fine-grained material, as the Petit Ponar sometimes does. The grab may also produce a shock wave that can disturb the bottom and some less-dense material may be selectively undersampled, as has been noted for the Van Veen (Wigley, 1967). Biased results can be expected in both cases.

Finally, if the objective is to evaluate the validity of an acoustic measurement, one must consider that what is actually being calculated is the mean grain size for all the sediment layers that were sampled by the grab sampler and not the mean grain size for the top layer. In some situations, this is a very important issue, as the acoustic energy will not necessarily penetrate to the same extent, but will be restricted to the top layers.

#### **3.2.4 Sediment analysis (grain-size and organic content)**

In 2005, sediment grain-size analysis was done by SAIC using sieves for the sand fraction (US standard sieve sizes: 10, 20, 40, 60, 100 and 200) and a hydrometer for silt and clay fractions, but only the percentage of gravel, sand, silt and clay was reported. The moisture content of the sediment was also determined (SAIC, 2005a).

The 2006 sediment-sample analyses followed procedures based on the methods used at the UNH Coastal Geology Laboratory and at the Marine Geology Department of the Portuguese Hydrographic Institute.

Laser diffraction was selected for particle-size analysis since it is relatively fast, more precise (Sperazza *et al.*, 2004) and permits determination of finer grain sizes, and most importantly, because it allows the analysis of the entire sample with the same method. The available laser diffraction equipment was the Malvern Mastersizer 2000 with a Hydro G dispersion unit from the Portuguese Hydrographic Institute. This equipment allows particle-size measurements from 0.02 to 2000  $\mu\text{m}$  with an accuracy  $\pm 1\%$  on the  $D_{v50}$ , using the Malvern Quality Audit Standard, and an instrument-to-instrument reproducibility better than 1% Relative Standard Deviation. Even though a maximum grain size of 2000  $\mu\text{m}$  is specified, the stirrer pump of the dispersion unit only holds 1500  $\mu\text{m}$ . After several tests it was found that the 500  $\mu\text{m}$  sieve limits particles to a size that does not clog the pump, because elongated particles with dimensions larger than the square mesh will pass through the sieve. Because of this, every sample was wet sieved at 500  $\mu\text{m}$ . For the coarser samples, this meant that the samples needed to be split at the upper limit of medium sand (500  $\mu\text{m}$ ) leaving the rest of the sample to be measured with sieves.

HARS samples have a wide range of grain sizes so a pre-evaluation was made to decide whether to split the sample at 500  $\mu\text{m}$  or 62.5  $\mu\text{m}$ . Photos were taken on all collected samples using a SLR 6MP digital camera with a Micro Nikkor 105 mm f/2.8 lens at a fixed distance from the sediment surface (0.75:1 magnification). A 500  $\mu\text{m}$  mesh was put in place of the sample surface as a reference. From the photos, 75% of the samples fall below the 500  $\mu\text{m}$  size, and 80% of the samples have more than 90% of their weight within that limit (based on a visual estimation of the area). Based on that, the decision was to sieve at 500  $\mu\text{m}$  in order to have most of the samples, or at least the most significant part of them, analyzed with only one method. The same procedure was applied to all the samples for consistency. Figure 3.3 illustrates the criteria used.

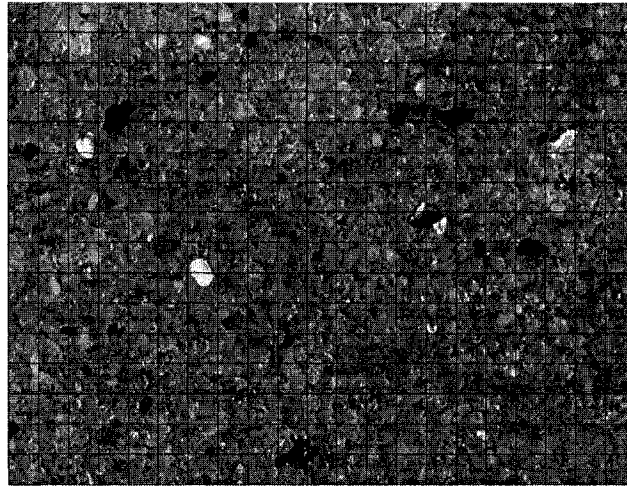


Figure 3.3 - Portion of the photograph taken to sample 20028\_A showing more than 90% of the area below 500  $\mu\text{m}$ .

In addition to laser diffraction, grain-size analysis was also performed with classical sieve and pipette methods for comparison. The weight Lost On Ignition (LOI) was also determined as a rough estimation of the percentage of organic material present in the sediments.

Each sediment sample was thoroughly mixed and two to five aliquots were removed depending on the size of the sample and visual estimation of the grain size. The remaining material was stored. The following table summarizes the analysis performed on each aliquot; the detailed procedure is described in Appendix C.

Aliquot	Procedure
1 <sup>st</sup>	Standard grain size analyses procedure, wet sieved at 500 $\mu\text{m}$ followed by sieving of the coarser fraction and laser diffraction for the finer fraction.
2 <sup>nd</sup>	Measurement of the natural occurring particle size and the effect of organic content on particle agglomeration, wet sieved at 500 $\mu\text{m}$ , finer fraction analyzed with laser diffraction following a different procedure, without particle dispersion and ultrasonication.
3 <sup>rd</sup>	Measurement of the effect of drying the sample, wet sieved at 500 $\mu\text{m}$ , finer fraction analyzed with laser diffraction following the normal procedure but without drying the sample.
4 <sup>th</sup>	Comparison with the pipettes method, wet sieved at 62.5 $\mu\text{m}$ , followed with sieving of the coarser fraction and pipette analysis of the finer fraction.
5 <sup>th</sup>	Organic content estimation by weight loss on ignition.

Table 3.1 - Analysis performed on each aliquot of 2006 sediment samples.

To compare grain-size data with acoustic data, all particles collected in the sample that act as scatterers were included, namely material of biogenic and anthropogenic origin (glass, brick pieces, etc).

### **3.2.5 Uncertainties in sediment analysis**

In standard grain-size analysis, “size” is defined as the diameter of a sphere of the same volume as the particle - true nominal diameter (Wadell, 1932). Sieves, pipettes, laser diffraction and other grain-size analysis methods involve the division of the sediment sample into a number of bins, where particle-size limits are related by a ratio of 2 (Udden, 1914; Wentworth, 1922). This scale was later modified to a logarithmic scale in phi values:  $\Phi = -\log_2 d$ , where  $d$  is the particle diameter in mm (Krumbein, 1934, 1936). Therefore, grain-size distribution is constructed from the weight or volume percentage of each fraction. In this study, an interval of 0.5  $\Phi$  was used for sieving and 1  $\Phi$  for pipettes. The resolution of the laser diffraction is higher, but was binned into 0.5  $\Phi$  groups to match the sieve interval.

Different analytical methods measure different properties that are all referred to as size. The pipette method measures the weight of the particles with a given settling velocity and relates it to particle radius by Stokes' law. Particle radius refers to the “radius of a sphere of the same specific gravity and of the same terminal uniform settling velocity as a given particle in the same sedimentation fluid” (Wadell, 1934, p. 281). Below 6 or 7  $\Phi$ , the settling velocity is affected by particle shape, degree of disaggregation, electrical charges, etc. (Folk, 1980). Temperature affects the viscosity of the fluid but it is usually well controlled.

The sieve method measures the weight of the particles retained in a sieve and relates the weight to the diameter of a sphere with the same size as the mesh. However,

elongated particles with larger volumes may pass through the sieve, so that grains are sorted according to the smallest cross sectional area that may or may not have the same volume as the reference sphere. Sieving time also influences the degree of sorting but that is a well-controlled factor. Sieve and pipette analysis can be quite time consuming and relatively imprecise with an error in excess of 40% (Sperazza et al., 2004).

Low-angle laser light-scattering systems (laser diffraction) measure the angular distribution and intensity of a laser diffracted by particles in suspension. A theoretical model based on the diffraction of particles with particular properties and grain-size distributions is then fitted to the actual measurements. Grain size is reported as volume percentage for each size bin. Sperazza et al. (2004) analyzed the size distribution of fine grained sediments (1 to 50  $\mu\text{m}$ ) and quantified method and instrument uncertainty associated with laser diffraction analysis of grain size as less than 6% ( $2\sigma$ ). The standard operating procedure of the Portuguese Hydrographic Institute is different from the one described by Sperazza et al. (2004) and is optimized for continental shelf sediments. Several factors contribute to the uncertainty in the measurement.

The amount of material required for analysis ranges from 0.1 g for clay-size samples to 1 to 2 g for sand-size samples. The way the aliquot is withdrawn from the sample material is determinant, as laser diffraction is a volume-based measurement technique, and therefore, sensitive to small changes in the amount of large material in the sample. The procedure the Portuguese Hydrographic Institute found to produce the most reproducible results is to remove the aliquot from a paste, which is easier to homogenize than a liquid or a solid. Sperazza *et al.* (2004) used three other methods: 1) drying a sample and removing an aliquot; 2) directly removing material from the original sediment sample with a spatula and; 3) extracting the aliquot with a pipette from a sample previously dispersed with sodium hexametaphosphate. Uncertainty among the different methods varied between 2.4% for  $D_{50}$  to 4% for  $D_{90}$ . The direct method caused

the highest uncertainty in the measurement, 5.9% for  $D_{50}$ , and a little more than 10% for  $D_{90}$ . Sperazza *et al.* (2004) obtained these values in clays; measurements of grain size in silts and sands will have higher uncertainty.

Wet dispersion in a solution of deionized water with sodium hexametaphosphate is commonly used to ensure particle dispersion and prevent particle agglomeration and flocculation. The dispersant has to be transparent to the laser beam and needs to have a different refractive index from the particles being measured. Dispersion increases with concentration, but beyond a certain point the solution becomes unstable causing flocculation. There is an optimum value for each type of dispersant and sediment (2 g/l is used at the UNH Coastal Geology Laboratory, 2.55 g/l is suggested by Folk (1980), 3 g/l is the value used at the Portuguese Hydrographic Institute, 4 g/l is used at the University of Rhode Island and Sperazza *et al.* (2004) suggest 5.5 g/l). The use of a dispersant may increase the formation of air bubbles during sample analysis and shift results (Duarte, J. personal communication, 2006).

Ultrasonication is used to disaggregate clay agglomerates. Sperazza *et al.* (2004) found an increase in clay dispersion up to 60 s. After 60 s, some samples showed a decrease in grain size interpreted as grain fracturing, whereas others showed an increase in grain size, interpreted as the flocculation of clays. Portuguese Hydrographic Institute standard operating procedure defines a disaggregation time of 120 s but the average grain size of the samples is different than those of Sperazza *et al.* (2004).

Another variable is the amount of material to be analyzed. For the Malvern Mastersizer 2000, an obscuration level between 15 and 20% produces consistent results (Sperazza *et al.*, 2004; Duarte, J. personal communication, 2006). The pump speed also influences results and an optimum value must be reached in order to keep the sample in suspension and minimize turbulence.



The Malvern Mastersizer 2000 system uses the Mie solution to adjust a theoretical diffraction pattern to the measurements (Singer *et al.*, 1988; Agrawal *et al.*, 1991; Loizeau *et al.*, 1994). This model requires knowledge of the refraction and absorption indices for the particles being analyzed. However, natural occurring sediments contain diverse mineralogical compositions, with each mineral having a unique set of optical properties that can affect the outcome of the laser diffraction results. In this study, a value of 1.544 for particle refraction index (quartz), 1.330 for dispersant refraction index and 1.5 for particle absorption, were used. Sperazza *et al.* (2004) report variations in the outcome that ranged from unimodal to bimodal distributions depending on the absorption index used and refraction indices varying from 1.43 to 3.22 for the minerals in the sediments analyzed.

Finally, when results for the entire sample are calculated, data from sieves (percent weight) and data from laser diffraction (percent volume) have to be joined. In this process all the grains are assumed to have the same density, which may add uncertainty to the results.

### **3.3 Sediment Profile Imaging (SPI) and Plan View Image**

Sediment Profile Imaging (SPI) was developed as a benthic monitoring tool during the 1970s and the middle 1980s (Rhoads and Cande, 1971; Rhoads and Germano, 1982, 1986) and it has been used extensively for monitoring the impacts of open-water dredged material disposal (the Disposal Area Monitoring System/USACE web site presents an extensive list of references). A camera is mounted horizontally on top of a wedge-shaped prism with a Plexiglas faceplate at the front and a mirror placed at 45° to reflect the profile image at the faceplate to the camera. A strobe mounted inside the back of the wedge provides illumination and the chamber is filled with distilled water

to provide a clear optical path. The assembly is mounted on a frame lowered to the seafloor by a winch at a rate of approximately 1 m/s (Fig. 3.4). Immediately prior to landing on the seafloor, a plan-view image is acquired. When the frame comes to rest on the seafloor, the winch wire goes slack and the camera prism descends into the sediment at a slow rate (approximately 6 cm/s) controlled by the dampening action of a hydraulic piston so as not to disturb the sediment-water interface. A trigger activates a 13 s time delay on the shutter release to allow maximum penetration before acquiring the profile image.

The optical prism penetrates the sediment under a static driving force imparted by its weight, acting like a static load penetrometer. The weight of the camera prism is adjusted according with the expected sediment type in order to maximize penetration and maintain a record of the water/sediment interface.

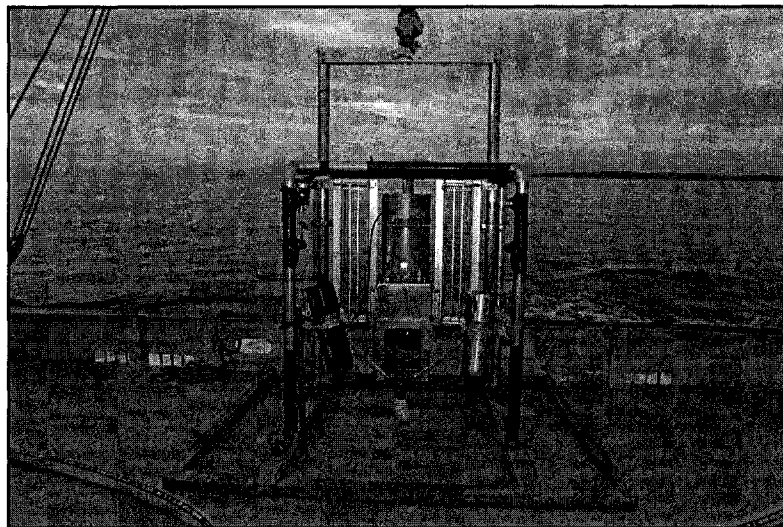


Figure 3.4 – SPI used by SAIC during 2005 and 2006 sample collection.

At least two replicate SPI casts and one plan-view image were acquired for each station. Sediment profile images were acquired on August 29<sup>th</sup>, 30<sup>th</sup> and September 2<sup>nd</sup> and 3<sup>rd</sup>, 2005. In 2006 profile images were simultaneously acquired with grab samples. Images view an area of 20 x 13 cm (HxW) and were acquired with an 8-bit 6MP digital camera at a resolution of 2240X1448 pixels. Plan-view images are sometimes difficult to interpret due to turbidity and were only sparsely used in this study to confirm the consistency of profile images and grab samples.

## CHAPTER 4

### GROUND TRUTH AND ACOUSTIC REMOTE SENSING RESULTS, COMPARISON AND DISCUSSION

#### 4.1 Mean Grain Size

The number of variables that need to be controlled in each grain-size-analysis technique is particularly large, as discussed in section 3.2.5. Therefore, it is important to compare the final results and assess the discrepancies.

##### 4.1.1 Calculation of mean grain size

Statistics using the method of moments, arithmetic, geometric and logarithmic, as well as using Folk and Ward (1957) graphical methods, were calculated for each sample using GRADISTAT software (Blott and Pye, 2001). Although moment measures are more accurate and more sensitive to environmental processes than are graphical measures (Friedman and Sanders, 1978), moment measures employ the entire sample population and are more affected by outliers in the tails of the distribution than the other measures. Therefore, moment measures should not be used unless the size distribution is fully known (McManus, 1988). Folk and Ward (1957) graphic measures appear to provide the most robust basis for routine comparisons of compositionally variable sediments (Jackson and Richardson, 2007) and are used in this study.

The difference in this dataset, between the mean grain size determined logarithmically by the method of moments compared to that by the Folk and Ward (1957) graphical method is on average  $0.15 \Phi \pm 0.16 \Phi (1\sigma)$ . The sample that presents the highest difference (A11\_C;  $0.88 \Phi$ ) has the grain size distribution open on the coarsest fraction, which means that the grab sampler did not capture the full range of grain sizes.

A plot of grain size distribution by weight for all samples collected in 2006 is shown in Figure 4.1. Samples were analyzed with the standard operating procedure (SOP), using sieves up to  $1 \Phi$  and laser diffraction for finer sizes. Samples range from clay to gravel with the majority of the material in the medium and fine sand size classes.

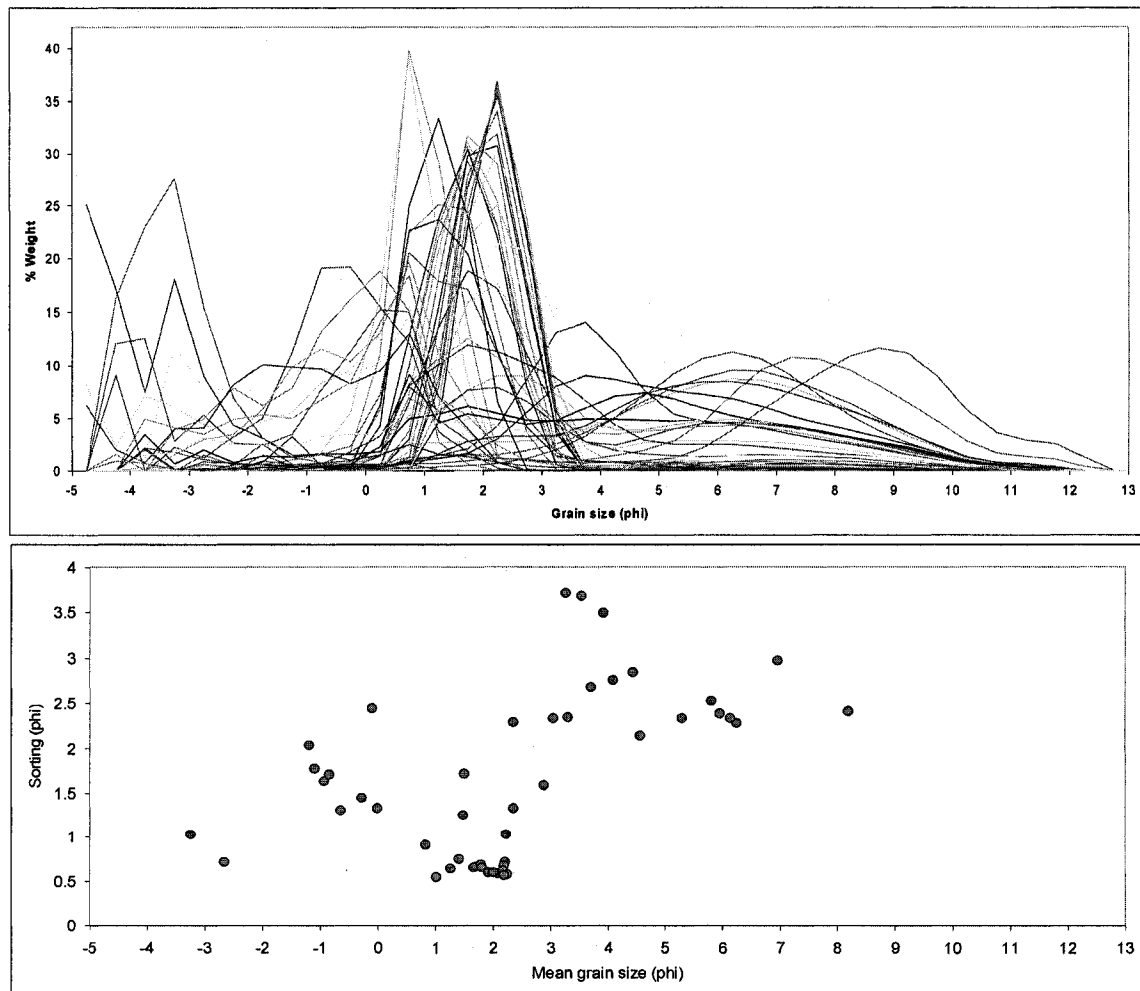


Figure 4.1 - HARS sediment samples collected in 2006: frequency distribution by weight of grain size in  $\Phi$  units (top) and sorting versus mean grain size in  $\Phi$  units (bottom).

There was no grain-size distribution for samples collected in 2005 and the only data available was in percentage of major fractions (gravel, sand and mud), as is the case for many databases constructed for benthic-habitat mapping studies. Data from 2006 shows a good correlation between percentages of gravel plus sand and the mean grain size (Fig. 4.2), at least up to the point where no mud is present in the sediment and mean grain size continues to increase. The same relation is likely present in samples collected in 2005.

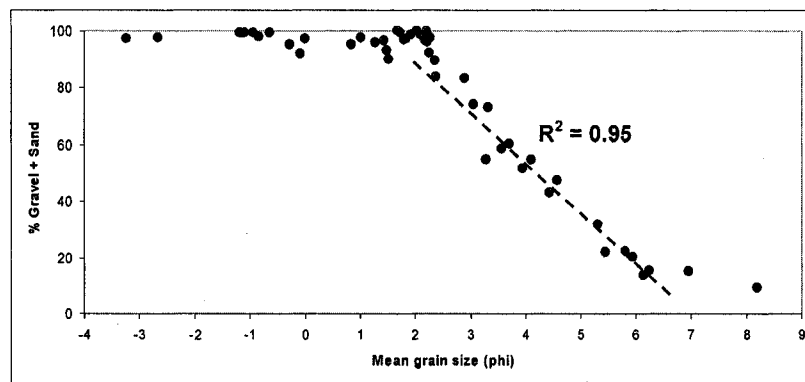


Figure 4.2 - Mean grain size versus percentage of gravel plus sand for sediment samples collected in 2006. There is a good correlation between the percentage of gravel plus sand and the mean grain size up to the point where no mud is present in the sample and the grain size continues to increase.  $R^2 = 0.95$  for samples with a percentage of gravel plus sand from 10% to 90%.

#### 4.1.2 Error introduced by drying the sample

During the normal SOP, samples were dried and concerns arose regarding possible agglomeration of clay particles. A comparison was made using only the portion of the sample that was analyzed with laser diffraction. In the standard procedure, the material left in the pan of the sieves stack was added to the fraction that was going to be analyzed with laser diffraction. It may be assumed that the material left in the pan would be evenly distributed through a wide range of finer sizes. However, to minimize errors, only those samples with material left in the pan that constituted less than 1% by weight

of the fraction finer than  $1 \Phi$  were considered. Figure 4.3 shows the effect of drying on the mean grain size. As expected, drying the sample slightly increases the mean grain size (lower  $\Phi$  values) in finer sediments, with a difference of  $0.2 \Phi$  for sample 17\_A ( $M_z = 6.3 \Phi$ ) and  $0.4 \Phi$  for sample 97007\_C ( $M_z = 7.5 \Phi$ ).

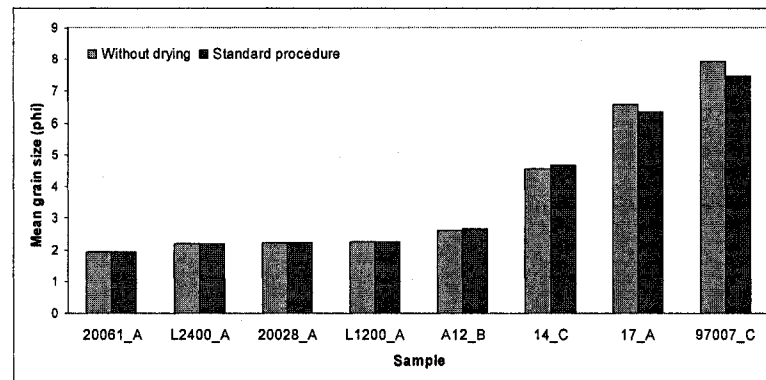


Figure 4.3 - Mean grain size for samples that were always kept wet (blue bars) and for those that followed the SOP (red bars). For finer sizes, drying the sample increases the mean grain size (lower  $\Phi$  value).

#### 4.1.3 Error in the estimation of the mean particle size

In order to estimate the effect of particle desegregation caused by the SOP, an attempt was made to characterize the naturally occurring particle size using minimal processing of a subset of samples. Twenty three samples, ranging from sand to clay, were not digested with hydrogen peroxide, thus preserving organic content, and not washed and centrifuged to remove salts. Nevertheless, samples had to be wet sieved at  $500 \mu\text{m}$  in order to prevent clogging the pump of the laser diffraction system, and since deionized water was used, salts were partially washed, therefore promoting some grain dispersion. Sodium hexametaphosphate was not used to disperse the samples and ultrasound was not applied in the laser diffraction system. Twenty measurements were made at 20 s interval. Figure 4.4 shows the evolution of the grain-size distribution by

volume for samples 14\_C, 17\_A and 97007\_C caused by mechanical stirring. The agglomeration effect is more pronounced for smaller grain sizes with the extreme shown in sample 97007\_C as a clear bimodal distribution.

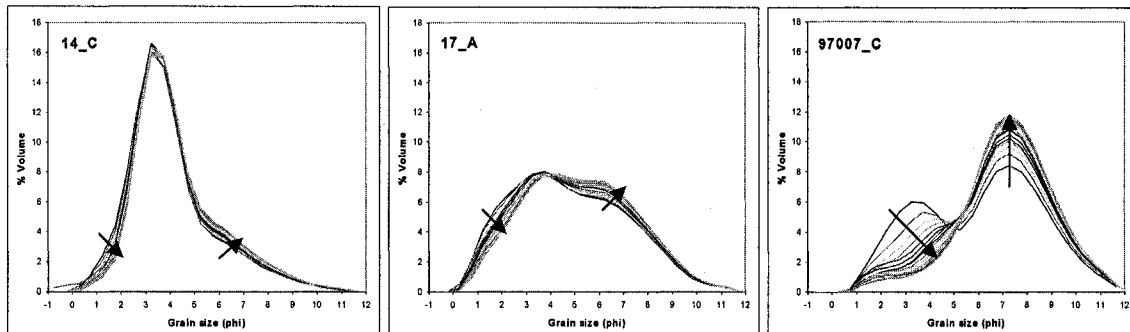


Figure 4.4 - Frequency distribution by volume of grain size in  $\Phi$  units for samples 14\_C, 17\_A and 97007\_C (from left to right). Each line corresponds to the distribution measured with 20 s interval. As time progressed the distribution moved to smaller sizes. Arrows point the evolution of the grain size with time.

Figure 4.5 compares the mean grain size calculated using the standard procedure with the mean grain size obtained using the first measurement of those samples that went to the laser diffraction without any treatment. Again, in order to minimize errors only those samples with material left in the pan that constituted less than 1% by weight of the fraction finer than 1  $\Phi$  were considered.

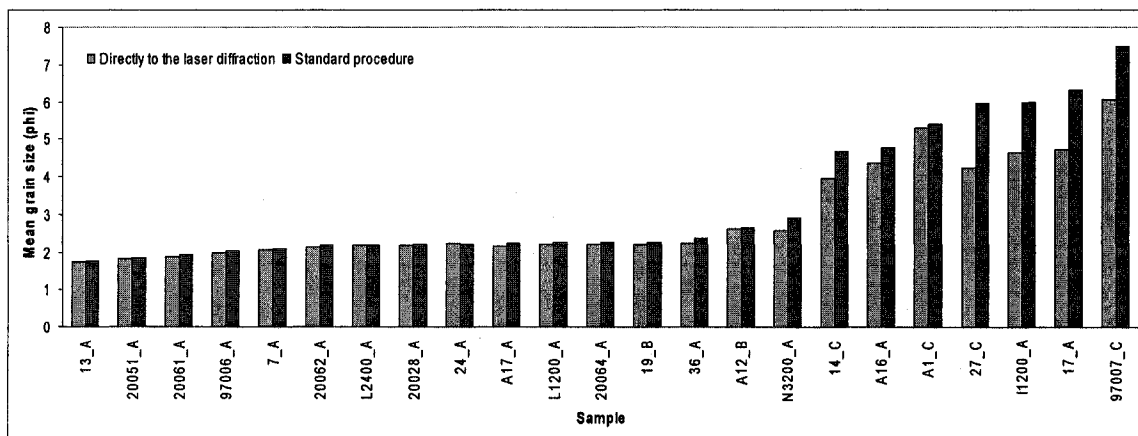


Figure 4.5 - Mean grain size for samples that followed the SOP (red bars) and for those analyzed by laser diffraction without any treatment (blue bars). The difference in mean grain size increases as samples become finer (higher  $\Phi$  value).



Samples that represent the sediment closer to its natural occurrence have a larger mean grain size (lower  $\Phi$  value) and this difference is accentuated in finer sediments. Particle agglomeration is also directly related to the organic content of the sample (Fig. 4.6).

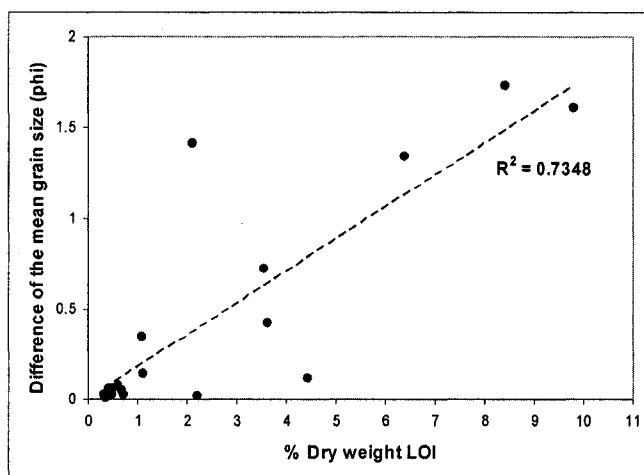


Figure 4.6 - Difference between the mean grain size in  $\Phi$  units of the samples that followed the SOP and those analyzed by laser diffraction without any treatment versus the organic content (percentage in weight of material lost on ignition). The mean particle size in the natural sediment is higher than the mean grain size determined by normal grain size analysis, and this difference is directly related with the organic content of the sample, with a coefficient of determination  $R^2 = 0.73$ .

#### **4.1.4 Comparison between the SOP (sieve-laser diffraction) and the sieve-pipette method**

A subset of samples was also analyzed with the conventional sieve-pipette method in order to compare results from a method that measures distributions by weight with one that measures distributions by volume.

Figure 4.7 shows mean grain size and sorting obtained with sieve-laser diffraction and sieve-pipette methods. Sieve-pipette consistently biases the mean grain size towards the finer fractions and results in poorer sorting of the finer samples. This may be due to the lack of resolution of the pipette method where the concentration of

grains smaller than  $10 \Phi$  is divided by bins  $11 \Phi$  to  $14 \Phi$ . Another explanation lies in the way grain size is measured; sizes between  $1 \Phi$  and  $4 \Phi$  were measured with sieves in the sieve-pipette method and sieves tend to retain coarser grains than those measured for the same class in laser diffraction.

The difference in mean grain size between sieve-pipette and sieve-laser diffraction is on average  $0.35 \Phi \pm 0.14 \Phi$  ( $1\sigma$ ). In sample 17\_A, this difference reaches  $2 \Phi$  but the pipette method is more prone to human error so this measurement was considered as a blunder.

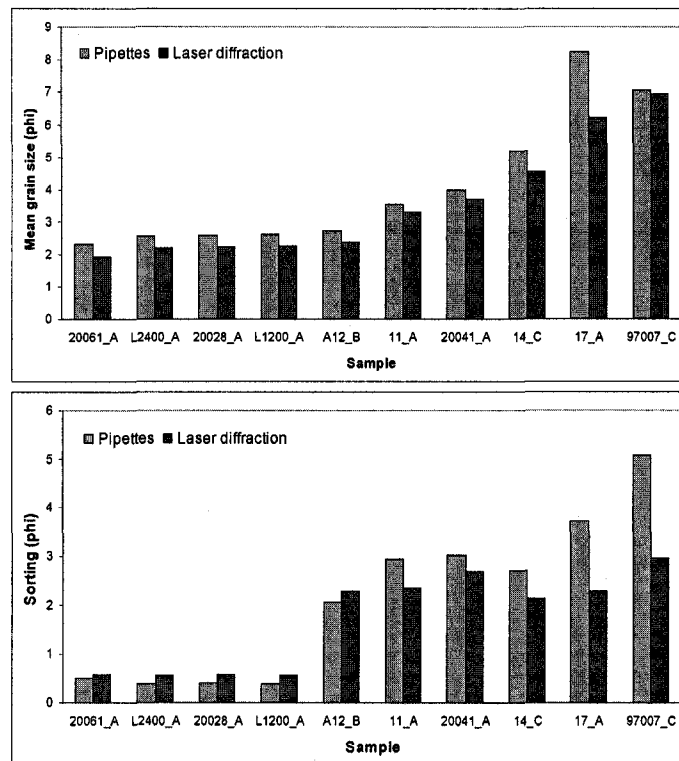


Figure 4.7 - Mean grain size (top) and sorting (bottom) in  $\Phi$  units for samples analyzed with sieve-laser diffraction (red bars) and sieve-pipette methods (blue bars). The sieve-pipette method systematically results in a smaller mean grain size.

#### **4.1.5 Estimated uncertainties in the determination of mean grain size**

Instrumental uncertainties were evaluated only for the automated method of laser diffraction. For a population of 50 samples with three replicate measurements per sample, the overall uncertainty in the measurement is  $0.024 \Phi \pm 0.026 \Phi$  ( $1\sigma$ ). The maximum uncertainty found in the determination of mean grain size for a single sample, with three replicate measurements, is  $0.082 \Phi \pm 0.054 \Phi$  ( $1\sigma$ ).

Uncertainties in mean grain size due to the effect of drying the sample in the SOP increase as the grain size decreases (higher  $\Phi$ ). For medium or fine sands, the effect of drying the sample is almost negligible whereas for silt and clay sizes the difference can reach  $0.2 \Phi$  and  $0.4 \Phi$ , respectively.

Differences between sieve-laser diffraction (SOP) and sieve-pipette methods are on average  $0.35 \Phi \pm 0.14 \Phi$  ( $1\sigma$ ) towards smaller grain sizes (higher  $\Phi$ ) for sieves-pipettes.

The highest degree of uncertainty seems to arise from the basic premise of grain-size analysis. From a sedimentological perspective, the objective is to obtain the grain size of the clastic particles as they were deposited (Folk, 1980) in order to get information about the parental source, transport and depositional processes. Decomposing the sample to its elementary particles accomplishes this objective and sets a standard for data comparison. But this process may not adequately characterize the mean grain size as a descriptor for geoacoustic properties.

In spite of not being representative of the natural sediment, samples that received minimal preparation for analysis compared to those analyzed with the SOP, show a difference in the mean grain size of  $0.2 \Phi$  or less for medium and fine sands, approximately  $0.3 \Phi$  for very fine sands,  $0.5 \Phi$  for coarse and medium silts, and approximately  $1.5 \Phi$  for fine silts to clays. The natural sediments are expected to show

higher differences because it was not possible to analyze the samples without disturbing the sediment.

Figure 4.8 summarizes results for samples 20061\_A (medium sand), A12\_B (fine sand), 14\_C (very coarse silt) and 17\_A (medium silt).

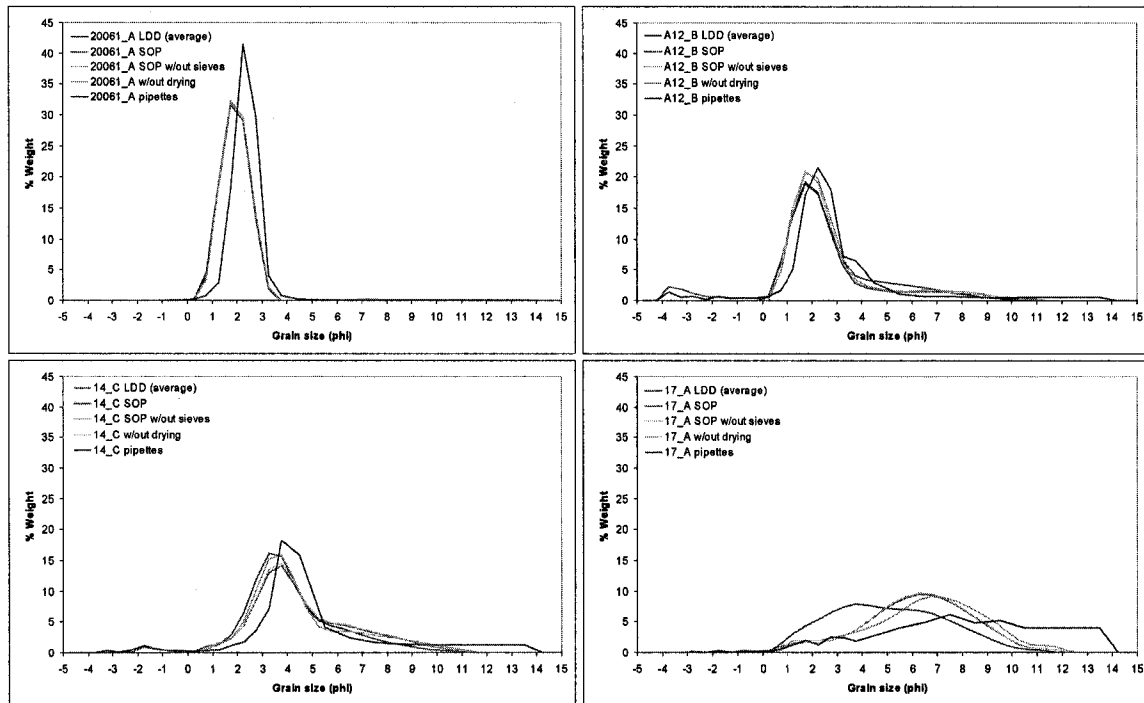


Figure 4.8 - Grain size versus percentage of weight for samples 20061\_A, A12\_B, 14\_C and 17\_A. The distribution of grain sizes obtained with the SOP (sieve-laser diffraction split at 1  $\Phi$ ) is shown for comparison with the sieve-pipette method (split at 4  $\Phi$ ). Results considering only the portion analyzed with laser diffraction are shown for comparison with the effect of not drying the sample and of sending the sample directly to the laser diffraction without going through the standard preparation (average of 20 measurements).

#### 4.1.6 Mean grain size versus penetration of the optical prism

In order to estimate if mean grain size can be used as a proxy for geotechnical properties of the seafloor, the penetration of the optical prism is compared with the mean grain size. Figure 4.9 relates the penetration of the optical prism with the percentage of gravel plus sand for data collected in 2005 and 2006. Although the penetration increases for finer sediments, there is no apparent correlation with the force exerted over the prism

(number of weights). Calculated penetration is the average of all the replicas in each nominal station for 2005 data (SAIC, 2005a). For data collected in 2006, only those stations where the SPI image and the grab sample were obtained in the same replica were considered.

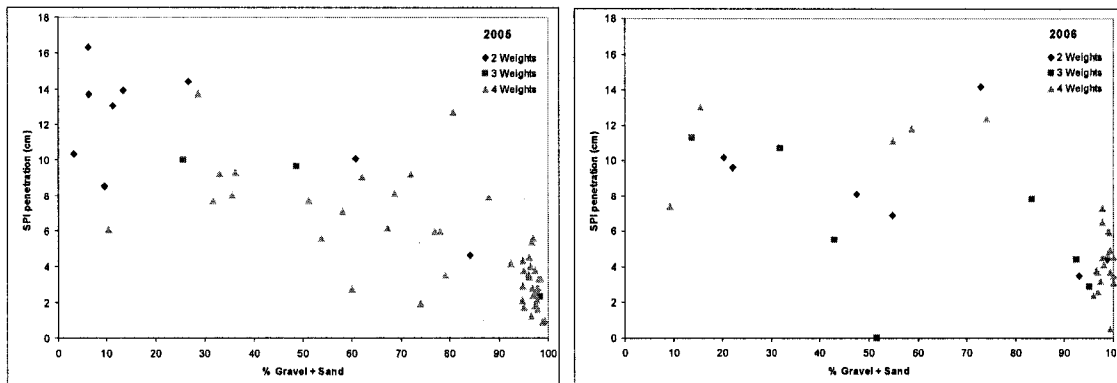


Figure 4.9 - Penetration of the optical prism versus percentage of gravel plus sand for each year. The weights in the camera were adjusted in order to obtain more penetration in harder bottoms. Although an apparent correlation can be observed for data collected in 2005 there is no differentiation by number of weights. Also, for data collected in 2005, the penetration of the optical prism is the average for all profile images within the same station and the percentage of gravel plus sand is calculated as the average of all the samples collected within the same station. For data collected in 2006 the same correlation is not observed, in this plot the penetration of the optical prism versus the percentage of gravel plus sand was calculated for each replica within the station.

If mean grain size is plotted against the penetration of the optical prism, instead of the percentage of gravel and sand (Fig. 4.10), a correlation is seen between the two, thus explaining why mean grain size is sometimes used as a proxy for geotechnical properties of the seafloor.

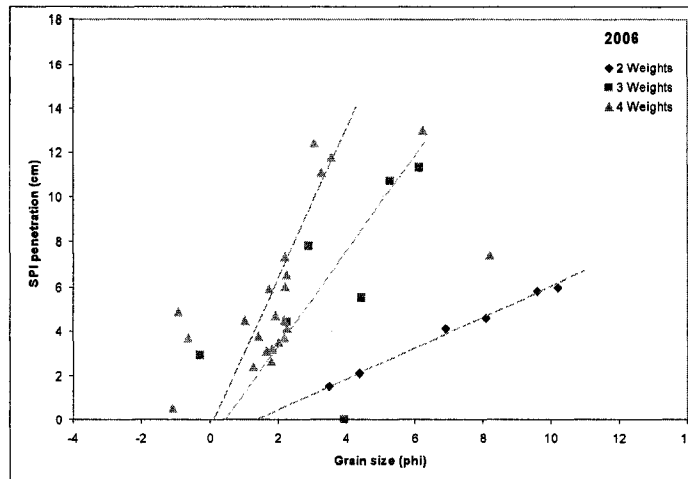


Figure 4.10 – Penetration of the optical prism versus mean grain size for samples collected in 2006. Lines reflect the general trend for each number of weights.

## 4.2 Backscatter Strength

### 4.2.1 Backscatter strength versus mean grain size

The observed relationship between percentage of gravel plus sand and mean backscatter strength, calculated within the uncertainty area of each sediment sample, is depicted in Figure 4.11. A general trend is observed with backscatter strength increasing with the percentage of gravel plus sand in 2005 but the same trend is not observed for data collected in 2006. Sediment samples collected in 2005 are composite samples whereas each sample collected in 2006 corresponds to a single deployment of the grab sampler. The average backscatter strength is also calculated over different areas, the size of the uncertainty area of the sediment samples collected in 2005 is on average 4 times the size of the uncertainty area of the sediment samples collected in 2006.

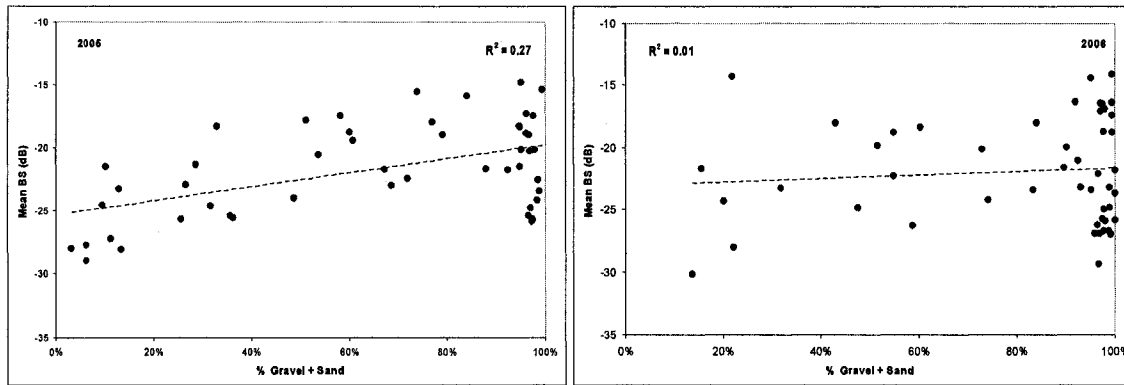


Figure 4.11 - Percentage of gravel plus sand versus mean backscatter strength calculated within the uncertainty area of each sample for 2005 (left) and 2006 (right).

The relation for data collected in 2006 seems to improve when mean grain size rather than percentage of gravel plus sand is considered (Fig. 4.12, left), but though a general trend can be observed, the correlation is weak ( $R^2 = 0.14$ ). Several factors may contribute to the lack of a strong correlation: 1) uncertainty in sample position; 2) measurement of a grain size that does not correspond to the size of the particles in the natural sediment and; 3) inability of the grain size to represent the acoustic response size of the seafloor. As will be discussed below, an attempt was made to consider all these factors with the results presented in Figure 4.12 right, showing an improvement in the correlation with backscatter strength, with a coefficient of determination  $R^2 = 0.74$ .

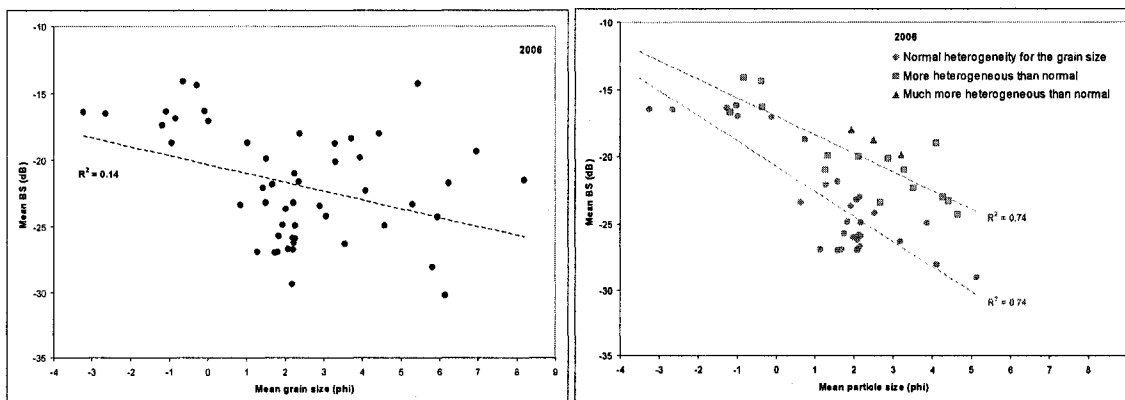


Figure 4.12 - Relation between mean grain size and mean backscatter strength (left) and between inferred mean particle size and mean backscatter strength for the deposit the sample was attributed (right). The correlation with backscatter strength improves with supervised positioning of the sample and estimation of the mean particle size. There is some differentiation by degree of sediment heterogeneity.

First, the uncertainty in sample position was considered. As an example, within the area of uncertainty of sample 26\_B (Fig. 4.13), two distinct backscatter areas can be observed. In this case, based on the analysis of the entire deposit and on the comparison with other similar sediment samples obtained in contiguous areas of high backscatter, and with samples corresponding to finer sediments obtained in contiguous areas of low backscatter, the sample was attributed to the area of high backscattering strength. The average backscatter was recalculated considering only the area of high backscatter strength. In station 4, replica 4\_A, the analysis of the backscatter revealed only one type of sediment within the uncertainty area of the sediment sample. The area that corresponds to replica P2800\_B presents some heterogeneity but it wasn't possible to clearly identify different sedimentary deposits, so the average backscatter within the whole area of uncertainty of the grab sample was considered.

Next, two samples that presented significant differences from the SPI image were removed (97007\_C and K0800\_C). The removed samples correspond only to red clay whereas the SPI images show mostly sand. Although several cases exist where there are differences between the sediment sample and what is observed in the SPI, these cases represent the extreme situation where only one component of the surface sediment was sampled.

The next step was taken to correct for the difference between measured mean grain size and the actual mean particle size, using the relation shown in Figure 4.5 and Figure 4.6 and assuming that the organic content is directly related with the degree of agglomeration of finer particles. The mean grain size was corrected assuming the relation between the mean particle size and the percentage of weight lost on ignition: mean particle size = mean grain size + (% dry weight LOI x 0.2). This relation mainly affects particles in the silt and clay range.



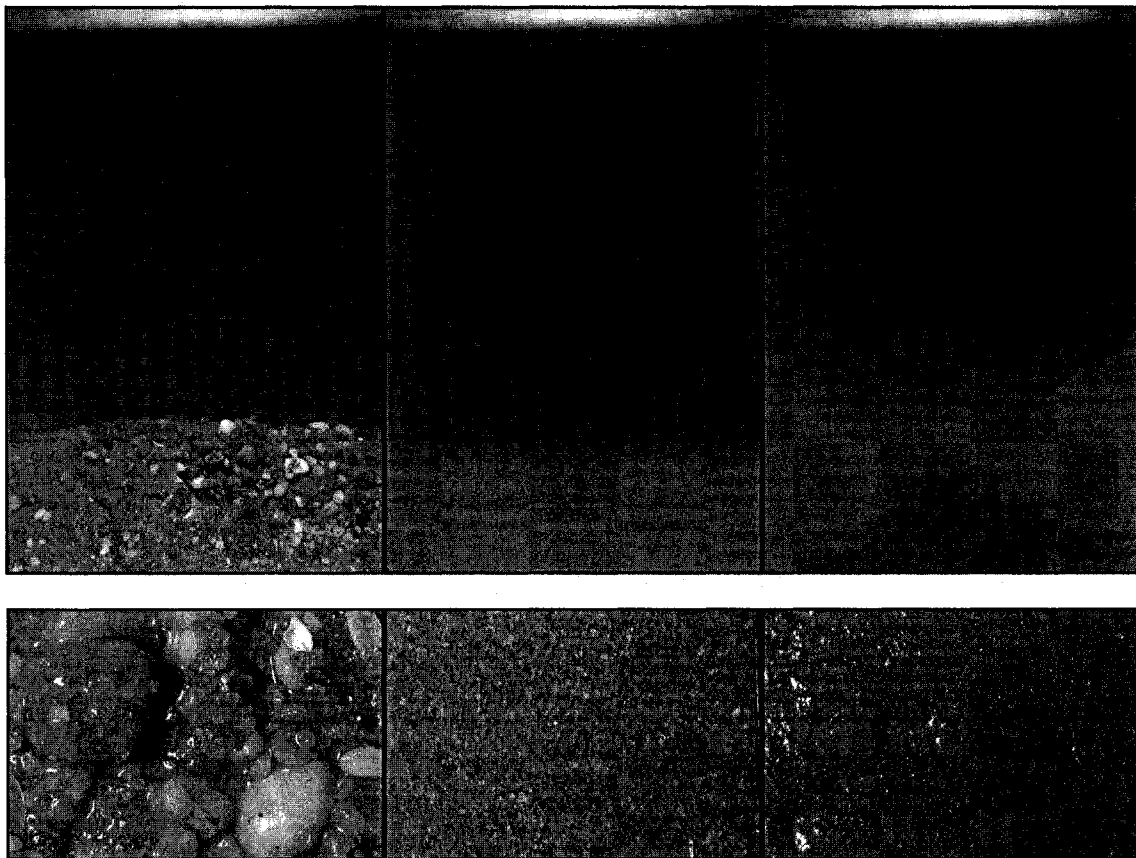
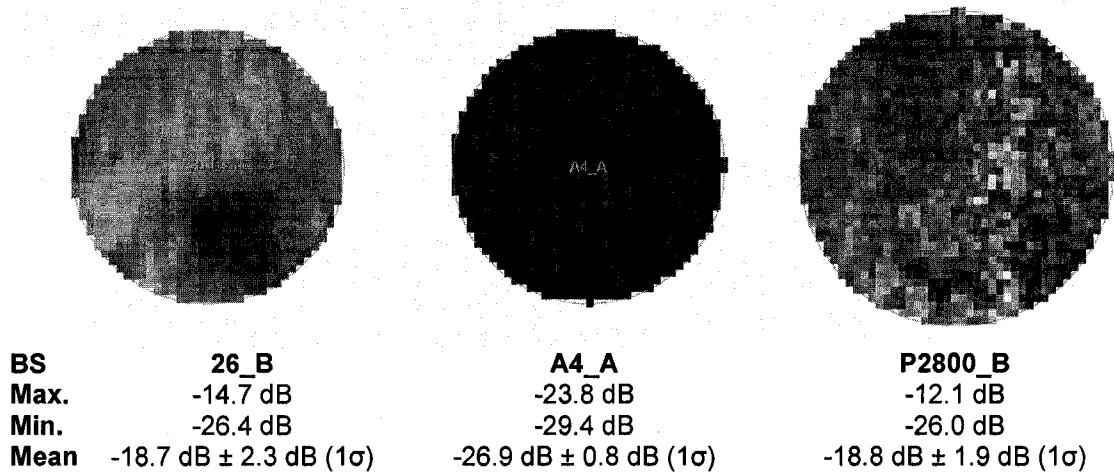


Figure 4.13 - From top to bottom: backscatter strength in the uncertainty area of the grab sample, SPI images and photographs of the grab sample for stations 26\_B, A4\_A and P2800\_B. Each pixel in the the backscatter mosaic corresponds to 1m. SPI images correspond to 20 x 13 cm (HxW) and grab sample photos to 2.2 x 3.3 cm (HxW).

Finally, two of the factors that contribute to the scattering of the acoustic wave were also considered; surface roughness and volume heterogeneity. In the HARS, the

two main sources of heterogeneity are biological reworking and dumping of varied material, both of which equally affect scattering on the surface and volume scattering in the first few centimeters of sediment. Based on SPI images, the seafloor was classified as: 1) having normal heterogeneity for the sediment type; 2) as being more heterogeneous than expected or; 3) as having much more heterogeneity than expected. All the SPI image replicas for the same station that presented the same type of sediment as the grab sample were used in the decision process due to the “point sample” nature of the SPI compared with the spatial variability of the area. Figure 4.13 illustrates the criteria; stations 26 and A4 have normal roughness and volume heterogeneity and P2800 much more roughness and volume heterogeneity than expected for the type of sediment.

Obviously, the criteria used are subjective, but illustrate the factors that may contribute to the lack of correlation between mean grain size and backscatter strength, which is sometimes observed in areas with high spatial heterogeneity.

#### **4.2.2 Comparison of backscatter strength for the same type of sediment**

One way of evaluating the consistency of results is to compare backscatter strength for the same type of sediment. This comparison was made only for data collected in 2006 because detailed granulometric distributions are not available for sediment samples collected in 2005.

Samples 20028\_A, 20064\_A, L1200\_A and L2400\_A collected in 2006, are from different locations but consist of the same sediment facies; a moderately well sorted fine sand, symmetrical and mesokurtic (Fig. 4.14 and Fig. 4.15). Backscatter values calculated as the average within the area of uncertainty of each sample are:  $-26.7 \text{ dB} \pm 1.7 \text{ dB} (1\sigma)$ ,  $-24.9 \text{ dB} \pm 1.0 \text{ dB} (1\sigma)$ ,  $-25.9 \text{ dB} \pm 1.4 \text{ dB} (1\sigma)$  and  $-25.8 \text{ dB} \pm 1.0 \text{ dB} (1\sigma)$ ,

respectively. All the mean values fall within  $\pm 1$  dB, which reflects the effectiveness of Geocoder in applying the necessary corrections. A standard deviation between 1.0 and 1.7 dB for the backscatter strength in a circular area on average 40 m diameter, suggests even better results if a point sample could be considered.

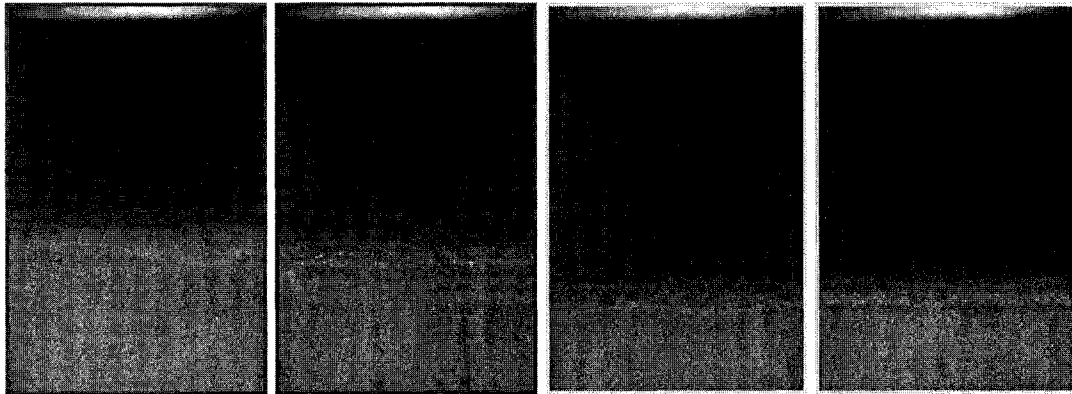


Figure 4.14 - SPI images from samples 20028\_A, 20064\_A, L1200\_A and L2400\_A (left to right) obtained with a load of 4 weights. Photos correspond to 20 x 13 cm (HxW).

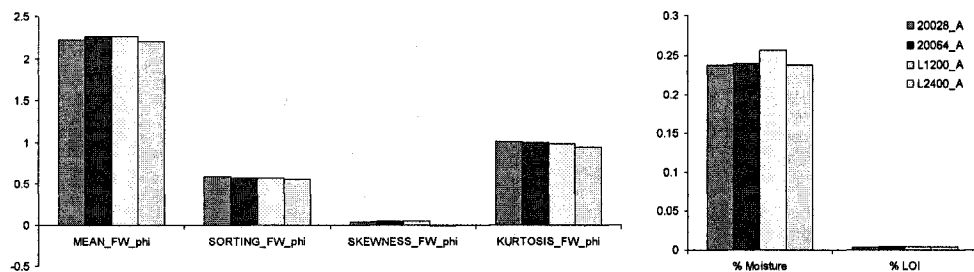


Figure 4.15 - Mean, sorting, skewness and kurtosis determined by the Folk and Ward (1957) graphical method, in  $\Phi$  units, for samples 20028\_A, 20064\_A, L1200\_A and L2400\_A (left). Percentage in weight of moisture and percentage of material LOI relative to the dry weight for the same samples (right).

#### 4.2.3 Differences in backscatter strength between 2005 and 2006 and temporal evolution of the seafloor

Multibeam sonar data was acquired at the same frequency (240 kHz) and with the same system (Reason 8101) in 2005 and 2006, so it is possible to calculate changes

in backscatter strength from year to year and estimate the consistency of results. Mosaics were assembled following the same procedure described in Chapter 3. The average difference in backscatter strength between the two years is  $-1.0 \text{ dB} \pm 2.8 \text{ dB}$  ( $1\sigma$ ), this bias was corrected by leveling the average difference in backscatter strength to 0 dB. Figure 4.16 depicts the difference in backscatter strength between 2006 and 2005.

Variations in backscatter strength seem to be collocated with variations in bathymetry (Fig. 4.17 and Fig. 4.18), corresponding to the deposition of new capping material in PRAs 1 and 2. Considering the relation between mean grain size and backscatter strength determined in section 4.2.2 it is possible to infer changes in sediment type relatively to the previous year. Recently deposited coarser material (positive difference in backscatter) in PRAs 1 and 2, seems to concentrate more than recently deposited finer material (negative difference in backscatter) that has spread over a larger area. Some scour depressions in PRA 1 and 3, which are probably caused by anchoring (Fig. 4.16), seem to be filled with new material. There seems to be a generalized transport of coarser material to the southeast across the HARS as evidenced by the distribution of positive values on both sides of the mounds in the center of the area. There is some noise concentrated around the sonar nadir, but that does not affect the observation of major variations in backscatter strength.

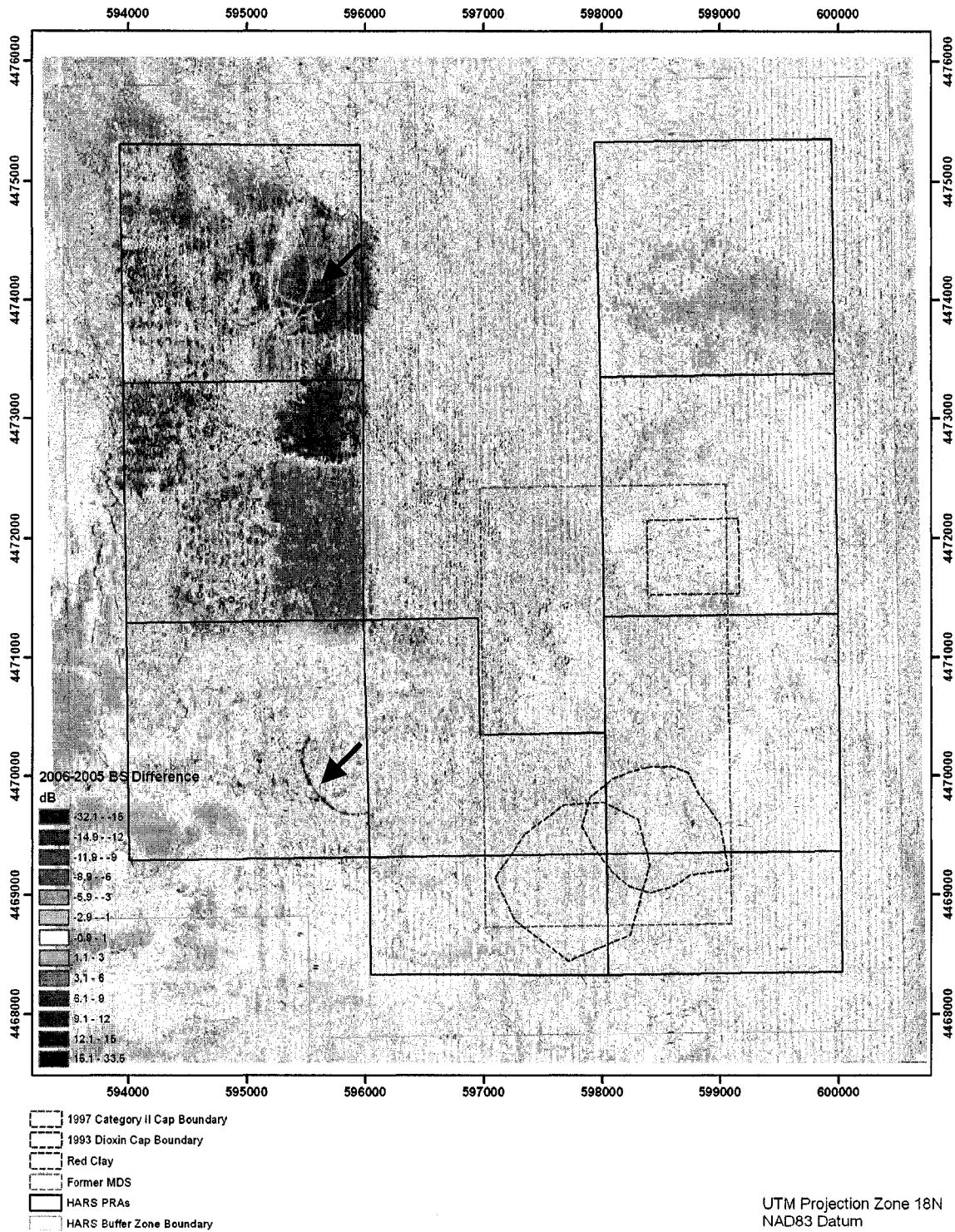


Figure 4.16 - Difference in the 240 kHz backscatter strength between 2006 and 2005, positive values are depicted in pink and correspond to an increase in grain size. Negative values are depicted in blue and correspond to deposition of finer material. Scours are indicated by arrows.

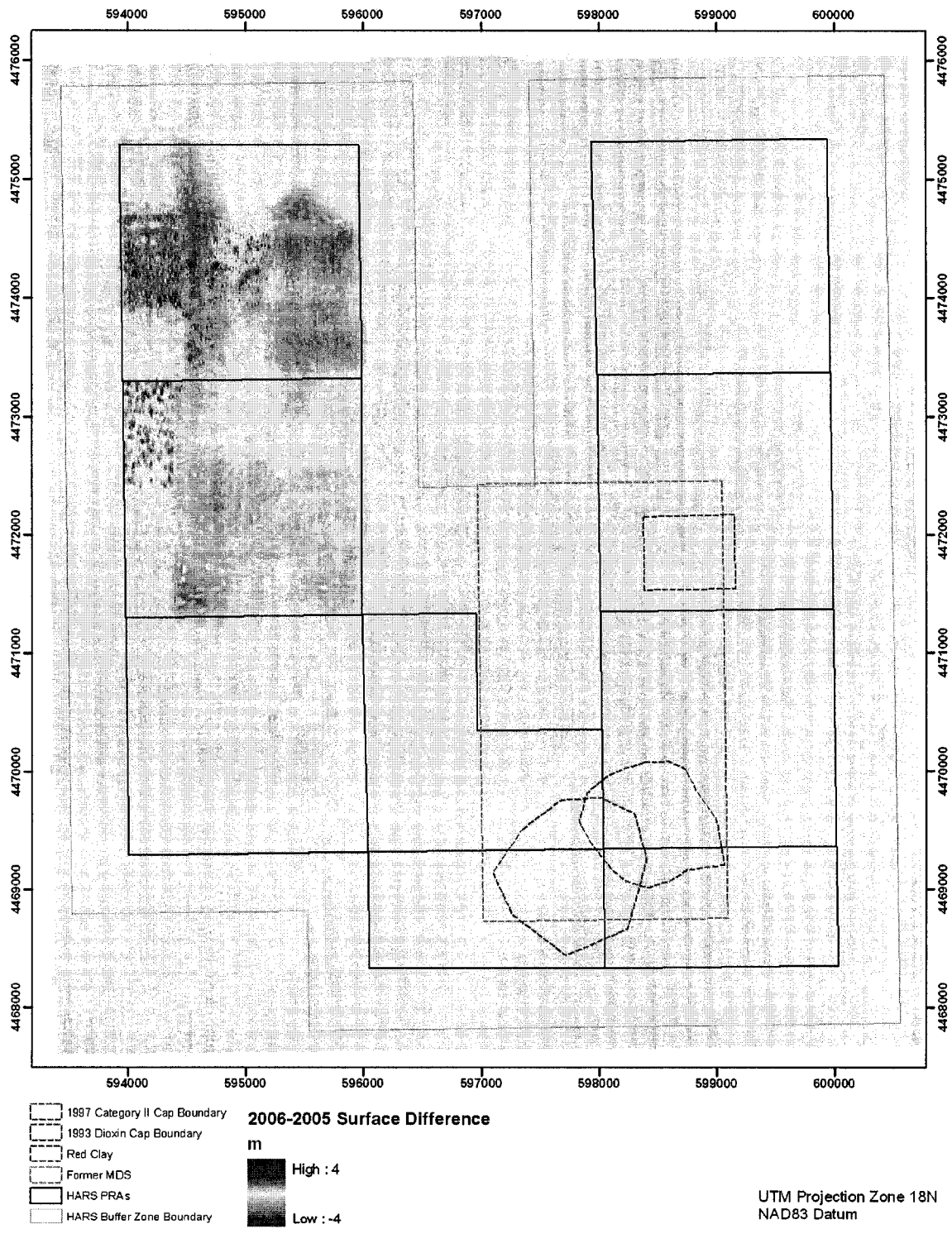


Figure 4.17 - Difference in bathymetry between 2006 and 2005, positive values are depicted in blue and are mainly concentrated in PRAs 1 and 2 where new material was deposited. Some erosion is also observed in the mounds that were already formed in 2005 (PRAs 1 and 2), corresponding to negative values depicted in brown.

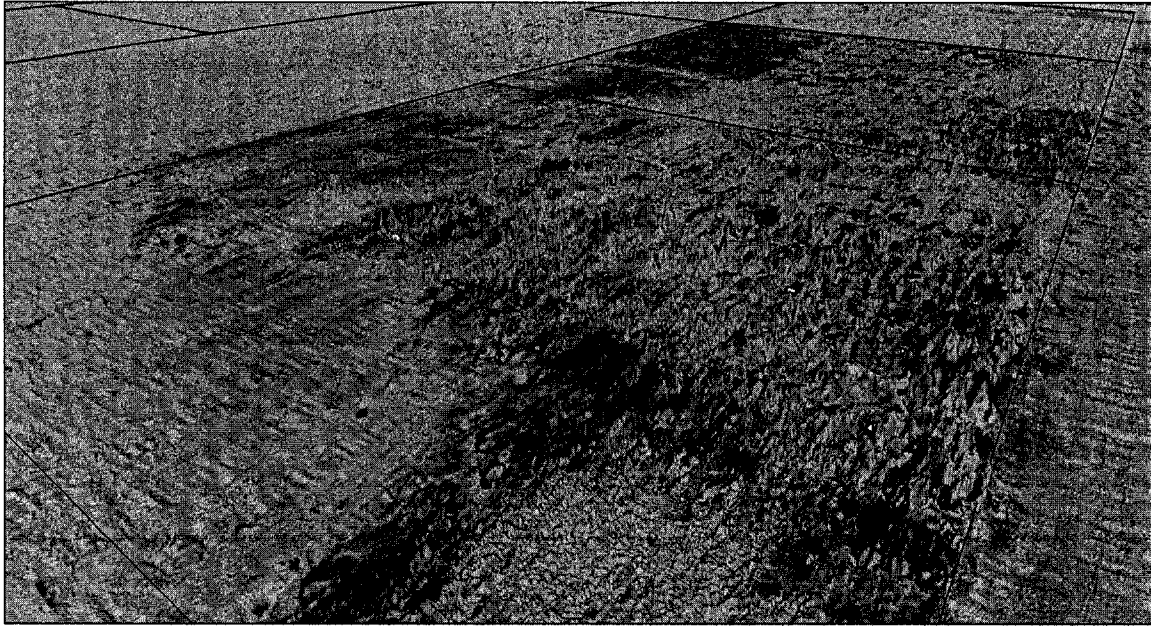


Figure 4.18 – View from northwest over PRAs 1 and 2. The difference in backscattering strength between 2006 and 2005 is draped over the difference in bathymetry. Positive values are depicted in red and correspond to coarser sediments. Negative values are depicted in blue and correspond to deposition of finer material. Vertical exaggeration: 15x.

#### 4.2.4 Backscatter strength versus penetration of the optical prism

Considering the results shown in Figure 4.10 (correlation between mean grain size and penetration of the optical prism), it would be expected that backscatter strength should present the same degree of correlation when compared with the penetration of the optical prism. The correlation observed in Figure 4.19 does not indicate backscatter as a good predictor of the geotechnical properties of the sediment. The lack of correlation might be explained by the uncertainty in sample position. In 2006 the optical and the sediment sample were taken 10 m apart, plus the deviation derived from cable angle. However, the mean backscatter was calculated as the mean within the uncertainty area of the sediment sample, with an average area of 1257 m<sup>2</sup>. An apparent correlation seems to exist in 2005 but the penetration of the optical prism was calculated

as the average for all the replicas that fall within a radius of 40 m and the mean backscatter was calculated as the mean within an uncertainty area of 5027 m<sup>2</sup>. In both years, there is no differentiation by number of weights.

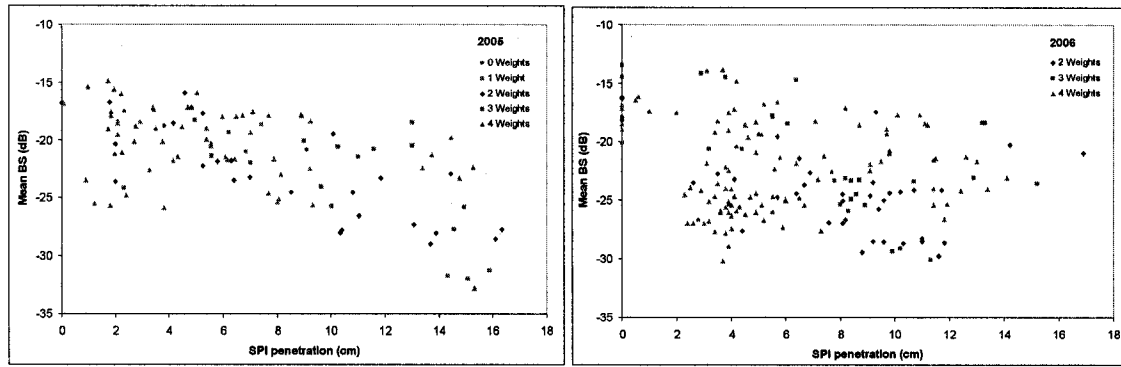


Figure 4.19 - Mean backscatter strength within the area of uncertainty of each sample versus penetration of the optical prism for 2005 (left) and 2006 (right). The value presented for the penetration of the optical prism in 2005 corresponds to the average of all replicas within a station.

### 4.3 Angular Range Analysis

#### 4.3.1 ARA in normal mode

ARA was performed in normal mode resulting in one ARA solution for each resolution cell, defined by the half-swath width of the sonar in the across-track direction and a stack of 30 pings in the along track direction. Appendix D shows some examples of the angular response for different types of sediments and model fits to the angular responses. Thiessen polygons (a polygon defined by the perpendicular bisectors of the lines connecting points in a triangular irregular network, whose boundaries delimit the area that is closest to each point comparatively to all other neighboring points) were constructed around each ARA solution and the mean grain size as predicted by the



model is depicted in Figure 4.20. The observed segmentation of the seafloor is very similar to the one that a geologist would have generated by visual interpretation of the backscatter mosaic, but with the great advantage that the characterization of the seafloor in terms of mean grain size is objective. It is derived from the measurement of a geoacoustic property and is not dependant on the human interpretation of a backscatter mosaic that can have a different outcome depending on which AVG was applied.

The 1993 dioxin, and the 1997 Category II capping projects are easily recognized, and capping material is predicted to be medium to fine sands. A deposit of fine sediment aligned with the axis of the Hudson Shelf Valley (Fig. 1.1) is also recognized, with a predicted mean grain size of coarse to medium silt. Another alignment of fine sediment exists to the west, and is more easily recognized than in the backscatter mosaic, in agreement with sediment transport to the head of the Hudson Canyon on the west flank of the topographic highs in the center of the HARS. The area corresponding to rock outcrops on the east side of the HARS is predicted to have  $M_z = -1 \Phi$ , the lower limit of the ARA model. Mounds of remediation material placed on PRAs 1, 2, 3 and 4 are predicted to have a mean grain size ranging from granules to fine sand. Preexistent sediment that is exposed on the sides of these mounds is classified as fine sand to coarse silt, which agrees with what is observed in the SPI images.

In spite of the good results at a regional scale, the limitations are evident when comparing ARA solutions with the backscatter mosaic at a local level. Figure 4.21 shows the predicted grain size at station A12 in PRA 9. A general trend can still be recognized, but HARS variability at a decameter scale can not be resolved by the spatial resolution of a method that employs the half-swath of the sonar (around 50 m for this region).

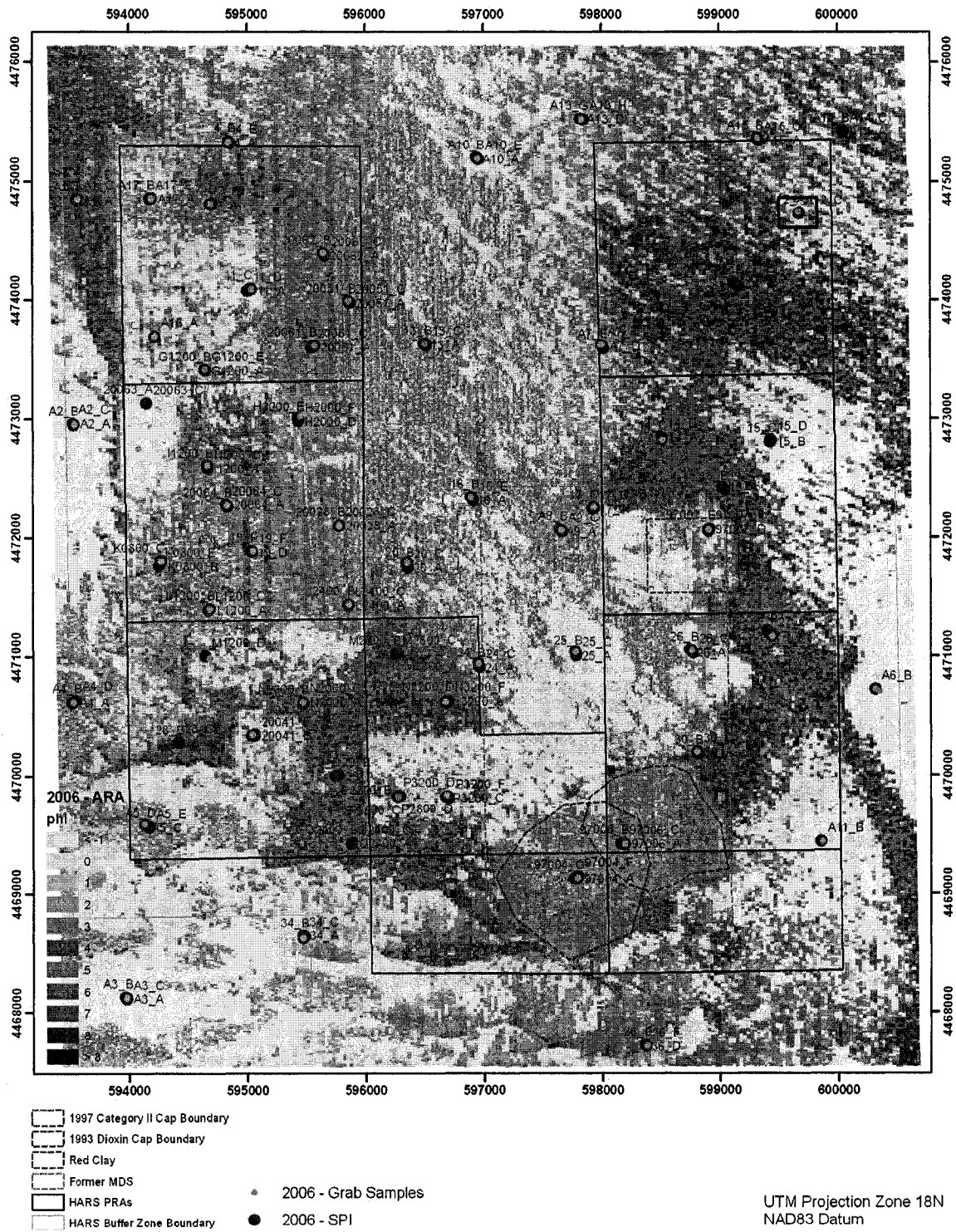


Figure 4.20 - Predicted mean grain size from the Angular Range Analysis for data collected in 2006. The area marked with a dark blue rectangle is zoomed in Figure 4.21.

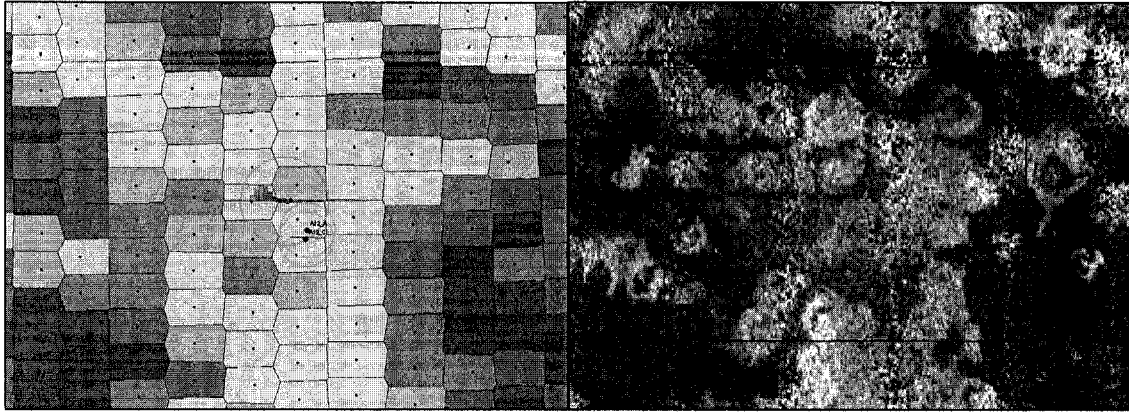


Figure 4.21 - Left: predicted mean grain size from the ARA for station A12 (2006). Polygons were constructed using ARA solutions represented by black dots (the color scheme is the same as the one used in Figure 4.20). The green circle represents the area of uncertainty of the grab sample and yellow circles the SPI uncertainty. Right: backscatter mosaic for the same area, the red rectangle corresponds to 150 x 200 m and marks the area where ARA was applied in “theme” mode.

#### **4.3.2 Comparison of ARA results with mean grain size**

Comparison of the mean grain size as predicted by the ARA with ground truth data is made considering the measured mean grain size and not the inferred mean particle size as in Figure 4.17. It is assumed that sediment samples used in the original measurements, that gave rise to the regression equations used in the ARA model, followed the normal preparation used in the majority of the grain-size analysis methods.

When the average of the ARA solutions inside the area of uncertainty of the grab sample is plotted against the measured mean grain size the result is a scatter of points (figure 4.22).

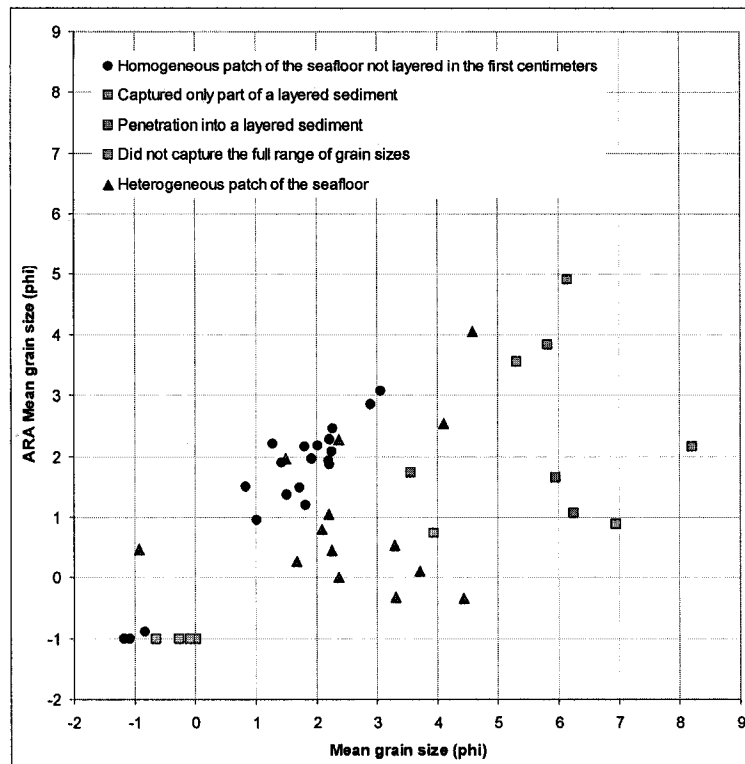


Figure 4.22 - Predicted mean grain size from the Angular Range Analysis for 2006 data versus measured mean grain size from sediment grab samples for sizes finer than  $-1 \Phi$ . Stations where the seafloor is homogeneous and without sediment layering in the first centimeters show a good correlation between ARA solutions and mean grain size determined by grab sampling and sediment analysis. Other points deviate from this trend, when the seafloor is heterogeneous, when the grab sample did not capture the full range of grain sizes or when the seafloor is homogeneous but the grab penetrated into a layered sediment.

The biggest difference is for station K0800 located in PRA 2 at the base of a mound of remediation material. ARA solutions that fall inside the area of uncertainty of the grab sample are relatively consistent (1.20, 2.26, 2.50 and 2.69  $\Phi$ ) but far from the measured mean grain size of 8.2  $\Phi$ . Backscatter strength inside the area of uncertainty of the sediment sample varies between -16 dB and -27 dB but most of the region falls in areas of higher backscatter and although some heterogeneity exists it is not enough to explain this discrepancy. However, the sediment was recovered from the SPI frame in the absence of a successful grab sample and represents only the upper millimeters. SPI images are smeared by red clay that exists on the surface but it is possible to observe a

few centimeters of remediation material (medium to fine sand on top of silts) that agrees well with ARA predictions.

The same correspondence of ARA prediction and grain size occurs at station 97007 situated near the base of a mound in the red clay deposition area inside PRA 6. Even though collected with a grab sampler, the recovered red clay only corresponds to a surface layer less than 1 cm thick as observed in the SPI. It is difficult to evaluate the grain size of the subsurface material on the SPI due to smearing by red clay but it appears to be sand. Two ARA solutions that fall in this area are both sands ( $0.63 \Phi$  and  $1.15 \Phi$ ). Considering an attenuation of only 0.2 dB/cm for the first layer of red clay at  $45^\circ$  grazing angle (Appendix A), it is likely that the contribution to scattering is mostly from the subsurface sand layer.

Grab samples 27\_C, A1\_C and N2000\_C are coarse and medium silts recovered from the frame and are situated in relatively homogeneous areas. The recovered sediment agrees relatively well with what is observed in the SPI images, except for a thin surface layer of fine sand that is not represented in the sample from the SPI frame. This probably explains why ARA predictions are coarser by 1 to 2  $\Phi$ . These are examples of sampling procedures that failed to adequately characterize the sediment to the extent that is penetrated by the acoustic wave.

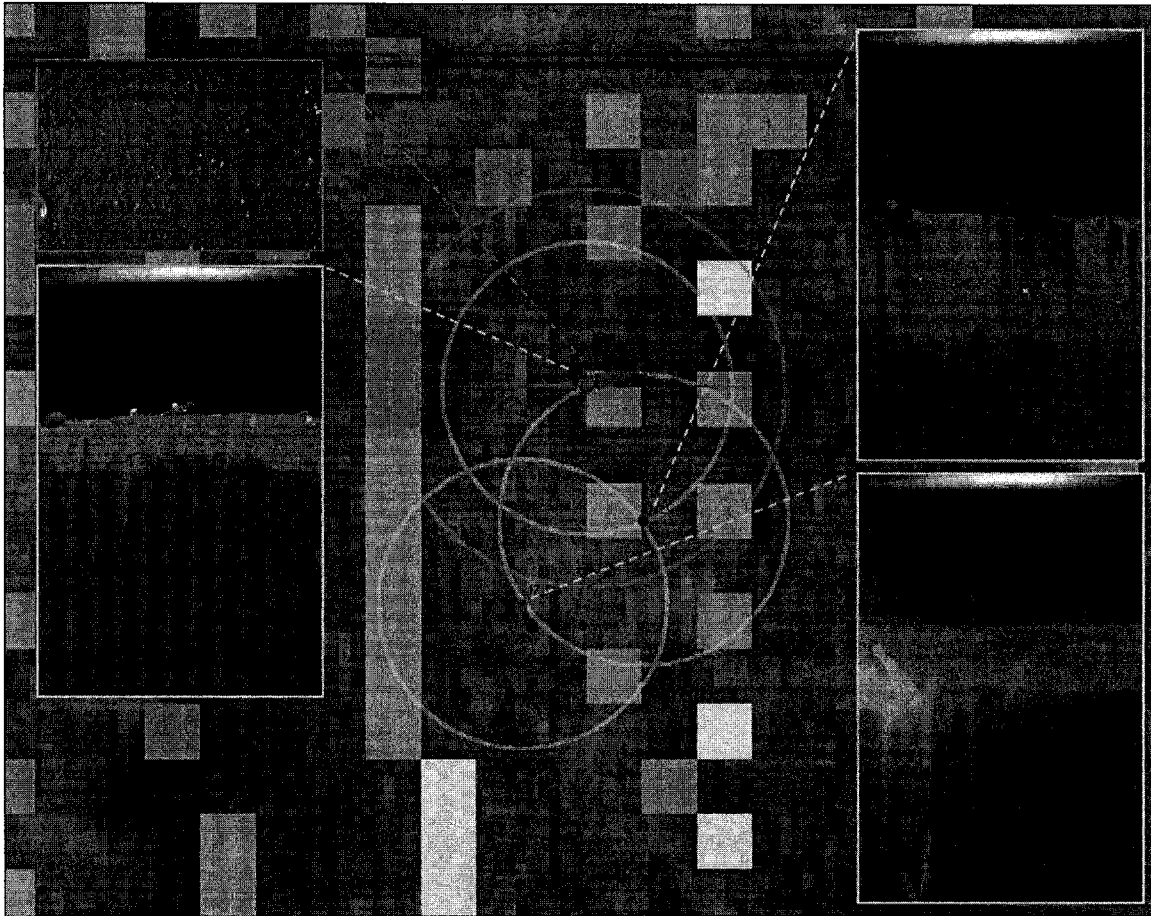


Figure 4.23 - ARA mean grain size solutions (the color scheme is the same as for Figure 4.20) over the backscatter mosaic for the area of station 17 (2006). The area of uncertainty for each sample is indicated by yellow circles for SPI images and with a green circle for the grab sample. Sediment profile images are 20x13 cm (HxW) and the grab sample image corresponds to 2.2 x 3.3 cm (HxW).

The opposite effect seems to arise when the material is sampled to a depth beyond what is penetrated by the acoustic wave. Station 17 (Fig. 4.23) is situated in an area where backscatter variations are subtle ( $-21.7 \text{ dB} \pm 1.2 \text{ dB } 1\sigma$ ) and different deposits cannot be clearly defined. ARA solutions fall in the medium sand size class but the determined mean grain size for the grab sample is in the fine silt size. SPI images reveal from 2 to 5 cm of sand over fine grained material. The grab sampler penetrated several centimeters into the bottom and the mean grain size is an average of more sediment than what is contributing to scattering in the direction of the transducer (approximately 2 cm in medium sands - Appendix A). Stations A9 and I1200 are similar

cases. They are in areas of relatively homogeneous backscatter and ARA predictions agree with what is observed in the first centimeters of the SPI.

Observations in stations 17, A9 and I1200 appear consistent with 2.3 dB/cm of attenuation for medium sand ensonified at 45° grazing angle, and with an expected acoustic penetration depth around 2 cm (Appendix A). They also seem consistent with the vertical structure of the sediment. The second layer appears to be an homogeneous very fine silt and the main contribution for scattering is at the wavelength scale,  $0.1 \lambda - 10 \lambda$  (Greaves and Stephen, 2000), that has its lower limit for 240 kHz at medium to coarse sand, close to the grain size of the top layer.

Other consequences of inadequate physical sampling may occur in coarse material when the size of the grab is not enough to capture the full range of grain sizes. Stations M1200, A2 and A3 are in relatively homogeneous areas and comparisons with SPI images suggest that the mean grain size is probably higher than what was captured by the grab sampler. ARA predictions are  $-1 \Phi$  but this is the lower limit of the model. Still, results are within  $1 \Phi$  of the measured mean grain size. Another example is from station A16 where the grab sample spreads over the sand and silt size class with  $M_z = 3.9 \Phi$  but the SPI did not penetrate into the bottom and on the surface reveals 2 cm pebbles. ARA results are  $0.7 \Phi$ , a coarse sand. All areas where the measured mean grain size is smaller than  $-1 \Phi$  are adequately classified by the ARA model.

When the backscatter strength within the uncertainty area of the grab sample is relatively homogeneous and it is not possible to clearly identify different sedimentary deposits, and when profile images show homogeneity in the first 2 to 5 cm, ARA predictions are within  $\pm 0.4 \Phi$  of the measured value for mean grain size. This is consistent for fifteen samples in the very coarse to fine sand range. Three other samples

present worse correlations, two medium sands with 0.5 and 0.9  $\Phi$  difference, and one coarse sand with 0.6  $\Phi$  difference.

Station 20051 corresponds to a homogeneous area of the seafloor but there is some striping in the backscatter caused by survey lines run on different days. ARA results differ by 0.6  $\Phi$  from the measured value at this station.

In areas of relative horizontal and vertical homogeneity, ARA solutions correlate well with the mean grain size determined by grab sampling except in the cases where the grab sampler failed to take a representative sample of the sediment. When horizontal and vertical heterogeneities exist, there is no apparent correlation between the two determinations of mean grain size.

#### **4.3.3 ARA in supervised segmentation mode (in areas of horizontal heterogeneity)**

Until now, only samples were considered that had been collected in places where the backscattering strength is relatively homogeneous over a patch of the seafloor approximately 50 m wide. In all these cases, the ARA model matched the observations, or the physical sample did not characterize adequately the sediment that is being ensonified.

The backscatter strength for 14 stations varies considerably within the uncertainty area of the grab sample and this brings up two different issues. First, the sample has to be attributed to the sedimentary deposit where it came from. This can be accomplished by supervised positioning of the sample, using information from contiguous areas. Second, the backscatter angular response uses half the swath width of the sonar which does not provide enough spatial resolution for areas like the one depicted in Figure 4.21. In order to overcome this limitation polygons of 200 by 150 m



were defined around each station. Each polygon was manually segmented into smaller areas with similar textural characteristics (themes) assuming that each theme corresponds to areas on the seafloor with similar physical and geoacoustical properties.

In the normal ARA mode, the observation is the average angular response of a certain number of stacked pings in the along track direction (30 in this study), whereas in the ARA theme mode, the observation is the average of all the snippets that fall within each theme, even if they come from different acquisition lines. ARA was executed for each theme, which means that inside each rectangle there are as many observations as the number of themes and as many solutions as themes.

Taking station A12 (2006) as an example, the backscatter mosaic allows differentiating two major deposits (Fig. 4.24): one corresponding to areas of high backscatter (depicted in light blue) and the other to areas of low backscatter (depicted in dark pink). SPI replicas for the same station reveal high variation over a short range (Fig. 4.25), showing a gravelly bottom and a layered sediment with 4 cm of sand over silt. The grab sample with  $M_z = 2.4 \Phi$  was attributed to the deposit depicted in dark pink. Two themes were defined for ARA, each one corresponding to a sedimentary deposit. ARA solutions are  $-1 \Phi$  (gravel) for the area in light blue and  $1.61 \Phi$  (medium sand) for the area in dark pink. Angular responses for each theme are depicted in Figure 4.26.



Figure 4.24 - Manual segmentation of the area marked by the red rectangle in Figure 4.21 right, 200 x 150 m. Although subtle variations can be observed in the backscatter mosaic only two different types of deposits could be clearly identified, transitional terms are probably included in each of the themes defined.

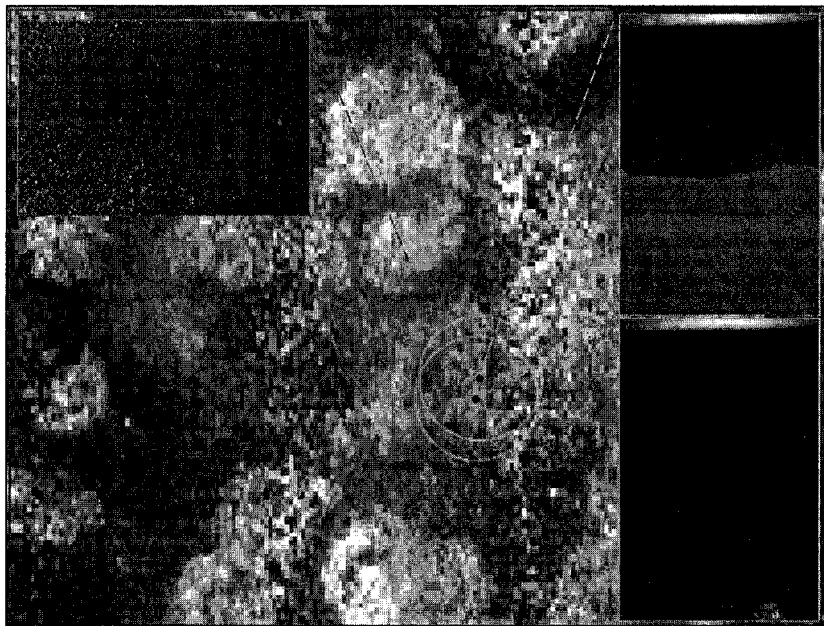


Figure 4.25 - 20 x 13 cm (HxW) SPI images and 2.2 x 3.3 cm (HxW) grab sample photo for station A12 (2006). The distance between the two red dots corresponding to SPI positions is 5 m and the uncertainty radius 15 m. The uncertainty radius for the grab sample is 24 m.

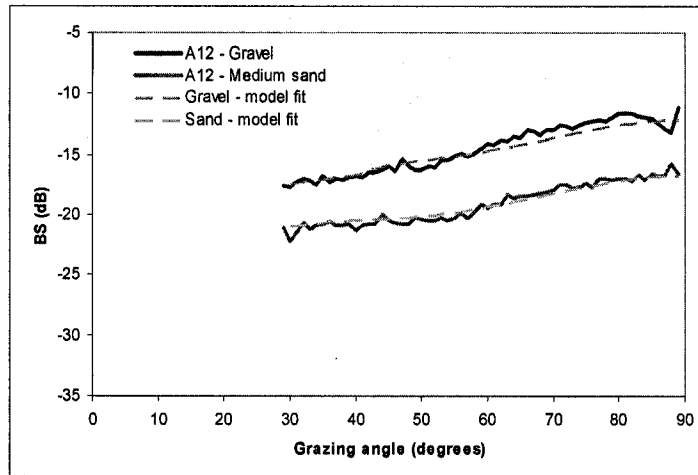


Figure 4.26 – Angular response and model fit in “theme” mode for station A12 (2006). The blue line corresponds to the light blue area depicted in Figure 4.24, and the pink line to the area in dark pink.

Although the segmentation method considerably improves ARA results in areas where the normal mode does not have enough spatial resolution, when the medium is layered in the first few centimeters, ARA predictions and grab samples do not match. This is a similar case to the one already observed in section 4.3.2 for stations 17, A9 and I1200.

#### **4.3.4 Comparison of ARA results with the estimated mean grain size for the top layer (in areas of vertical heterogeneity)**

If SPI observations are considered valid to a lateral extent of 10 to 20 m, it can be assumed that the same sediment was collected by the grab sampler, if no significant difference between the two is observed. In the majority of the cases, the uppermost layer of sediment corresponds to remediation material, usually sand, deposited over silt. The mean grain size varies to the extent the grab penetrated the sediment. If the sampler collected mostly the top layer of the sediment, then the mean grain size will be larger. If the sampler collected mostly the subsurface layer, then the mean grain size will be

smaller. Therefore, the mean grain size is not a measure of sediment properties that will influence its acoustic behavior but only a measure of grab efficiency. Although there seems to be a general trend, if the penetration of the grab fluctuated as much as the SPI penetration for the same type of sediment (Fig. 4.14 and Fig. 4.15), mean grain size can hardly be used as a geotechnical indicator either.

ARA solutions seem to characterize well the few first centimeters of the seafloor for the frequency of interest (240 kHz). Considering that when layering is present, each layer is relatively homogeneous and corresponds to a different type of sediment, it is possible to infer the grain size of the top layer by looking at the grain-size frequency distribution. The grain size histogram usually has one mode for each type of sampled sediment (Fig. 4.27) and the agreement with ARA solutions is remarkable as seen in Figure 4.28.

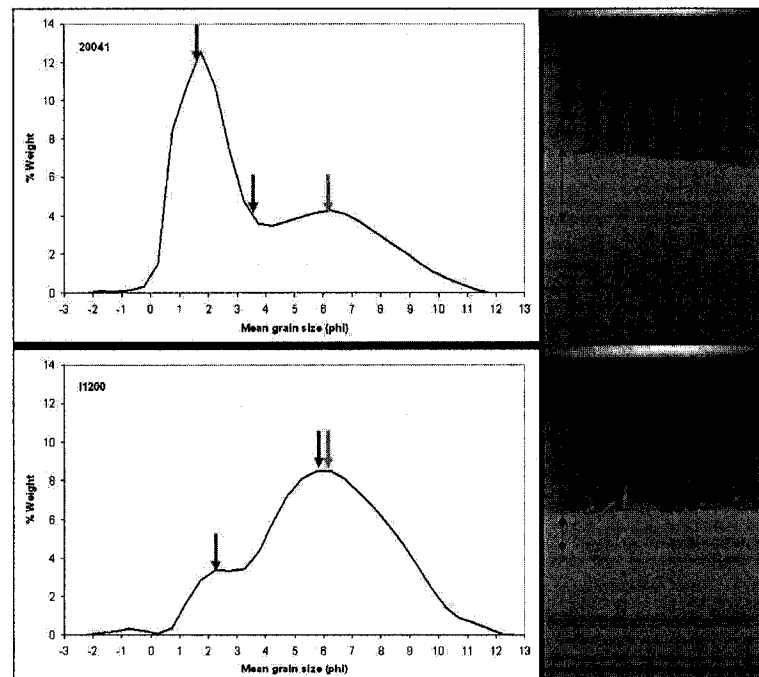


Figure 4.27 - Grain size frequency distribution and profile images for samples 20041\_A (top) and I1200\_A (bottom), from 2006. A first layer of remediation material, medium to fine sand, with a few centimeters, overlays a layer of medium to fine silt. The blue arrow represents the mean grain size for the sampled sediment and the red and green arrows the mode corresponding to each layer.

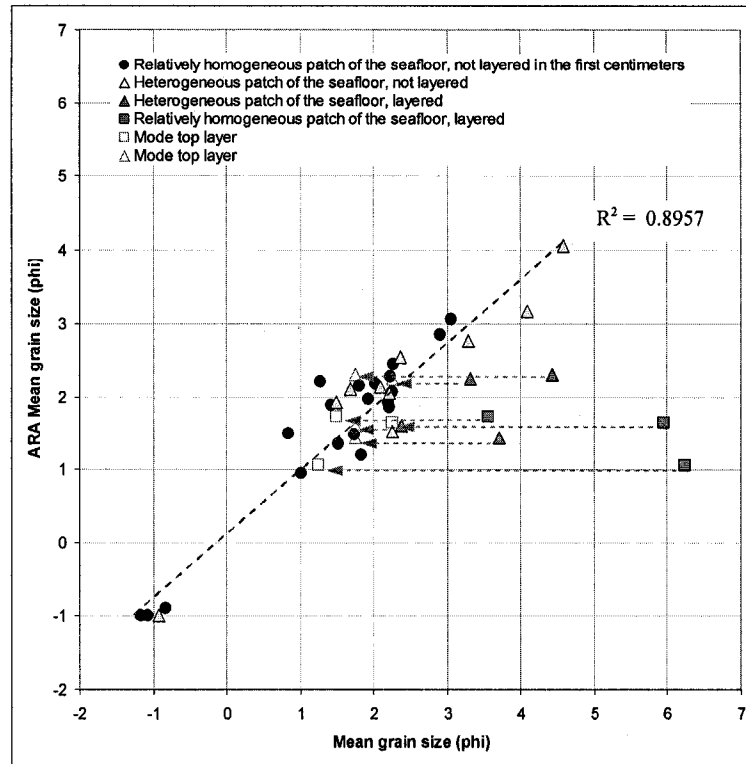


Figure 4.28 - Predicted mean grain size from ARA for 2006 data versus measured mean grain size from sediment grab samples. Samples depicted by squares in Figure 4.22 that did not capture the full range of grain sizes were removed. ARA solutions for samples depicted by triangles in Figure 4.22, corresponding to high spatial variability, were obtained using segmentation and definition of themes. The mean grain size of the top layer was approximated by considering the mode corresponding to the top layer. Green arrows connect the mean grain size of a layered sediment to the mode of the top layer of the same sediment sample. The red line represents the linear regression after correcting for horizontal and vertical heterogeneities.

After correction for vertical heterogeneities as well, the correlation between ARA solutions and mean grain size is high (coefficient of determination  $R^2 = 0.90$ ). However, since points are mainly concentrated between 1 and 3  $\Phi$ , more data is needed to validate this correlation.

#### 4.3.5 Estimation of the consistency of ARA results

When considering samples 20028\_A, 20064\_A, L1200\_A and L2400\_A collected in 2006 (Fig. 4.14 and Fig. 4.15) that were used to estimate the consistency in backscatter strength, it is observed that ARA predictions calculated as the average of the solutions that fall within the area of uncertainty of the sediment sample are (Table 4.1):

Sample	ARA solutions ( $\Phi$ )	Mean grain size - grab sample ( $\Phi$ )
20028_A	1.9 $\pm$ 0.6 (1 $\sigma$ )	2.2 $\pm$ 0.6 (1 $\sigma$ )
20064_A	2.5 $\pm$ 0.0 (1 $\sigma$ )	2.3 $\pm$ 0.6 (1 $\sigma$ )
L1200_A	2.1 $\pm$ 0.2 (1 $\sigma$ )	2.3 $\pm$ 0.6 (1 $\sigma$ )
L2400_A	1.9 $\pm$ 1.4 (1 $\sigma$ )	2.2 $\pm$ 0.6 (1 $\sigma$ )

Table 4.1 – ARA solutions calculated as the average within the area of uncertainty of the grab sample and correspondent mean grain size determined from sediment analysis.

For these four samples, mean ARA solutions are within a range of 0.6  $\Phi$  and only 0.2 to 0.3  $\Phi$  apart from the correspondent value determined by grab sampling. These values suggest that the entire workflow, from data acquisition by SAIC with the Reson 8101 multibeam system to ARA in Geocoder, yields consistent results within  $\pm 0.3 \Phi$  for the same type of seafloor. Considering all the samples in Figure 4.28, after correcting for horizontal and vertical heterogeneities, the average difference between ARA solutions and mean grain size determined by grab sampling is  $\pm 0.4 \Phi$  (1 $\sigma$ ).

## CHAPTER 5

### CONCLUSIONS

Before confidence can be acquired for a remote sensing tool, to the point where the need for ground truth is minimized or eventually eliminated, a comparison has to be made between remote sensing results and ground truth data in different types of environments. The present study tried to estimate the applicability of the Angular Range Analysis implemented in Geocoder (Fonseca and Mayer, 2007) to an area of high spatial variability (the Historical Area Remediation Site – HARS).

The parameter chosen as the object of comparison was mean grain size because it is the most commonly measured seafloor property, widely used to define dredging areas for beach nourishment, to predict sediment transport, seafloor geotechnical behavior, and to define benthic habitats. Although it may not yield the desirable predictive relationship with other physical and geoacoustic properties of the sediment, it can be easily measured with low cost. However, any measurement is affected by an uncertainty and, before assuming mean grain size as determined by common methods of ground truth and grain size analysis as an absolute value, we have to determine the sources of uncertainty in the measurement and when possible, quantify them.

The major source of uncertainty in the determination of mean grain size by grab sampling derives from the peculiarities of the HARS and sampling efficiency. In a natural environment on the continental shelf it is expected that the major sediment types have a horizontal continuity on the order of decameters to kilometers and a vertical continuity on

the order of decimeters to meters. The anthropogenic actions at the HARS shaped the seafloor and variations are at a meter/decameter level horizontally and vertically at a centimeter level. The grab sampler was not precisely positioned and position uncertainty is on the order of decameters. Penetration of the grab sampler usually follows a trend with sediment type but has variations in the order of centimeters. This brings up two issues. Where is the sample from? And what is being sampled?

Uncertainties in sampling position on a small boat using DGPS were found to vary between  $\pm 15$  m to  $\pm 25$  m in the HARS, and in several cases the area of uncertainty falls between different deposits. In spite of not reflecting the true normalized average backscatter strength for each pixel due to the application of an AVG, the backscatter mosaic is suitable for the identification of different deposit types and even to recognize subtle variations. Using ground truth information from contiguous areas that are homogeneous within the uncertainty area of sediment samples it was possible, to a certain extent, to execute a supervised positioning of samples that fall between deposits.

Another type of uncertainty due to sediment sampling arises when the grab is not able to capture the full horizontal and/or vertical range of grain sizes. This particular type of uncertainty would be minimized with the use of larger and heavier grabs.

It was found that instrumental uncertainties associated with an automated method of grain size analysis, such as laser diffraction, appear to be negligible. Although there were not enough analyses to make statistically meaningful conclusions, it was observed that the procedure of drying the sample, in order to calculate its weight and split it between different analytical methods, increased the mean grain size by 0.01 to 0.05  $\Phi$  for sand, 0.1  $\Phi$  for coarse silt, 0.2  $\Phi$  for fine silt and 0.4  $\Phi$  for very fine silt/clay sizes. Determination of mean grain size by sieve-laser diffraction and sieve-pipette methods was on average higher 0.35  $\Phi \pm 0.14$   $\Phi$  ( $1\sigma$ ) for the sieve-pipette method. Although it seems that uncertainties associated with the instruments, procedures and



methods are relatively low, it must be considered that mean grain size determined by the Folk and Ward (1957) graphical method is much less affected than the full distribution curve.

The major uncertainty in the determination of the size of the particles in the sediment seems to be caused by the common analytical procedure of decomposing the sample into its elementary particles. The standard analytical procedure is reasonable from a sedimentary perspective but causes an underestimation of the mean particle size of the sediment of at least  $1.5 \Phi$  for fine silts to clays,  $0.5 \Phi$  for coarse to medium silts and  $0.3 \Phi$  for very fine sands.

How representative a grab sample is of the surficial facies a region is directly associated with the spatial variability of the seafloor under investigation. Although good results can be expected in many natural environments, this is not the case for the HARS. Comparison of results with remote seafloor characterization proved to be difficult, but possible only because of profile images and the full grain-size distributions, which suggests that unless the medium is relatively homogeneous, grab samples by themselves, and grain size expressed in terms of major fractions do not have much value in describing the surficial sediment.

Remote seafloor characterization in terms of mean grain size using Angular Range Analysis implemented in Geocoder (Fonseca and Mayer, 2007) showed good results at a regional scale and the limitations associated with the resolution of the method in normal mode (stack of pings x half-swath) do not affect the general regional trend. At a local level, however, and given the heterogeneity of the HARS, the lack of spatial resolution is evident. When there is an homogeneous patch of the seafloor where several ARA solutions fall, results are in agreement with the measured mean grain size provided the sediment is roughly homogeneous over the first centimeters of depth.

When there is horizontal and/or vertical heterogeneity, the ARA's solutions deviate considerably from the measured mean grain size.

When the sediment is vertically homogeneous over the first centimeters but varies horizontally within the half-swath width of the sonar, it was found that segmenting the backscatter mosaic to define regions of the seafloor with similar properties yields good results. The definition of different "themes" and calculation of the average angular response for each theme, gave results similar to the ones determined by grab sampling.

Vertical heterogeneity in the HARS (here considered as layering between sediment types with marked differences) consists of two main types; an upper layer of red clay (approximately 1 cm) overlying sand, and a few centimeters of sand (2 to 5 cm) overlying medium to fine silt. In both cases the angular response of the sediment is characteristic of sand. This suggests that, in the first case the sound penetrated in the clay and was mainly scattered in the sandy layer and that, in the second case, scattering occurred mostly in the sandy layer without significant penetration and scattering in the underneath silt. When the mean grain size for the sandy layer is inferred from the mode of the grain size distribution, results agree relatively well with the mean grain size predicted by the analysis of the sediment angular response.

In all these cases, 1) vertical and horizontal homogeneity; 2) horizontal heterogeneity with determination of the angular response in "theme mode"; 3) vertical heterogeneity with approximation of the mean grain size by the mode corresponding to the top sandy layer; ARA solutions are within a maximum range of  $\pm 0.9 \Phi$  of the mean grain size determined by ground truth, with an average difference of  $\pm 0.4 \Phi$  ( $1\sigma$ ) and a coefficient of determination  $R^2 = 0.90$ . However, these values also reflect the uncertainty in the determination of mean grain size by grab sampling and sediment analysis.

In order to better evaluate the consistency of ARA predictions and also of the backscatter mosaics assembled in Geocoder, acoustic remote sensing results were

compared with four sediment samples taken in different places but corresponding to the same sediment. The areas that were sampled are horizontally and vertically homogeneous. ARA predictions for the mean grain size are within  $\pm 0.3 \Phi$  and the backscatter averaged over the area of uncertainty of the grab sample is within  $\pm 1$  dB. Angular Range Analysis proved to be an effective remote sensing tool at regional scale in normal mode and at a local scale, when the seafloor is heterogeneous, in "theme" mode.

Mosaics assembled by Geocoder, which were corrected for geometric and radiometric distortions, allowed the observation of the temporal evolution of the seafloor. Changes in backscatter are collocated with variations in bathymetry, mainly corresponding to the deposition of new remediation material. Between two different years, the same workflow, from multibeam data acquisition to processing in Geocoder, showed a bias of 1 dB, and some noise in the order of  $\pm 10$  dB concentrated near nadir that did not affect the interpretation.

Special care has to be taken when trying to validate remote sensing measurements, especially when a grab sample might be the only possible ground truth method; results should not be assumed *a priori* as being true. One possibility to overcome this limitation is to execute the acoustic survey first, build the backscatter mosaic in the field and choose homogeneous areas of the seafloor within the predicted radius of uncertainty of the grab sample. To ensure that samples represent vertically what is being sampled by the acoustic wave, one possibility is to estimate the degree of penetration of the acoustic wave, collect a relatively undisturbed sediment sample with a larger grab, like a Smith-McIntyre, and remove a core from the center of the grab.

The idea that "The most reliable method to obtain information on the ocean sediment grain size is the gathering of bottom samples followed by a laboratory grain

size analysis.” (van Waaij and Ainslie, 2006, p. 2555) does not seem to be particularly valid in the case of the HARS and probably in other regions of high spatial variability.

### **Future Work**

A definitive test for the Angular Range Analysis, or for any acoustic remote sensing tool, will probably never be completed unless all types of seafloor and all possible variations are covered. Further comparisons of results should focus on common oceanic environments with low spatial variability and/or on areas of high spatial variability but using box corers with acoustic positioning. It would also be interesting to see the effect of layering at different scales and frequencies in the angular response of the seafloor.

The application of the ARA in “theme” mode yielded good results for areas of high spatial heterogeneity but it is not feasible to manually segment regions of similar properties in large mosaics. An automated segmentation method usually requires *a priori* definition of the number of classes but for large areas or for areas with gradual variations, that is almost impossible. It might be possible to overcome this limitation by dividing the area of study into smaller regions, and using the backscatter mosaic and bathymetric data, define statistically different populations for each region and correlate populations from different regions to segment the seafloor into different “themes”, each one corresponding to an area of the seafloor with similar properties.

## **APPENDICES**

## APPENDIX A

### PENETRATION OF THE SOUND INTO THE SEDIMENT

An estimation of how much the sound is attenuated in the first layer can be made by considering regression equations between mean grain size and  $k$  ( $\text{dB m}^{-1} \text{ kHz}^{-1}$ ), a constant used to calculate the attenuation  $\alpha$  expressed in dB/m, defined by Hamilton (1972) as:

$$\alpha = kf^n \quad (\text{A.1})$$

where  $f$  is the frequency in kHz and  $n$  the exponent of the frequency.

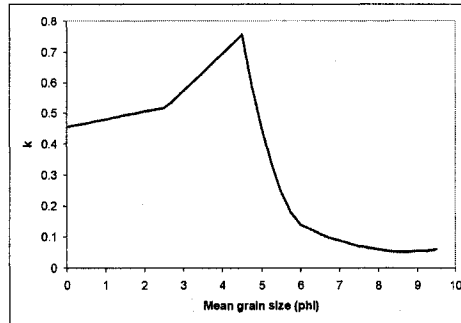


Figure A.1 - Mean grain size versus  $k$  (adapted from Hamilton, 1972).

The path traveled by the sound inside the sediment can be estimated considering Snell's law for a grazing angle  $\theta_1$ :

$$\frac{\cos \theta_1}{c_1} = \frac{\cos \theta_2}{c_2} \quad (\text{A.2})$$

where  $c_1$  is the sound speed in the water (1500 m/s) and  $c_2$  the sound speed in the sediment (Fig. A.2),

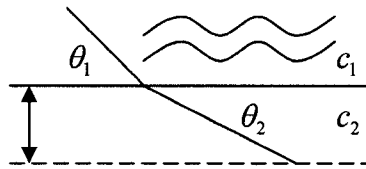


Figure A.2 - Refraction of the ray that describes the incident sound wave with 45° grazing angle.

and the relation between sound speed in the sediment and mean grain size referenced by Hamilton and Bachman (1982):

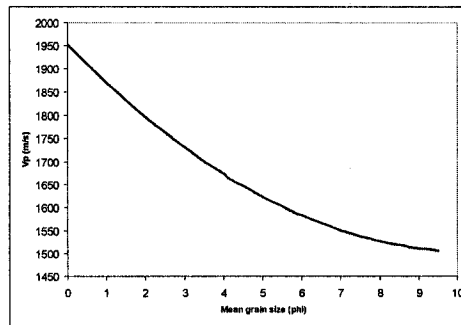


Figure A.3 - Mean grain size versus compressional sound speed in the sediment (adapted from Hamilton and Bachman, 1982).

The attenuation in dB per each cm of layer thickness, for 45° grazing angle and the 240 kHz frequency used in this study, considering  $n \approx 1$ , becomes:

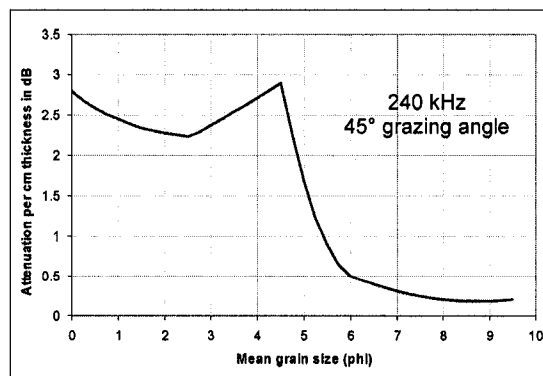


Figure A.4 - Mean grain size versus attenuation per each cm thickness of the first layer for a grazing angle of 45° and a frequency of 240 kHz.

Given the attenuation of sound in the sediment, it is possible to roughly estimate the maximum penetration of the acoustic wave making some assumptions and considering the sonar equation for an active sonar (Urick, 1983):

$$SL - 2TL + TS = NL - DI + DT \quad (A.4)$$

The source level (SL) is specified as 210 dB re 1  $\mu\text{Pa}@1$  m (manufacturer's data). Calculation of the transmission loss (2TL) considers spherical spreading and absorption, for scattering on a rough bottom it is:

$$2TL = 40 \log R + 2\alpha R \quad (A.5)$$

where R is the range to the target, considered here as 35.4 m at a depth of 25 m with 45° grazing angle, and  $\alpha$  the absorption coefficient with a value of 0.55 dB/m for 240kHz (Kinsler *et al.*, 1999), using these values, 2TL = 101dB.

The noise level (NL) for 240 kHz is mainly due to the thermal noise effect (Urick, 1983) and is calculated by:

$$NL = N_0 + 10 \log(Bw) \quad (A.6)$$

$N_0 = 33$  dB re 1  $\mu\text{Pa}/\text{Hz}^{1/2}$  (Urick, 1983), and the receiver bandwidth (Bw) can be approximated by  $Bw = 0.88/\tau$ , where  $\tau$  is the pulse length, equal to 75  $\mu\text{s}$  in our case, so Bw = 11.7 kHz and NL = 73 dB.

Not having information about the detection threshold (DT) and the receive directivity index (DI), it is possible to consider DI – DT as the “increase in signal-to-background ratio produced by the entire receiving system” (Urick, 1983, p. 21), here assumed to be equal to 5 dB.

The seafloor is the target, and the acoustic backscattering strength BS is (Lurton, 2002):

$$BS = S_B + 10 \log(A) \quad (A.7)$$



where  $A$  is the area ensonified by a sound pulse with length  $\tau$ , with beam width  $\varphi$ , at a distance  $R$  and at a grazing angle  $\theta$ , and with a speed in the water  $c$ :

$$A = \varphi R \frac{c\tau}{2\sin\theta} \quad (\text{A.8})$$

and  $S_B$  is the angular dependant acoustic backscattering strength that can be approximated considering the graph in Figure A.5, as  $-21$  dB for a medium sand. So  $10\log(A) = -10$  dB and  $BS = -31$  dB.

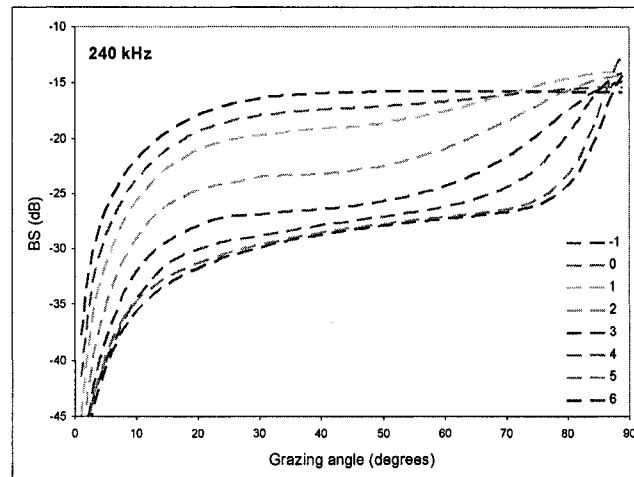


Figure A.5 -  $S_B$  versus grazing angle calculated using the implementation of Jackson *et al.* (1986) model in Geocoders's ARA with default values of input parameters. Each colored line corresponds to a different mean grain size, expressed in  $\Phi$  units.

Considering the sonar equation and the assumptions made, an estimate can be made on how much loss is allowed for bottom penetration (BL):

$$DT - DI + NL = SL - 2TL - BL + BS \quad (\text{A.9})$$

which results in 10 dB for bottom loss in medium sands. This value corresponds to a penetration of approximately 2 cm at  $45^\circ$  grazing angle (considering an attenuation of 2.3 dB/cm for medium sand at 240 kHz in Figure A.4, and two-way travel of sound in the sediment). Given all the assumptions made, it is expected that the calculations are subject to large errors but the order of magnitude of the results is consistent with the

observations. Figure A.6 depicts results of the calculations for different types of sediments.

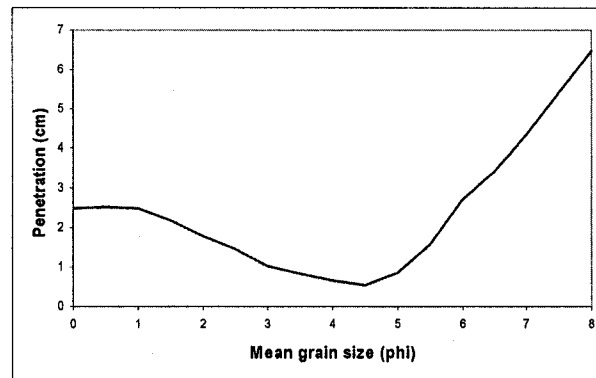


Figure A.6 - Rough estimation of acoustic wave penetration into the sediment for different mean grain sizes at 45° grazing angle and 240 kHz. The penetration is estimated to vary between 1 and 10 wavelengths depending on the type of sediment.

## APPENDIX B

### BACKSCATTER MOSAICS APPLYING DIFFERENT AVGs

Several mosaics were assembled in order to compare the influence of applying an Angular Varying Gain to normalize the acoustic response across the swath. Three AVGs from Geocoder were selected for this comparison: "Trend", "Flat" and "Lambert".

In the case of the "Trend" and "Flat" AVG corrections, the AVG for each ping is constructed from the average angular response calculated over 300 pings centered on the ping. In the "Flat" AVG correction, the reference level is the mean of the two average backscatter values calculated for each side of the sonar, between 35 and 55° grazing angles. In the "Trend" AVG correction, the reference level is the trend line between the average backscatter values (calculated between 35 and 55° grazing angles) of each side of the sonar. The "Lambert" AVG correction considers an angular variation of the backscatter following Lambert's law ( $BS(\theta) = BS_0 + 20\log(\cos\theta)$ , where  $\theta$  is the incident angle and  $BS_0$  the average backscatter between 35 and 55° grazing angles).

The choice of which AVG curve to apply is subjective. Figure B.1 depicts the backscatter mosaic without any AVG correction, the interpretation of this image is relatively difficult due to high backscatter near nadir (the result of coherent reflection), and a rapid drop in backscatter beyond the critical angle. Figures B.2, B.3 and B.5 depict the backscatter mosaic with the AVG "Trend", "Flat" and "Lambert" corrections, respectively. The standard Lambertian correction is not effective in removing the effect

of the seafloor angular response. The AVG "Trend" and "Flat" corrections produce a backscatter mosaic with a smooth response across the sonar swath.



Figure B.1 - 2006 backscatter mosaic assembled with Geocoder without any AVG. The angular response of the sediment makes interpretation of the backscatter mosaic relatively difficult.



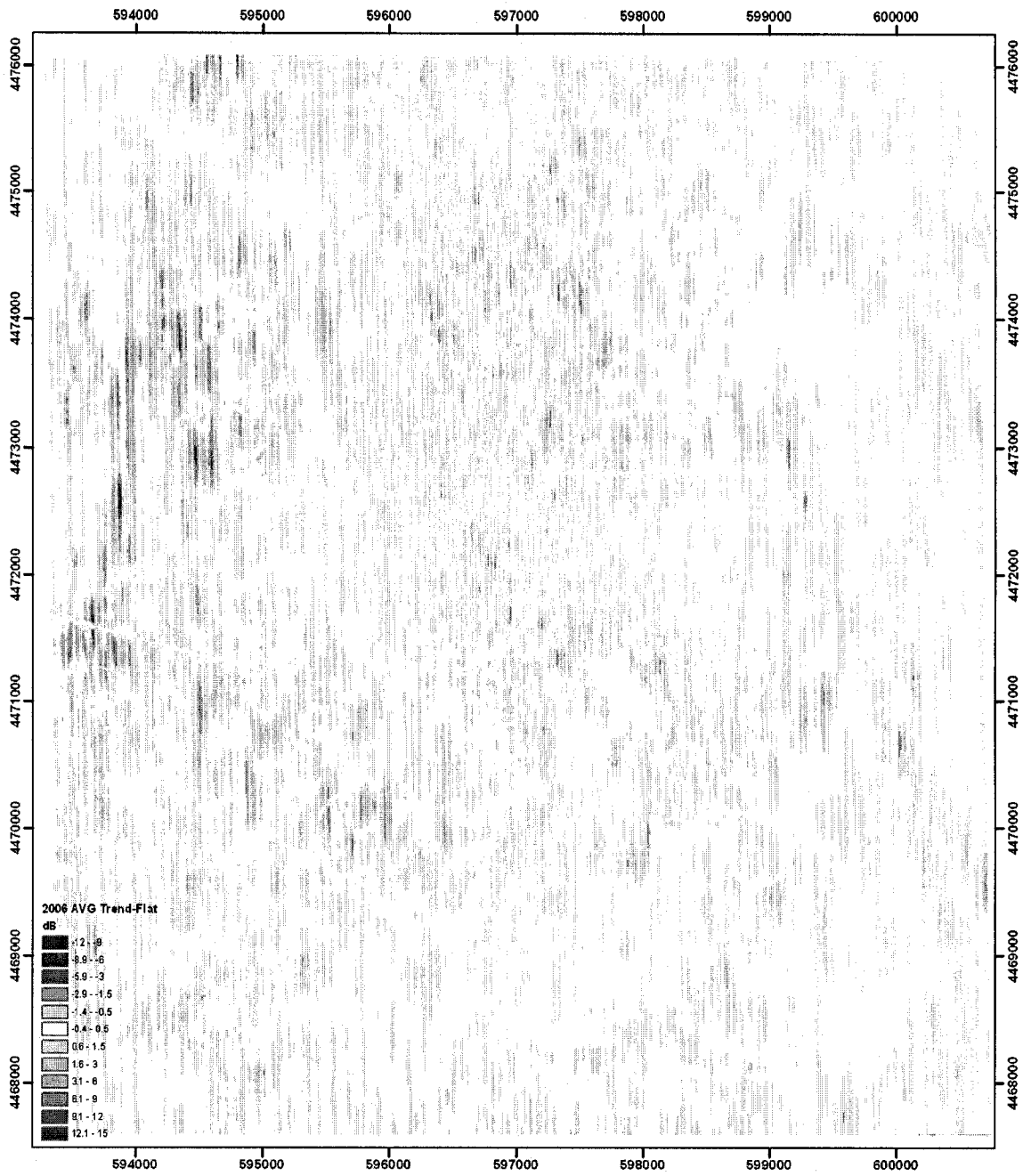
2006 AVG Trend  
 dB  
 High : -2.17  
 Low : -53.7

UTM Projection Zone 18N  
 NAD83 Datum

Figure B.2 - 2006 backscatter mosaic assembled with Geocoder with AVG Trend.



Figure B.3 - 2006 backscatter mosaic assembled with Geocoder with AVG Flat.



Mean = 0.12 dB  
 Standard deviation = 0.52 dB

UTM Projection Zone 18N  
 NAD83 Datum

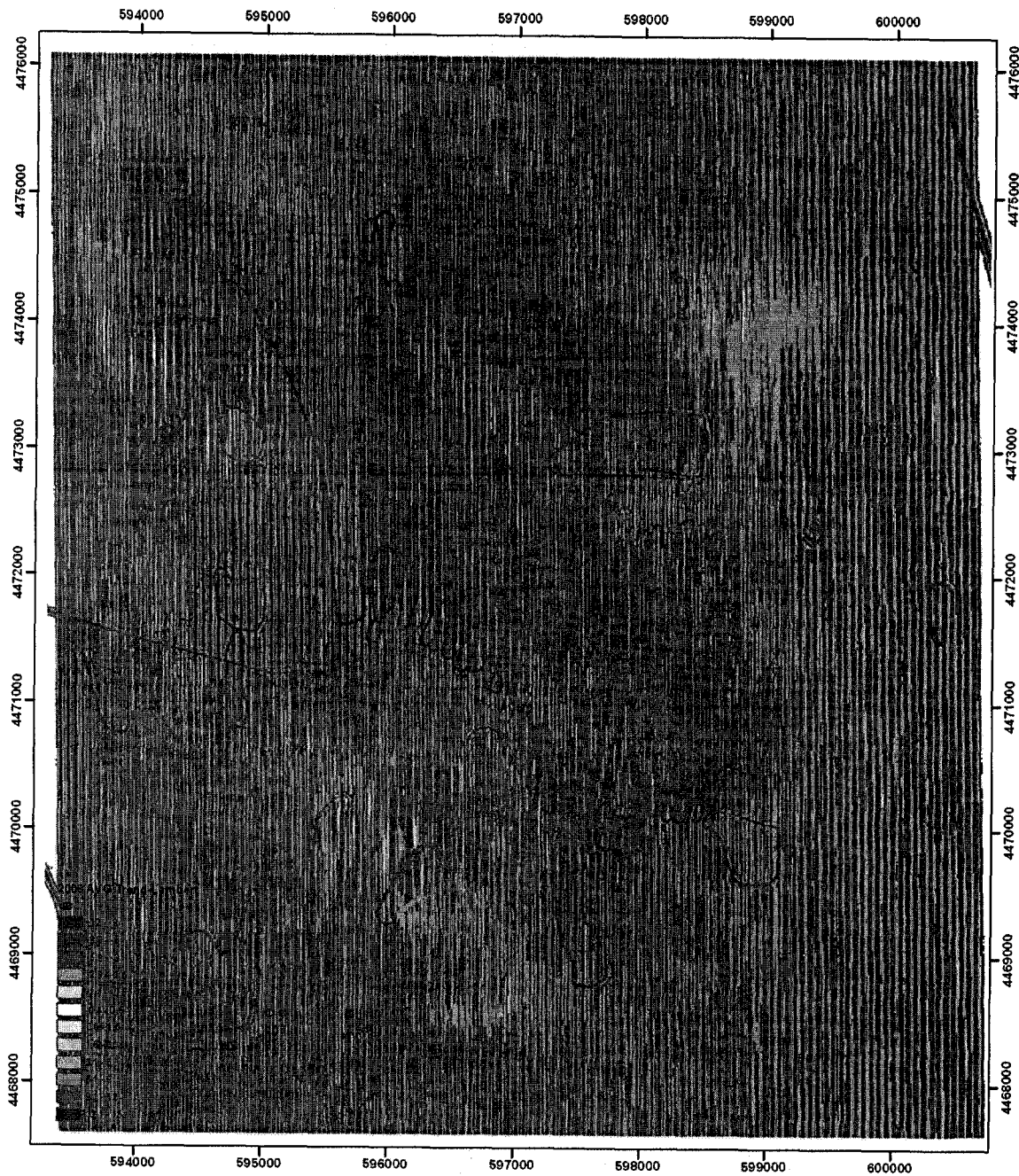
Figure B.4 - Difference between AVG Trend and AVG Flat for the 2006 backscatter mosaic. The difference can reach more than 10 dB.





Figure B.5 - 2006 backscatter mosaic assembled with Geocoder with a Lambertian correction.





Mean = -4.45 dB  
 Standard deviation = 2.29 dB

UTM Projection Zone 18N  
 NAD83 Datum

Figure B.6 - Difference between AVG Trend and a Lambertian correction for the 2006 backscatter mosaic.

## APPENDIX C

### PROCEDURES FOR GRAIN SIZE ANALYSIS

#### C.1 Normal procedure for grain size analysis

##### C.1.1 Removal of organic material

Each sediment sample was placed in a large beaker, covered with 10 ml of 30% hydrogen peroxide and stirred. Deionized water was added to remove any sample material from the beaker walls and to prevent foaming over the top of the beaker. The sample was left to digest for 2 to 5 days until the foaming stopped, then another 10 ml of hydrogen peroxide were added. The procedure continued for about two weeks until all the organic material was oxidized, or until a total 40 ml of hydrogen peroxide had been added and no significant bubbling was observed.

##### C.1.2 Washing salts from the sample

Deionized water was used to transfer the sample from the beaker to centrifuge bottles; each bottle was filled with deionized water up to 80%, closed and thoroughly shaken. Centrifuging took place for 30 min and the clear supernatant water was decanted.

##### C.1.3 Wet sieving at 500 $\mu\text{m}$

A 500  $\mu\text{m}$  sieve was placed over a funnel and a large pre-weighed beaker to collect the finer fraction passing through the sieve. The sample was transferred from

the centrifuge bottle to the sieve with the aid of a squeeze bottle with deionized water. The sediment was rinsed with deionized water and stirred on the sieve with a “rubber policeman” until no small grains were observed on the sieve and the water passing through the sieve remained clear. Care was taken to limit the volume of deionized water plus finer sediment to the size of the beaker. The sieve was turned upside down over a glass bowl and rinsed with deionized water to collect any coarse sand. The excess water was decanted and the sediment rinsed into a small pre-weighted beaker. Both beakers, with sediment fractions larger and smaller than 500  $\mu\text{m}$  were dried at 55  $^{\circ}\text{C}$ .

After all the water evaporated (usually after 3 days for the large beakers with the finer fraction), the beakers were left to cool to room temperature in a desiccator and reweighed. The total weight of the sample is the sum of the two fractions.

#### C.1.4 Dry sieving

The fraction coarser than 500  $\mu\text{m}$  was disaggregated and dry sieved in 0.5  $\Phi$  intervals for 15 min on a sieve shaker. The content of each sieve was transferred to a pre-weighted aluminum dish and reweighed. The fraction left in the pan was also weighed and added to the sediment to be analyzed with laser diffraction.

#### C.1.5 Laser diffraction (Malvern Mastersizer 2000 with the dispersion unit Hydro G)

Dried samples smaller than 500  $\mu\text{m}$  were transferred to plastic jars and a solution of 3 g/l sodium hexametaphosphate was added until the dried sample became a paste. Samples were thoroughly mixed until homogeneous and shipped to the Portuguese Hydrographic Institute for analysis. A small portion of this homogeneous paste was removed and put in the tank of the dispersion unit of the laser diffraction system until the obscuration level settled between 10 and 20 %. Ultrasound was applied to the sample for 120 s and stopped immediately prior to analysis. Three measurements were made,

each with 12 s integration time. Results are reported as the average of the three measurements.

Configuration values used in the Malvern Mastersizer 2000 were 1.544 for particle refraction index (quartz), 1.330 for dispersant refraction index and 1.5 for particle absorption.

## **C.2 Measurement of the natural occurring particle size**

In order to estimate the particle size as close as possible to the original sediment, samples underwent minimal processing. The sample was not digested with hydrogen peroxide and was not washed and centrifuged to remove salts, but was wet sieved at 500  $\mu\text{m}$  to prevent clogging the pump of the laser-diffraction system.

The fraction coarser than 500  $\mu\text{m}$  was discarded. The fraction finer than 500  $\mu\text{m}$  was collected in the beaker and left to rest for more than a week, then partially decanted, left to settle again for a few more days and the remaining supernatant liquid removed with a pipette.

Each sample was analyzed with the laser-diffraction system without adding any dispersant and without ultrasound. The sample was only stirred in order to keep grains in suspension.

Comparison with the samples that followed the normal SOP was made considering only the portion that was analyzed in the laser diffraction. There is one difference, for the samples that followed the normal SOP the sediment left in the pan when sieving was added to the portion analyzed with laser diffraction. It is assumed that the effect of adding dried sediment is worse than the errors introduced if the fraction left in the pan doesn't follow the same distribution as the entire fraction to be analyzed with laser diffraction. In order to minimize errors the comparison was made only for those

samples analyzed with the normal SOP with material left in the pan less than 1% by weight of the fraction finer than 1  $\Phi$ .

The samples considered for this experiment have on average 97 % of their weight distributed below the 1  $\Phi$  size class.

### **C.3 Measurement of the effect of drying the sample**

Drying the sample is part of the standard procedure used at the Portuguese Hydrographic Institute in order to determine the weight of the two portions to be analyzed with sieving and laser diffraction. It is assumed that the sample analyzed with laser diffraction will be separated in its constituent particles when dispersing the sample with sodium hexametaphosphate, applying ultrasound and stirring. To evaluate the error introduced by this method, some samples were analyzed with the standard procedure but without drying for weight determination. The comparison was made only for the portion analyzed with laser diffraction with the same assumptions as in C.2.

### **C.4 Pipette analysis**

A subset of samples was analyzed with pipettes to compare results obtained with two methods that measure different properties of the sediment. This technique used the following steps:

#### **C.4.1 Removal of organic material**

Each sediment sample was placed in a large beaker, covered with 10 ml of 30% hydrogen peroxide and stirred. Deionized water was added to remove any sample material from the beaker walls and to prevent foaming over the top of the beaker. The

sample was left to digest for 2 to 5 days until the foaming stopped, then another 10 ml of hydrogen peroxide were added. The procedure continued for about two weeks until all the organic material was oxidized, or until a total 40 ml of hydrogen peroxide had been added and no significant bubbling was observed.

#### C.4.2 Washing salts from the sample

Deionized water was used to transfer the sample from the beaker to centrifuge bottles; each bottle was filled with deionized water up to 80%, closed and thoroughly shaken. Centrifuging took place for 30 min and the clear supernatant water was decanted.

#### C.4.3 Dispersing the sample

The sample was placed in a 1000 ml beaker and filled up to 66% with dispersant, a solution of 2.18 g/l sodium hexametaphosphate in deionized water, stirred until dispersed and left to sit for one day. After verification that flocculation did not occur, the sample was ready for wet sieving.

#### C.4.4 Wet sieving

After rinsing a 1000 ml graduated cylinder, the funnel, a 2mm sieve and a 62  $\mu\text{m}$  sieve (rinsing the 62  $\mu\text{m}$  sieve is also important to reduce surface tension on the sieve's mesh), the dispersed sediment was poured over the 2 mm sieve and rinsed with dispersant in the squeeze bottle and with the aid of a "rubber policeman". The sediment that passed through the 2 mm sieve was removed and the gravel fraction was rinsed into a glass bowl using deionized water and then to a pre-weighted beaker. Rinsing continued in the 62  $\mu\text{m}$  sieve until the dispersant passing through the sieve was clear. The sieve was removed and the sand fraction was transferred to a glass bowl and then

to a pre-weighted beaker with deionized water. Both beakers were placed to dry at 55 °C.

The volume of dispersant plus mud was limited to less than 1000 ml. The graduated cylinder was topped up to 1000 ml with dispersant.

#### C.4.5 Dry sieving

The gravel and sand fractions were weighted after they were completely dried and cooled to room temperature. The sand and gravel fraction were sieved together for 15 min in 0.5  $\Phi$  intervals, the content of each sieve was placed on a pre-weighted aluminum dish and reweighed and the portion remaining in the pan was also weighed and added to the mud fraction to be analyzed with the pipettes.

#### C.4.6 Pipettes

Each sample in the graduated cylinder was thoroughly mixed during 15 min less than 0.5 hr from the start of the analysis and stirred with a rod for the last 2 min. The first aliquot was removed with a 20 ml pipette 20 cm below the surface, 20 s after stirring stopped, and expelled into a pre-weighted beaker. An additional 20 ml of deionized water was used to rinse out the remaining sediment and expelled into the same beaker. The beaker was placed to dry at 55° C in an oven for one day, cooled in a desiccator to room temperature and reweighed. The first withdraw is a representative sample of the entire sediment present in the graduated cylinder. Additional withdraws were taken at the times and depths presented in table B.1, each sequential withdrawal sample all the sediment at 1  $\Phi$  finer intervals.

Time (h:mm:ss)	Depth (cm)	Fraction
0:00:20	20	<4 $\Phi$
0:01:56	10	<5 $\Phi$
0:07:44	10	<6 $\Phi$
0:31:00	10	<7 $\Phi$
2:03:00	10	<8 $\Phi$
8:01:00	10	<9 $\Phi$
23:00:00	7	<10 $\Phi$

Table C.1 - Withdrawal times and depths used for 20° C water temperature.

Samples were dried, weighed and corrected for dispersant weight and related to the volume of the suspension from which the aliquot was drawn. The last aliquot represents sediment finer than 10  $\Phi$  and was evenly divided between 10  $\Phi$  and 14  $\Phi$ .

### **C.5 Loss On Ignition (LOI)**

Ten to 20 g of sample were placed in a pre-weighted aluminum dish and weighed. The sample was dried in an oven at 55° C for 24 hr, removed and cooled in a desiccator to ambient temperature for one hour, then weighed again. The difference between the dry weight and the initial sample weight is a function of the percentage of moisture in the sample. The sample was heated in a muffle furnace during 4 hr at 450 °C, removed and cooled in a desiccator to ambient temperature and reweighed. The weight difference corresponds to the loss on ignition, assumed to be organic matter.



## APPENDIX D

### EXAMPLES OF ANGULAR RESPONSE

The variation of backscatter strength with grazing angle is an inherent property of the seafloor. Figure D.1 depicts the acoustic backscatter angular response for gravel and silt. Figure D.2 shows the angular response for medium sand in two different areas of the HARS. The sedimentary cover in one station is layered in the top few centimeters whereas in the other it is homogeneous up to the penetration depth of the optical prism.

A perfectly flat seafloor would behave as a partially reflecting acoustic mirror, reflecting sound at an angle equal to the angle of the incident sound, and no energy would return to the transducer except at normal incidence. However, at high frequencies, the seafloor has substantial irregularities at the scale of the acoustic wavelength and acoustic waves are scattered randomly. These irregularities include the roughness of the water-sediment interface, spatial variations in sediment physical properties and discrete inclusions such as shell pieces or bubbles (Jackson and Richardson, 2007).

Silts and clays usually have a smooth surface compared with the acoustic wavelength ( $\lambda = 6$  mm for 240 kHz) and backscatter near normal incidence is mainly dominated by coherent reflection. These sediments also have high porosity, and the acoustic impedance contrast between the sediment and the water is low. At oblique incidence, backscattering due to surface roughness may not be important due to the lack of impedance contrast and to the small surface roughness, the sound penetrates into the sediment more than in sands and gravels and scattering due to heterogeneities that exist within the sediment is expected to be stronger than scattering due to surface

roughness. In a gravelly seafloor, the impedance contrast between the water and the sediment is high and the water-sediment interface is rough; therefore, backscatter is dominated by scattering due to surface roughness at all incident angles. Beyond the critical angle there is a sudden drop in backscatter since almost no energy is transmitted into the sediment. A part of the small amount of energy that is scattered back beyond the critical angle comes from the surface whereas the other part may be due to some penetration into the sediment and scattering by volume heterogeneities within the sediment. Energy may penetrate into the sediment beyond the critical angle due to downward scattering at the sediment surface and/or to the Biot slow wave, which does not have a critical angle (Pouliquen *et al.*, 2000).

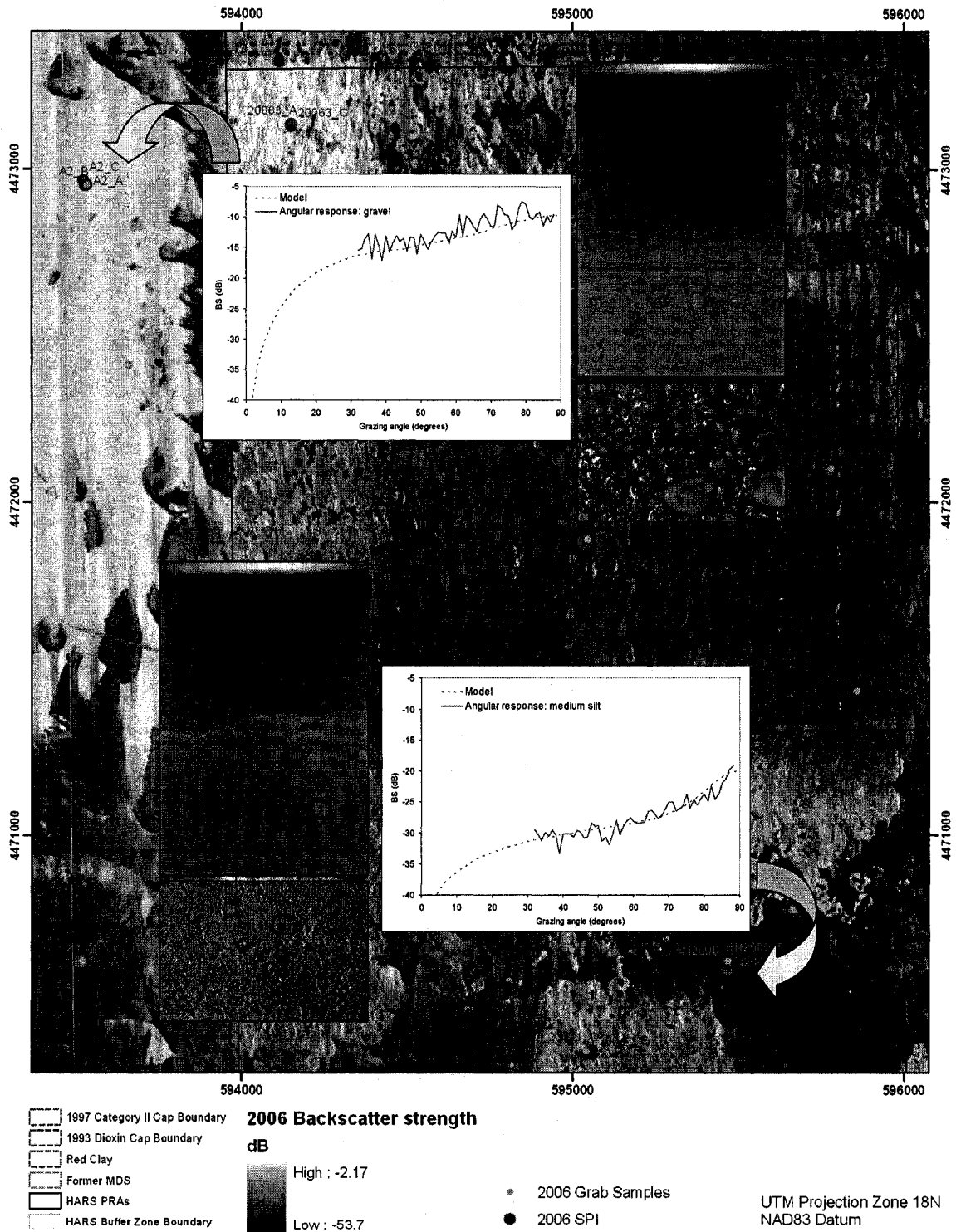


Figure D.1 – Examples of the angular response in the area of stations A2 (gravel) and N2000 (silt) from 2006. SPI images correspond to 20 x 13 cm (HxW) and sediment sample photos to 2.2 x 3.3 cm (HxW). The angular response, depicted in red, was obtained in normal mode (half-swath with x 30 pings) for one patch of the seafloor near each station. The blue line is the adjustment of the model to the observations.

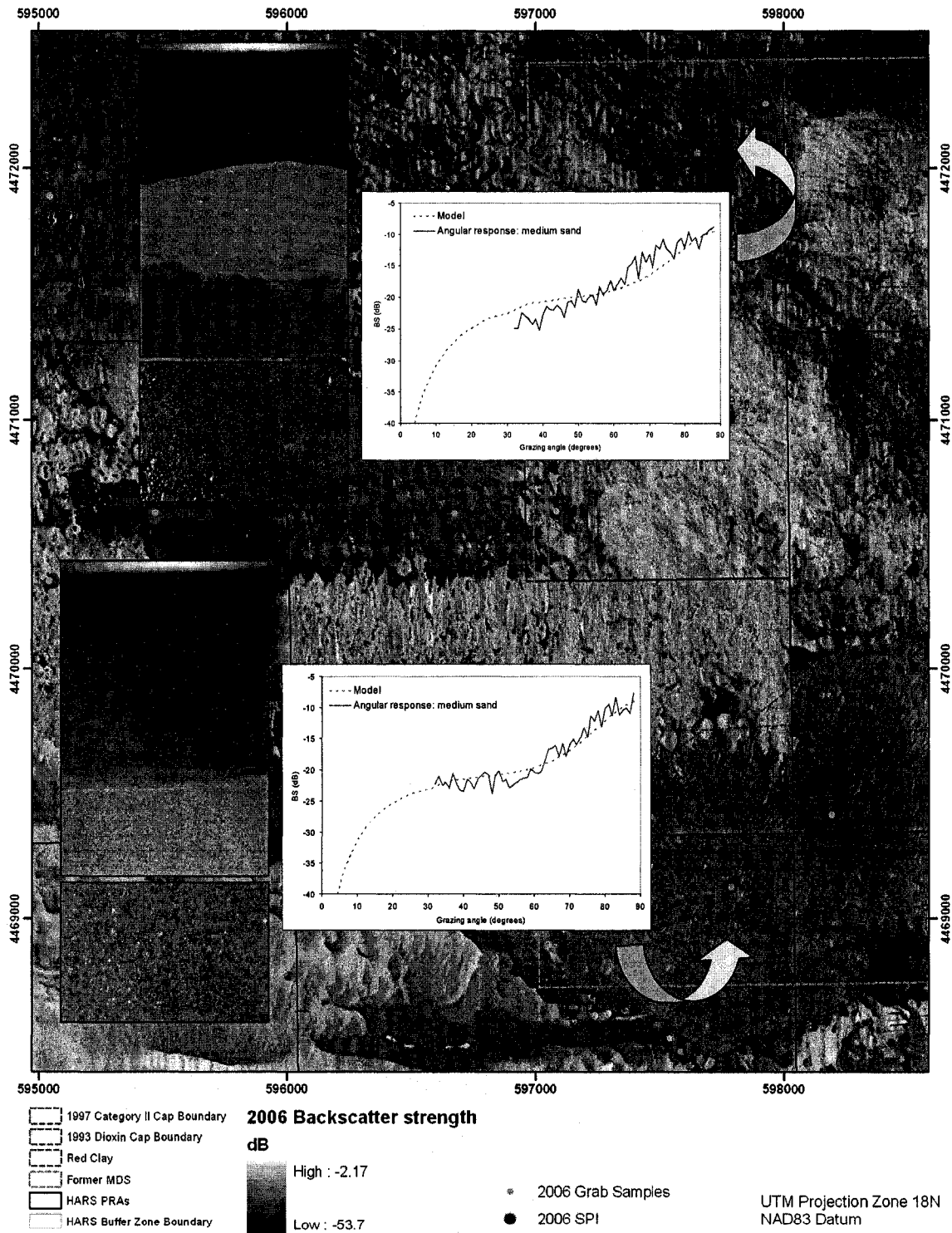


Figure D.2 – Examples of the angular response in the area of stations A9 and 97004 (2006), corresponding to a medium sand seafloor. The grab sample in station A9 captured also the underneath silty layer. SPI images correspond to 20 x 13 cm (HxW) and sediment sample photos to 2.2 x 3.3 cm (HxW). The angular response, depicted in red, was obtained in normal mode (half-swath with x 30 pings) for one patch of the seafloor near each station. The blue line is the adjustment of the model to the observations.

## REFERENCES

Agrawal, Y. C., McCave, I. N. and Riley, J. B., 1991, Laser diffraction size analysis, in: Syvitski, J. P. M., (Ed.), Principles, methods and application of particle size analysis, Cambridge University Press, p. 119-128.

Beaudoin, J. D., Hughes Clarke, J. E., Van Den Aemele, E. J. and Gardner, J. V., 2002, Geometric and radiometric correction of multibeam backscatter derived from Reson 8101 systems, Canadian Hydrographic Conference Proceedings, p.1-22.

Biot, M. A., 1956, Theory of propagation of elastic waves in a fluid-saturated porous solid. II. Higher frequency range, The Journal of the Acoustical Society of America, Vol. 28, No. 2, p. 179-191.

Biot, M. A., 1962, Generalized theory of acoustic propagation in porous dissipative media, The Journal of the Acoustical Society of America, Vol. 44, No. 9, p. 1254-1264.

Blott, S. J. and Pye, K., 2001, GRADISTAT: A grain size distribution and statistics package for the analysis of unconsolidated sediments, Earth Surface Processes and Landforms, Vol. 26, p. 1237-1248.

Butman, B., Danforth, W. W., Knowles, S. C., May, B. and Serret, L., 2002, Sea floor topography and backscatter intensity of the Historic Area Remediation Site (HARS), offshore of New York, based on multibeam surveys conducted in 1996, 1998 and 2000, U.S. Geological Survey Open File Report 00-503, 5 sheets.

Butman, B., Danforth, W. W., Schwab, W. C. and ten Brink, M. B., 1998, Multibeam Bathymetric and Backscatter Maps of the Upper Hudson Shelf Valley and Adjacent Shelf, Offshore of New York, U.S. Geological Survey Open File Report 98-616, 4 sheets.

Chivers, R. C., Emerson, N. and Burns, D. R., 1990, New acoustic processing for underway surveying, The Hydrographic Journal, Vol. 56, p. 9-17.

Collier, J. S. and Brown, C. J., 2005, Correlation of sidescan backscatter with grain size distribution of surficial seabed sediments, Marine Geology, Vol. 214, p. 431-439.

Collins, W., Gregory, R. and Anderson, J., 1996, A digital approach to seabed classification, *Sea Technology*, August 1996, p. 83-87. Damuth, J. E., 1975, Echo character of the western equatorial Atlantic floor and its relationship to the dispersal and distribution of terrigenous sediments, *Marine Geology*, Vol. 18, p. 17-45.

Damuth, J. E., 1980, Use of high-frequency (3.5-12 kHz) echograms in the study of near-bottom sedimentation processes in the deep-sea: a review, *Marine Geology*, Vol. 38, p. 51-75.

Dartnell, P. and Gardner, J. V., 2004, Predicting seafloor facies from multibeam bathymetry and backscatter data, *Photogrammetric Engineering & Remote Sensing*, Vol. 70, No.9, p. 1081-1091.

Dunsiger, A. D., Norman, A. C. and Vetter, W. J., 1981, Seabed characterization from broad-band acoustic echosounding with scattering models, *IEEE Transactions of Oceanic Engineering*, Vol. OE-6, No. 3, p. 94-106.

Environmental Protection Agency (EPA), 1996, New York-New Jersey Harbor Estuary Program, Final Comprehensive Conservation and Management Plan (CCMP), 280 p.

Folk, R. L., 1980, *Petrology of sedimentary rocks*, Hemphill Publishing Company, TX, 184 p.

Folk, R. L. and Ward, W. C., 1957, Brazos River bar: a study in the significance of grain size parameters. *Journal of Sedimentary Petrology*, Vol. 27, p. 3-26.

Fonseca, L., and Calder, B., 2005, Geocoder: an efficient backscatter map constructor, *Proceedings of the U.S. Hydrographic Conference 2005*, San Diego, CA.

Fonseca, L. and Calder, B., 2007, Clustering acoustic backscatter in the angular response space, *Proceedings of the U.S. Hydrographic Conference 2007*, Norfolk, VA.

Fonseca, L. and Mayer, L., 2007, Remote estimation of surficial seafloor properties through the application of angular range analysis to multibeam sonar data, *Marine Geophysical Researches*, Vol.28, No. 2, p. 119-126.

Friedman, G. M. and Sanders, J. E., 1978, *Principles of sedimentology*, John Wiley & Sons, NY, 792 p.

Greaves, R. J., Stephen, R. A., 2000, Low-grazing angle monostatic acoustic reverberation from rough and heterogeneous seafloors, *The Journal of the Acoustic Society of America*, Vol. 108, No. 3, p. 1013-1025.

Hamilton, E. L., 1970, Reflection coefficients and bottom losses at normal incidence computed from Pacific sediment properties, *Geophysics*, Vol. 35, No. 6 (December 1970), p. 995-1004.

Hamilton, E. L., 1972, Compressional-wave attenuation in marine sediments, *Geophysics*, Vol. 37, No. 4 (August 1972), p. 620-646.

Hamilton, E. L. 1974, Prediction of deep sea properties: state-of-the-art, in: Inderbitzen, A. L. (Ed.), *Deep-sea sediments, physical and mechanical properties*, Plenum Press, p. 1-43.

Hamilton, E. L., 1976, Sound attenuation as a function of depth in the sea floor, *The Journal of the Acoustical Society of America*, Vol. 59, No. 3, p. 528-535.

Hamilton, E. L., 1978, Sound velocity-density relations in sea-floor sediments and rocks, *The Journal of the Acoustical Society of America*, Vol. 63, No. 2, p. 366-377.

Hamilton, E. L., Bachman, R. T., 1982, Sound velocity and related properties of marine sediments, *The Journal of the Acoustical Society of America*, Vol. 72, No. 6, p. 1891-1904.

Hamilton, E. L., Shumway, G., Menard, H. W. and Shippek, C. J., 1956, Acoustic and other physical properties of shallow-water sediments off San Diego, *The Journal of the Acoustic Society of America*, Vol. 28, No. 1, p. 1-15.

Haralick, R. M., 1979, Statistical and structural approaches to texture, *Proceedings of the IEEE*, Vol. 67, No. 5, p. 786-804.

Jackson, D. R., Winebrenner, D. P and Ishimaru, A., 1986, Application of the composite roughness model to high-frequency bottom backscattering, *The Journal of the Acoustical Society of America*, Vol. 79, No. 5, p. 1410-1422.

Jackson, D. R. and Richardson, M. D., 2007, *High-frequency seafloor acoustics*, Springer, 616 p.

Lurton, X., 2002, An introduction to underwater acoustics: principles and applications, Springer, 347 p.

Kinsler, L. E., Frey, A. R., Coppens, A. B. and Sanders, J. V., 1999, Fundamentals of acoustics, 4<sup>th</sup> ed. , John Wiley & Sons, 548 p.

Krumbein, W. C., 1934, Size frequency distributions of sediments, Journal of Sedimentary Petrology, Vol. 4, No. 2, p. 65-77.

Krumbein, W. C., 1936, Application of logarithmic moments to size frequency distributions of sediments, Journal of Sedimentary Petrology, Vol. 6, No. 1, p. 35-47.

Krumbein, W. C. and Pettijohn, F. J., 1938, Manual of Sedimentary petrography, Appleton-Century-Crofts, NY, 549 p.

LeBlanc, L. R., Shock, S. G., DeBruin, D. L., Jenkins, M. and Munro, L., 1995, High-resolution sonar volume scattering measurements in marine sediments, The Journal of the Acoustical Society of America, Vol. 91, No. 1, p. 107-115.

Loizeau, J. -L., Arbouille, D., Santiago, S. and Vernet, J. -P., 1994, Evaluation of a wide range laser diffraction grain size analyser for use with sediments, Sedimentology, Vol. 41, p. 353-361.

Mayer, L. A. and LeBlanc, L. R., 1983, The chirp sonar: a new quantitative high-resolution profiling system, in: Pace, N. (Ed.), Acoustics and the Sea-Bed, Bath University Press, 436 p.

Mayer, L. A., Kraft, B. J., Simpkin, P., Lavoie, P., Jabs, E., and Lynskey, E., 2002, *In-situ* determination of the variability of seafloor acoustic properties: an example from the ONR GEOCLUTTER area, in: Pace, N. G. and Jensen, F. B. (Eds.), Impact of Littoral Environmental Variability on Acoustic Predictions and Sonar Performance, Kluwer Academic Publishers, The Netherlands, p. 115-122.

McKinney, C. M. and Anderson, C. D., 1964, Measurements of backscattering of sound from the ocean bottom, The Journal of the Acoustical Society of America, Vol. 36, No. 1, p. 158-163.

McMannus, J., 1988, Grain size determination and interpretation, in: Techniques in Sedimentology, Tucker, M. (Ed.), Blackwell, Oxford, p. 63-85.



de Moustier, C. and Matsumoto, H., 1993, Seafloor acoustic remote sensing with multibeam echo-sounders and bathymetric sidescan sonar systems, *Marine Geophysical Researches*, Vol.15, p. 27-42.

Murphy, L., Leary, T. and Williamson, A., 1995, Standardizing seabed classification techniques, *Sea Technology*, July 1995, p. 15-19.

Orlowski, A., 1984, Application of multiple echoes energy measurements for evaluation of sea bottom type, *Oceanologia*, No. 19, p. 61-78.

Pace, N. G. and Dryer, C. M., 1979, Machine classification of sedimentary sea bottoms, *IEEE Transactions on Geoscience Electronics*, Vol. 17, No. 3, p. 52-56.

Pace, N. G. and Gao, H., 1988, Swathe seabed classification, *Machine classification of sedimentary sea bottoms*, *IEEE Journal of Ocean Engineering*, Vol. 13, No. 2, p. 83-90.

Panda, S., LeBlanc, L. R. and Schock, S. G., 1994, Sediment classification based on impedance and attenuation estimation, *The Journal of the Acoustical Society of America*, Vol. 96, No. 5, p. 3022-3035.

Pouliquen, E. and Lyons, A. P., 2002, Backscattering from bioturbated sediments at very high frequency, *IEEE Journal of Ocean Engineering*, Vol. 27, No. 3, July 2002, p. 388-402.

Pouliquen, E., Lyons, A. P. and Pace, N. G., 2000, Penetration of acoustic waves into rippled sandy seafloors, *The Journal of the Acoustical Society of America*, Vol. 108, No. 5, p. 2071-2081.

Reed IV, T. B. and Hussong, D., 1989, Digital image processing techniques for enhancement and classification of SeaMARC II side scan sonar imagery, *Journal of Geophysical Research*, Vol. 94., No. B6, p. 7469-7490.

Rhoads, D. C. and Cande, S., 1971, Sediment Profile Camera for in situ study of organism-sediment relations, *Limnology and Oceanography*, Vol. 16, No. 1, p. 110-114.

Rhoads, D. C. and Germano, J. D., 1982, Characterization of organism-sediment relations using sediment profile imaging: an efficient method of remote ecological monitoring of the seafloor (Remots TM System), *Marine Ecology – Progress Series*, Vol. 8, p. 115-128.

Rhoads, D. C. and Germano, J. D., 1986, Interpreting long-term changes in benthic community structure: a new protocol, *Hydrobiologia*, Vol. 142, p. 291-308.

Richardson, M. D. and Briggs, K. B., 2004, Empirical predictions of seafloor properties based on remotely measured sediment impedance, in: High Frequency Ocean Acoustic Conference, Porter, M. B. and Siderius, M. (Eds.), AIP, Melville, NY, p. 12-21.

SAIC, 2005a, Results of the summer 2005 sediment toxicity and sediment-profile imaging survey at the Historic Area Remediation Site, SAIC Report No. 696, 90 p.

SAIC, 2005b, Results of the summer 2005 sediment multibeam, bathymetric and backscatter surveys at the Historic Area Remediation Site and the Shark River Reef, SAIC Report No. 697, 51 p.

Schock, S. G., LeBlanc, L. R. and Mayer, L. A., 1989, Chirp sub-bottom profiler for quantitative sediment analysis, *Geophysics*, Vol. 54, No. 4, p. 445-450.

Schwab, W. C., Denny, J. F., Butman, B., Danforth, W. W., Foster, D. S., Swift B. A., Lotto, L. L., Allison and M. A., Thieler, E. R., 2000, Sea floor characterization offshore of the New York-New Jersey metropolitan area using sidescan-sonar, U. S. Geological Survey Open-File Report 00-295, 3 sheets.

Singer, J. K., Anderson, J. B., Ledbetter, M. T., McCave, I. N, Jones, K. P. N. and Wright, R., 1988, An assessment of analytical techniques for the size analysis of fine-grained sediments, *Journal of Sedimentary Petrology*, Vol. 58, No. 3, p. 534-543.

Sperazza, M., Moore, J. N., Hendrix, M. S., 2004, High-resolution particle size analysis of naturally occurring very fine-grained sediments through laser diffractometry, *Journal of Sedimentary Research*, Vol. 74, No. 5 (September 2004), p. 736-743.

Stanton, T.K. and C.S. Clay. 1986, Sonar echo statistics as a remote-sensing tool: volume and sea floor, *IEEE Journal of Oceanic Engineering*, Vol. 11, p. 79-96.

Stewart, W. K., Chu, D., Malik, S., Lerner, S. and Singh, H, 1994, Quantitative seafloor characterization using a bathymetric sidescan sonar, *IEEE Journal of Ocean Engineering*, Vol. 19, No. 4, p. 599-610.

Udden, J. A., 1914, Mechanical composition of clastic sediments, *Bulletin of the Geological Society of America*, Vol. 25, p. 655-744.

Urick, R. J., 1954, The backscattering of sound from a harbor bottom, *The Journal of the Acoustical Society of America*, Vol. 26, No. 2, p. 231-235.

Urick, R. J., 1983, *Principles of underwater sound*, 3<sup>rd</sup> ed., Peninsula Publishing, CA, 423 p.

Wadell, H., 1932, Volume, shape, and roundness of rock particles, *The Journal of Geology*, Vol. 40, p. 443-451.

Wadell, H., 1934, Some new sedimentation formulas, *Physics*, Vol. 5, p. 281-291.

van Walree, P. A. and Ainslie, M., 2006, Mean grain size mapping with single-beam echo sounders, *The Journal of the Acoustical Society of America*, Vol. 120, No. 5, p. 2555-2566.

Wentworth, C. K., 1922, A scale grade and class terms for clastic sediments. *The Journal of Geology*, Vol. 30, p. 377-392.

Wentworth, C. K., 1926, *Methods of mechanical analysis of sediments: Univ. Iowa Studies in Nat. Hist.*, Vol. II, No. II.

Wigley, R. L., 1966, Comparative efficiencies of Van Veen and Smith-McIntyre grab samplers as revealed by motion pictures. *Ecology*, Vol. 48, No. 1, p. 168-169.

Williams, K. L., 2001, An effective density fluid model for acoustic propagation in sediments derived from Biot theory, *The Journal of the Acoustical Society of America*, Vol. 110, No. 5, p. 2276-2281.